IMPACT OF A BIOLOGICALLY-INSPIRED TAIL ASSEMBLY ON DRAG REDUCTION FOR LIGHTER-THAN-AIR NEAR SPACE PLATFORMS

by

JASON LAMBERT COTTINGHAM

A THESIS

Submitted in partial fulfillment of the requirements
for the degree of Master of Science in the
Department of Aerospace Engineering
in the Graduate School of
The University of Alabama

TUSCALOOSA, ALABAMA

2010

Copyright Jason Lambert Cottingham 2010
ALL RIGHTS RESERVED

ABSTRACT

The near space region is a vastly underused region of our atmosphere due to the extreme conditions present but makes up approximately 75% of the usable atmosphere. Although there are no weather patterns like rain, storms and clouds, the winds that are present at high altitudes are very challenging to overcome. Many have researched and designed high altitude platforms for exploration, but few have succeeded in experimental aircraft tests at altitude. Due to the low density, temperature and pressure in this region, fixed wing flight is almost impossible but lighter than air technology can be utilized to help overcome some of those challenges. Long endurance flight in the near space region is beginning to be heavily researched due to the many advantages of the capability from civilian uses to military uses. With the ever present winds in the near space region, lighter than air technology used in conjunction with its station keeping ability becomes an almost unconquerable task.

This research focuses on using the adaptations of nature to help solve the power requirement challenge surrounding high altitude/long endurance flight. With the use of a biologically inspired tail, the drag on an airship can be decreased, and thus the power required for station keeping abilities. Using computational modeling, a complete environmental model was created to represent the aspects of the atmosphere that directly affect airship flight. A model of a basic shaped airship and an airship fitted with a tail inspired by avian flight were created to be used in the environmental model. The approach used in this research is one approach that could be used to significantly reduce the drag on a high altitude airship and help enable the creation of viable near space vehicles.

LIST OF ABBREVIATIONS AND SYMBOLS

HAA	=	High Altitude Airship
UVA	=	Unmanned Aerial Vehicle
t/c	=	Thickness to chord ratio
C_{lmax}	=	Maximum lift coefficient
α_{clmax}	=	Angle of attack for maximum lift coefficient
α_{Lo}	=	Angle of attack for zero lift
C_{Lo}	=	Lift coefficient at zero angle of attack
C_{Lm}	=	Moment coefficient at zero angle of attack
$C_{L\alpha}$	=	Lift curve slope
Re	=	Reynolds number
ρ	=	Density
V	=	Velocity
l	=	General length
μ	=	Dynamic viscosity
C_{do}	=	Zero lift drag coefficient
R_{wf}	=	Wing/fuselage interference factor
R_{LS}	=	Lifting surface correction factor
C_f	=	Coefficient of friction
S_{wet}	=	Wetted surface area

S_w	=	Wing area
l_f	=	Length of fuselage
d_f	=	Diameter of fuselage
Re_f	=	Reynolds number of fuselage
Λ	=	Wing Sweep
M	=	Mach number
C_L	=	Lift Coefficient
W	=	Weight
q	=	Dynamic pressure
P(U)	=	Probability density function
k	=	Shape factor
c	=	Scale factor
U	=	Wind velocity
F(U)	=	Cumulative distribution function
σ_U	=	Standard deviation of velocity
$\bar{U}$	=	Average wind velocity
Γ	=	Gamma function
$U_{99\%}$	=	99^{th} percentile velocity
$U_{1\%}$	=	1^{th} percentile velocity
z	=	Altitude AGL
AGL	=	Above Ground Level
ω	=	Mixing ratio
M_w	=	Mass of water vapor

M_a = Mass of dry air

ν = Specific volume of moist air

ν_a = Specific volume of dry air

P = Pressure

P_o = Standard air pressure at sea level

T = Temperature

T_o = Absolute temperature at sea level

R_w = Universal gas constant for water vapor

R_a = Universal gas constant for dry air

ρ_a = Moist air density

L_{LG} = Lift generated by lifting gas

g = Gravitational constant

vol = Volume

ρ_{LG} = Density of lifting gas

R_{LG} = Universal gas constant for the lifting gas

D = Drag

V_∞ = Freestream velocity

C_{DV} = Volumetric drag coefficient

C_f = Friction Coefficient

C_{fl} = Laminar friction coefficient

C_{ft} = Turbulent friction coefficient

F = Force

A = Area

C_{fc} = Combination laminar/turbulent friction coefficient

Re_L = Reynolds number for total length

Re_c = Critical Reynolds number

P_R = Power required

T_R = Thrust required

M_{BB} = Pitching Moment

CB_{blimp} = Center of buoyancy for blimp

CP_{tail} = Center of pressure for tail

N_{BB} = Yawing moment

ACKNOWLEDGEMENTS

I am lucky to have worked closely with many of the faculty members of the Aerospace Engineering Department during my tenure as both and undergraduate student and a graduate student. First and foremost, I would like to thank my advisor, Dr. John Baker for his patience, motivation, guidance and persistence in both my studies and my research. I would also like to thank Dr. L. Michael Freeman and Dr. Amy Lang for serving on my committee and providing invaluable guidance and through this process. None of this research could have been possible without the help of Mrs. Bedingfield, Mrs. Hamric, and Mrs. Hinton from the Mechanical Engineering Department, Mr. Connell from the Aerospace Engineering Department, and everyone in the College of Engineering Machine Shop.

I would also like to thank the Near Space Engineering Research and Technology (NSERT) Program funded by NASA. Graduate school would not have been possible for me to attend without this resource.

Lastly, I would like to thank my family and friends for the support and encouragement during this process. The kind words and help throughout the years are irreplaceable and have always been greatly appreciated.

CONTENTS

ABSTRACT……...…....…ii

LIST OF ABBREVIATIONS AND SYMBOLS……...……....iii

ACKNOWLEDGEMENTS……...vii

LIST OF TABLES……...….....x

LIST OF FIGURES…….....xi

CHAPTER 1. INTRODUCTION/MOTIVATION…….……...…..…1

1.1 Designs…….…….....…1

1.2 Models/Modifications……..…….…...….3

1.3 Organization……..…….…….3

CHAPTER 2. REVIEW OF LITERATURE……..……....…5

2.1 Blimp/Airship Aerodynamics……..……...….5

2.2 Avian flight…….……...8

2.3 Near Space…….……..…13

2.4 Near Space Vehicles……..……..…15

CHAPTER 3. CONCEPTUAL VEHICLE DESIGN……..…….....22

CHAPTER 4. MODEL VEHICLE DESIGN…….…….27

4.1 Environmental Model…….....…27

4.1.1 Wind Model…….....….27

4.1.2 Buoyancy Model……...…...33

4.2 Basic Blimp Model……..……...……..…37

4.2.1 Dimensions……...…...……..…37

4.2.2 Aerodynamic Analysis…….…....……....38

4.2.3 Basic Blimp Power Model…….……...……....44

4.2.4 Stability/Control……..……...……...…46

4.3 Modified Blimp Model……..……..47

4.3.1 Modified Blimp Dimensions……...……...…….48

4.3.2 Modified Blimp Aerodynamic Analysis…….....49

4.3.3 Modified Blimp Power Model……...…….....53

4.3.4 Stability/Control……..…….....…55

CHAPTER 5. RESULTS AND DISCUSSION OF NEAR SPACE ANALYSIS…..…….....…56

5.1 Basic Blimp Results for Near Space……..……..56

5.2 Modified Blimp Results for Near Space……...…...…....58

5.3 Comparison of Results……..……...61

CHAPTER 6. CONCLUSIONS AND FUTURE WORK……...…..…....63

6.1 Models……...……...…63

6.2 Conclusions……..63

6.3 Potential Future Work…….....64

REFERENCES……...66

APPENDIX 1…….70

APPENDIX 2……..……...76

APPENDIX 3……..……...98

LIST OF TABLES

Table 1. HQ 3012 airfoil parameters (Selig, 2008). 22

Table 2. Lift generated at an altitude of 500ft. 25

Table 3. Lift generated at 100,000 ft. 25

Table 4. Velocities obtained from weibull distribution for Akron, OH. 29

Table 5. Velocities obtained from weibull distribution for White Sands, NM. 31

Table 6. U.S. Standard atmosphere mixing ratio at altitude. 33

Table 7. Basic Blimp dimensions. 37

Table 8. Mesh refinement data for Basic Blimp. 41

Table 9. Drag analysis results and comparison for Basic Blimp. 42

Table 10. Power analysis and comparison for Basic Blimp. 46

Table 11. Calculated moment for the Basic Blimp. 47

Table 12. Modified Blimp dimensions. 48

Table 13. Mesh refinement data for Basic Blimp. 50

Table 14. Drag analysis results and comparison for Modified Blimp. 51

Table 15. Power analysis and comparison for Modified Blimp. 55

Table 16. Moment comparison between Basic Blimp and Modified Blimp. 55

Table 17. Power required for Basic Blimp in Near Space. 58

Table 18. Power required for Modified Blimp in Near Space. 60

Table 19. Comparison of power required for the Basic Blimp and Modified Blimp. 61

Table 20. Comparison of power required for the Basic Blimp and Modified Blimp. 62

LIST OF FIGURES

Figure 1. Timeline of airship research and development (Liao 2009)……..……....6

Figure 2. Different adaptations of avian wings (Saville 1956).....9

Figure 3. Different possible configurations for *Microraptor* flight(Chatterjee 2007). 11

Figure 4.Visualization of Separation Bubble (Muti Lin, 1996). 16

Figure 5. Wind profile for airspace above Akron, OH. 30

Figure 6. Wind profile for airspace above White Sands, NM. 32

Figure 7. Plot of mixing ratio as a function of altitude.....34

Figure 8. SolidWorks drawing of Basic Blimp. 38

Figure 9. Volumetric Drag coefficient vs. altitude for Basic Blimp. 40

Figure 10. Mesh refinement convergence for Basic Blimp. 42

Figure 11. Velocity plot of Basic Blimp at ground level for Akron, OH. 43

Figure 12. Velocity plot of separation region for Basic Blimp at ground level for Akron, OH. 43

Figure 13. Power required vs. altitude for Basic Blimp over Akron, OH. 45

Figure 14. Power required vs. altitude for Basic Blimp over White Sands, NM. 45

Figure 15. Visualization of the reduction in wake height due to presence of tail. a). Full tail, b). Tail wedge only, c). No tail (Maybury and Rayner, 2001). 48

Figure 16. SolidWorks drawing of Modified Blimp. 49

Figure 17. Drag coefficient vs. altitude for Modified Blimp.....49

Figure 18. Mesh refinement convergence for Basic Blimp. 50

Figure 19. Profile view of velocity plot of the Modified Blimp for Akron, OH. 52

Figure 20. Magnified view of area of most likely separation. 53

Figure 21. Power required vs. altitude for Modified Blimp over Akron, OH. 54

Figure 22. Power required vs. altitude for Modified Blimp over White Sands, NM. 54

Figure 23. Relationship between power required and wind velocity for a basic airship over Akron, OH. 56

Figure 24. Relationship between power required and wind velocity for a basic airship over White Sands, NM. 57

Figure 25. Visualization of wake for Basic Blimp at Power Knee Region. 58

Figure 26. Relationship between power required and wind velocity for modified airship over Akron, OH. 59

Figure 27. Relationship between power required and wind velocity for modified blimp over White Sands, NM. 59

Figure 28. Visualization of wake for Modified Blimp at Power Knee Region. 61

CHAPTER 1

INTRODUCTION / MOTIVATION

High altitude flight has been brought to the forefront of research due to the need of a long endurance aircraft that can be used at high altitudes for a multitude of purposes including surveillance and communication abilities. According to the International Aeronautical Federation, the boundary between air and space is defined at the Karman line, or approximately 100 km (Knoedler, 2005). This region of the atmosphere is a vast, greatly underutilized region of the atmosphere that has much potential for military as well as civilian uses (Schmidt, 2007). In the near space region, a major concern in using aircraft that require aerodynamics to produce lift is the low air density, therefore, lighter than air technology may be used to utilize this region of the atmosphere.

1.1 Designs

Original near space platform designs focused on fixed wing aircraft for high altitude flight. Some simulations have been conducted including a NASA simulation by Murray et al.(1992) for high altitude aircraft. This simulation study involved deploying a high altitude aircraft from a balloon. One major concern for fixed wing flight in near space is a concern for low Reynolds number aerodynamics. Low Reynolds number aerodynamics creates a special problem in the form of a separation bubble on the airfoil that greatly reduces the effectiveness of the airfoil. Other designs for high altitude fixed wing aircraft were researched. Goraj et al.(1999)

conducted a study for the design of a high-altitude long-endurance unmanned aerial vehicle. The design study addressed four obstacles that must be confronted when designing this type of vehicle: 1. Low Reynolds number aerodynamics, 2. Light structures, 3. Propulsion technology, and 4. Flight control system. Of most relevance to this research is the low Reynolds number aerodynamics problem. For high altitude flight, the velocity at which the vehicle needs to fly at in order to stay aloft at a high altitude for an extended period is relatively high. Due to the extreme nature of the near space region the size of the aircraft needs to be relatively large in order to carry the amount of equipment needed, and to generate the amount of lift needed in this extreme environment.

One way to decrease the amount of lift needed from aerodynamics may be to utilize airship technologies. Benefits that come from using an airship include the potential to have wide-area surveillance for months at a time, along with other benefits like heavy lift capabilities that typical aircraft do not have. However a major challenge arises in finding a suitable renewable energy source to power the airship.

The concept of a hybrid airship using aerodynamic lift technology could be a feasible alternative to a high altitude aircraft. The ability of the hybrid airship to generate most of its lift by buoyancy forces and relying on aerodynamic lift for part of the overall lift generated could help solve some maneuverability problems seen in airship technology. The use of ailerons, elevators and rudders to control all aspects of the flight could make controlling a hybrid airship by flight control software easier than trying to utilize flight control software to control a conventional airship with different configurations of thrusters (Brooke, 2005).

1.2 Models/Modifications

For the design and analysis of an airship, different models were created to calculate the values needed for accurate analysis. An environmental model based on the 1976 US Standard Atmospheric Data as well as previously published wind data (NOAA Real Time Archive, 2004) was created that predicts different aspects of the atmosphere from sea level through near space. Temperature, pressure, density and mixing ratio were included in the environmental model. A statistical analysis of the previously published wind conditions (NOAA Real Time Archive, 2004) through the atmosphere was conducted and inserted into the model for a complete model of the atmosphere. A model of a basic airship and a modified airship was integrated into Solidworks and analyzed using Floworks, computational fluid dynamics software. A biologically inspired modification was applied to the basic blimp. The tail of the blimp was modified and lengthened to mimic the tail of some birds. It has been shown that the tail of birds acts as a natural drag reduction technique for avian flight. The tail interacts with the wake behind the body of the bird to decrease the overall wake height and thus the overall drag.

1.3 Organization

This research is organized into five chapters. A literature review of the topics surrounding fixed wing, high altitude flight, low Reynolds number aerodynamics, statistical analyses, avian flight evolution and airship aerodynamics and capabilities is presented in the second chapter. The third chapter presents some original work surrounding high altitude fixed wing flight and the multitude of challenges involved with successful flight. Chapter four presents the environmental model used for the airship analysis and the model of the basic airship and the

modified airship. The final chapter discusses the results of the computational and theoretical analysis of the two airships and the potential for future work.

CHAPTER 2

REVIEW OF LITERATURE

2.1 Blimp/Airship Aerodynamics

Airships have been utilized for civilian use and military use for many years. The first blimp can be traced back to 1852 and was built by the French engineer Henri Giffard (Liao, 2009). From that point airships continued to gain popularity because of their low cost of energy usage. Many different types of airships have been built, including: traditional airships, unconventional airships, non-rigid, semi-rigid, and rigid airships, hybrid airships, high altitude airships and more (Liao, 2009). Airships have a much longer range of performance than conventional fixed wing aircraft and helicopter. The main advantage over fixed wind and rotor craft vehicles is derived from the low operating cost and the ability to station keep for long periods of time without having to refuel (Liao, 2009). Even with the huge success of airships before the *Hindenburg* accident, airship interest and research severely lacked thereafter (Liao, 2009). Figure 1 shows the history of airship development before 1960 and shows the lack of research and development after the *Hindenburg* accident in 1937 (Liao 2009).

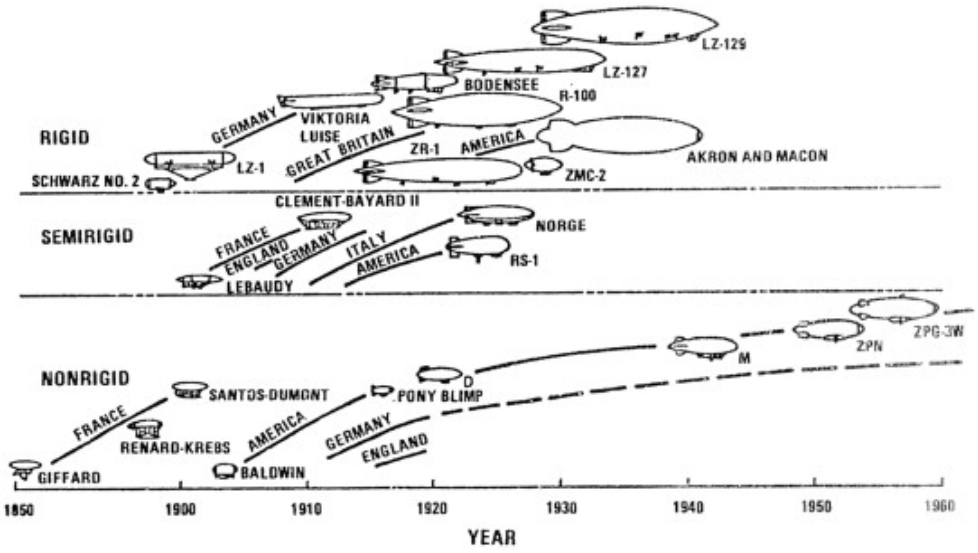

Figure 1. Timeline of airship research and development (Liao 2009).

In more recent years, with the increase in technology and capabilities in materials, propulsion and computer technology, many airship test vehicles have been built and tested in order to gain experience for the exploration of near space including but not limited to airships by Kantor (2001) and Nadakate (2005). Basic designs and tests were conducted by multiple parties on the basic structure and flight of an airship. One such low altitude airship was built and tested to calculate aerodynamic properties of an airship as well as how to construct a tail structure sufficient enough to withstand the forces being placed on it (Huang, 1995). Another low altitude airship was designed and used to test the capability of electric motors to successfully fly and operate a blimp (Sandlin, 1992). One flight test vehicle developed by the Japan Aerospace Exploration Agency was the SPF-2. The model built was tested and confirmed the ability of newer and lighter materials to be more effective in flight, as well as the ability of flight computers to control the airship effectively (Nakadate, 2005). With the anticipated exploration of near space, the current solution for regenerative energy is by the use of solar power. Although solar power is on the brink of major breakthrough, the technology is not yet available which limits the total endurance of an airship (Kantor et al., 2001).

Analyses and tests were conducted on different types of airships to try to verify the theoretical processes used and discover general trends in the estimation of drag on airship hulls. Dorrington (2006) calculated and tested the processes presented by Hoerner to estimate the drag over a streamlined body. Hoerner's method accurately estimates the drag for streamlined bodies, however doesn't extend to spherical airships. Dorrington theoretically proved that adding a cone shaped body to the back of a sphere would decrease the drag by almost 50%. After wind tunnel analyses were conducted, full scale flight tests were conducted to verify this theory; however the flight test results did not show a reduction in drag with the use of a cone attached to the back of the airship, and was in fact higher than anticipated. A hypothesis for this discrepancy may be high parasitic interference due to turbulent conditions during flight that could cause early separation over the body, but further tests have not been conducted to verify the hypothesis (Dorrington, 2006). Another experimental study that was conducted utilized a water towing tank to experimentally estimate the drag of a high altitude airship. Included in this particular study by Beheshti (2007) was the effect of wind speeds, crosswinds, and appendages of the High Altitude Airship (HAA) on the overall aerodynamics of the HAA. Tests were also performed on a sphere to compare data from other sources to verify the experimental approach. After testing, the numerical results using Hoerner's method, computational results and experimental data somewhat resembled each other. The discrepancies in the experimental, theoretical and computational results are due to the effect of laminar-to-turbulent transition, which was not accounted for in CFD and theoretical approaches. The experiment also showed that with the addition of appendages on the body, the drag was increased by around 23% compared to that of the hull alone. With Reynolds numbers ranging between approximately $5x10^5$ to approximately $2x10^5$ for the lower region of near space, and using the wind data that was available (NOAA

Real Time Archive, 2004) between 20-26 kilometers, the transition of the flow from laminar to turbulent moves forward on the airship with increasing altitude, resulting in a greater portion of the flow being turbulent thus increasing the drag.

2.2 Avian Flight

There have been hypotheses that aerodynamic theory can help explain the basic physics of flight as well as the origin of flight. Hendenström's (2002) research involved using aerodynamic theory to determine flight range, migration strategy, and flight speeds of birds as well as how birds evolved to the design they currently have. The very complicated motion of avian flight creates many problems when determining the instantaneous forces acting on the bird, including changing wing planform, wing twist, wing rotation, and elastic deformation of feathers during flight. When modeling the aerodynamics of avian flight, two methods are often used, a quasi-steady assumption, and an impulse of the wake momentum change caused by the flapping of the wings. From the different aerodynamic characteristics, the power curve can be derived. The power curve produces the most relevant data for ecologists to use for determining the evolution of avian flight (Hendenström, 2002). Saville (1956) proposed that avian wings have been products of adaptive evolution and can be grouped into multiple categories: the elliptical wing which was adapted to be used in confined spaces, the high speed wing, the high aspect ratio wing generally seen on oceanic birds, and the slotted high lift wing generally found on terrestrial soaring birds and predators carrying heavy loads. Figure 2 shows the different adaptations of the avian wing.

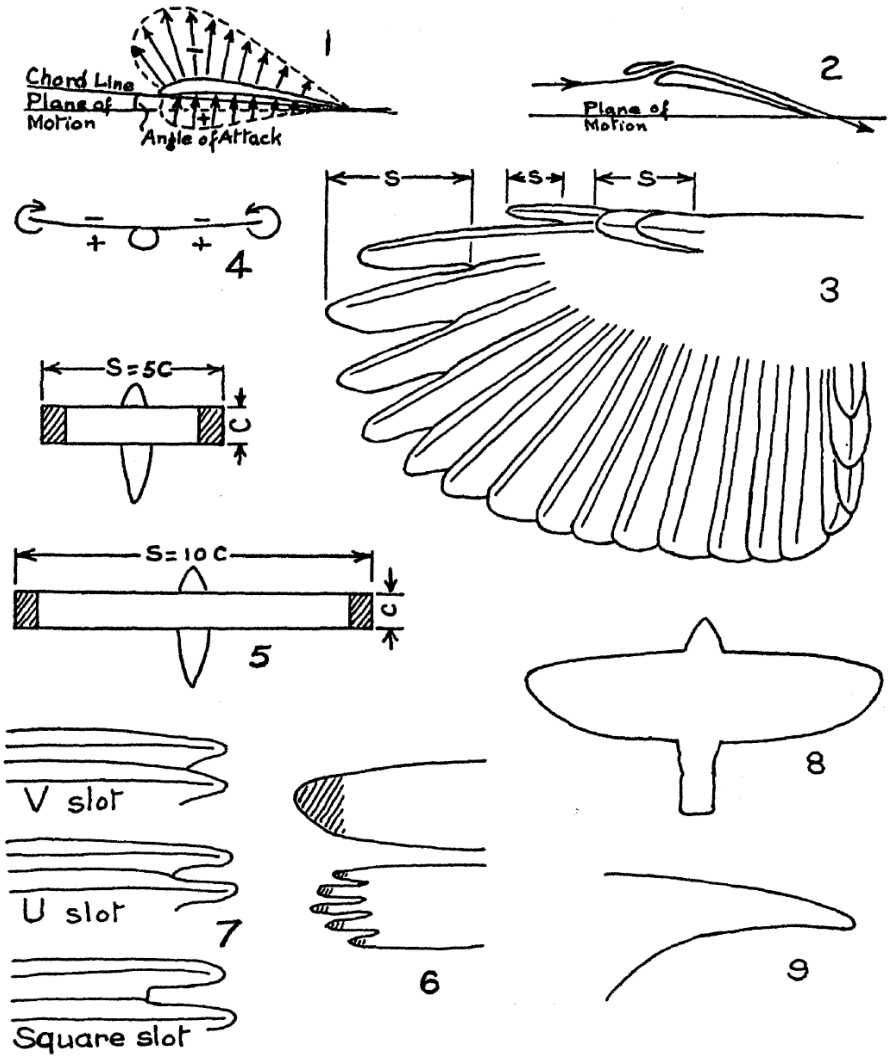

Figure 2. Different adaptations of avian wings (Saville, 1956).

Some of the different adaptations Figure 2 shows are:

1.) Wing section showing approximate magnitude and direction of lift at different locations.

2.) Wing section showing the effect of a slot in delaying the turbulent transition.

3.) Plan view of Catbird wing showing slotted portions make up 55% of length of wing.

4.) End view of bird showing wing tip vortices.

5.) Effect of increased aspect ratio on percentage of wing that is ineffective.

6.) Reduction of loss of lift by slotted wing tips.

7.) Types of slots; primitive v-slot, more advanced and efficient U-slot and highly efficient square slots found in birds of prey.

8.) Plan view of House Sparrow showing elliptical wing.

9.) Plan view of the wing of an American Golden Plover showing high speed capability.

The previous aerodynamic theories only take the wings and body into account, however the tail of a birds acts much like the tail of an aircraft, therefore cannot be neglected. Some theories suggested by scientists proposed that the tail could bend in the airflow causing the outer tail feathers to act much like the flaps of an aircraft which can help with maneuverability during slow and fast flight (Thomas, 1993). From early fossils, the ancestors of today's birds had feathers and wings. Some scientists believe earliest birds were more designed for gliding, including the *Microraptor gui,* one of the earlier ancestors of today's birds (Chatterjee, 2007). Simulations suggest *Microraptor gui* had the ability to use its wings and feathered hind limbs together like a biplane for undulating flight and its long tail for pitch dampening and overall stability (Chattterjee, 2007). Figure 3 shows the different possible configurations for the wings and limbs of the *Microraptor gui* during flight (Chatterjee, 2007).

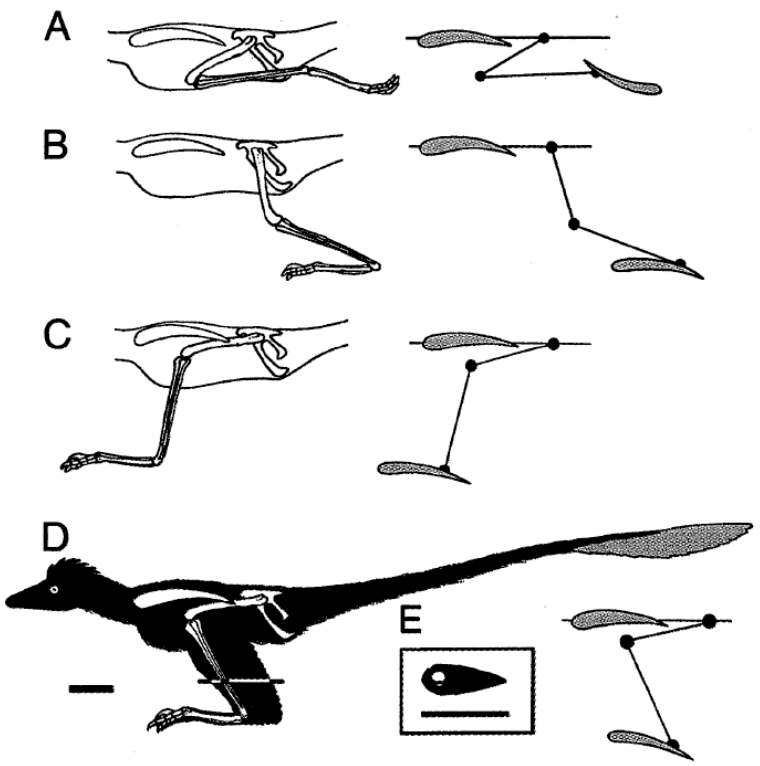

Figure 3. Different possible configurations for *Microraptor gui* flight (Chatterjee 2007).

Along with *Microraptor gui*, other dinosaurs had similar aspects including a long tail. Gatesy and Dial (1996) propose the long tail of early gliding dinosaurs was used primarily for stability. The tail's contribution to pitch control would have been limited to the changing in angle of attack of the tail by raising or lowering it. Because the tail was long, it created a large moment to ensure stability during gliding flight, and was much more stable than modern birds. A possible theory for this change in tails was presented by Smith (1952). He proposed the evolution of birds from stable, long tails to more unstable short tails could be in the evolution of the nervous system of early animals. Much like modern day fixed wing flight, the more stable or the better the ability of the airplane to return to steady flight after a disturbance, the easier the plane is to fly, however the less maneuverable the plane could be. With advancements in

technology, more specifically flight computer and autopilot technology, the closer to unstable a plane can be due to the ability of a much faster and precise computer to be able to handle the magnitude and complexity of inputs needed to fly. Smith uses this same observation and applies it to early avian flight to help explain the adaptations of early birds to a more unstable design. By having a more advanced nervous and muscular system, it was proposed that early birds could more effectively and efficiently control and maneuver with shorter tails. Norberg (1995) studied the effects of long tails versus short tails on flight power. It was seen that the longer the tail, the more power was required, whereas shorter tails needed less power and could have evolved to be more prominent due to natural selection.

Other scientists have proven other uses for the tail. For example, Maybury (2001) conducted experiments on wingless bodies of birds with no tail, partial tail, and full tails. The experiment followed the known knowledge that vortex shedding is induced behind bluff bodies. One common method to reducing the shedding is to introduce a splitter plate in the wake centerline. When the splitter plate interferes with the shedding, it reduces the mean wake height, which directly corresponds to a reduction in drag. With the use of the splitter plate, the drag can be reduced by as much as 36% at Reynolds numbers between 10^3 and 10^6. The results showed that by removing the tail, the drag was increased by as much as 25%. This result is affirmed by the known effects of drag on cylinders in a flow and the drag reducing effect that a splitter plate can have down the centerline of the body, in the wake. Therefore tails can help decrease the parasite drag created by the body of the bird.

2.3 Near Space

Near space makes up the majority of the usable atmosphere however is an overlooked region of our atmosphere for flight. The International Aeronautical Federation defines the boundary between air and space and thus the upper boundary of near space, to be at the Karman Line, or approximately 100 km (Fernandez, 2004). Many researchers consider the lower boundary of near space to be at approximately 20 km (Knoedler, 2005). Through basic geometry, it can be shown that the near space region accounts for almost 77% of the atmosphere below the Karman line. With such a vast amount of volume, it is a highly under used portion of the atmosphere. The environment in near space is very harsh, similar to that of space. There are significant differences that make it different than space, first, the concept of ambient temperature. The temperature in near space is cold, but actually between 20 km and about 36 km, the temperature actually increases to a maximum of around 250 Kelvin at approximately 36 km, whereas in space, the concept of ambient temperature doesn't exist due to the scarcity of molecules to determine temperature (Tomme, 2005). If an object is in the sun it is hot, if it is in the shade it is cold, due to the radiation from the sun. Another difference in space and near space is atmospheric pressure. In space there is no atmospheric pressure while in near space, atmospheric pressure can have a major effect on a vehicle. There is a growing worldwide interest in autonomous flight as well as the ability to have flight vehicles that operate at extended periods of time at high altitudes. The ability to have a flight vehicle that can operate at these high altitudes for extended periods is needed not only for potential military goals but also for potential commercial goals as well, all of which were once only accomplishable using spacecraft. There are very few vehicles that operate at these high altitudes, and when they do, it is only for a very short period of time. This interest in near space activity has increased because of the

potential for cheaper, more flexible missions than that of a space based mission, and because of the availability of lighter weight materials and the advancement of solar technology to make near space flight more feasible.

For the cases concerned with airship flight in near space, wind is a major reason for the lack of aircraft presence in near space. There is no appreciable wind in space however in near space wind is a major hindrance to flight (Tomme, 2005). Because wind is such a determining factor on the feasibility of near space flight, multiple statistical studies have been conducted on the topic. Roney (2007) explores the low near space region (20-22 km) and analyzes the wind for that region. The wind environment above 60,000ft was characterized using statistical data archived by the National Weather Service. This study focused on two locations, where airship testing was most likely and because of the difference in latitudes and traditional weather patterns, White Sands, NM, and Akron, OH. Roney (2007) verifies the method of using a Weibull distribution to estimate winds at altitude from previous year's data. Data from 2004 was analyzed for a fit with the Weibull distribution (Manwell, 2009). The method was used to forecast and hind-cast wind velocities and the results showed the Weibull distribution provided a very close approximation when compared with actual data from different years. From the study it was seen that the wind velocities changed significantly from month to month depending on the season, and the monthly variations should be taken into account as opposed to a year's averaged wind velocity.

Schmidt (2005) also did a statistical study on the wind environment in the near space region. He explored the power requirements needed in order to station keep at an altitude of 65,000 ft. The vehicle used for this study was the typical airship, due to its ability to carry larger payloads to such high altitudes. The drag was determined empirically and experimentally

validated. Using data based on Hoerner, the drag coefficient was approximated. Using wind tunnel tests of a small model, the approximated data was validated. Based on the wind statistics, modeling efforts have shown the ability to characterize the wind data using a Weibull distribution. Using the Weibull probability functions, the 50^{th}, 95^{th}, and 99^{th} percentile winds were determined. Schmidt showed that only at certain times of the year could a basic airship be utilized in near space. Certain months of the years have higher wind velocities making it very difficult for an airship to remain aloft using currently available technology.

2.4 Near Space Vehicles

The near space environment is not a very conducive environment for flight. Due to the low density, temperature and pressure, the flow in this region is a low Reynolds number flow for fixed wing aircraft. One major concern with low Reynolds number flow is the presence of a separation bubble that forces the flow to separate from the airfoil the reattach at a distance further downstream as seen in the representation shown by Muti Lin (1996) in Figure 4.

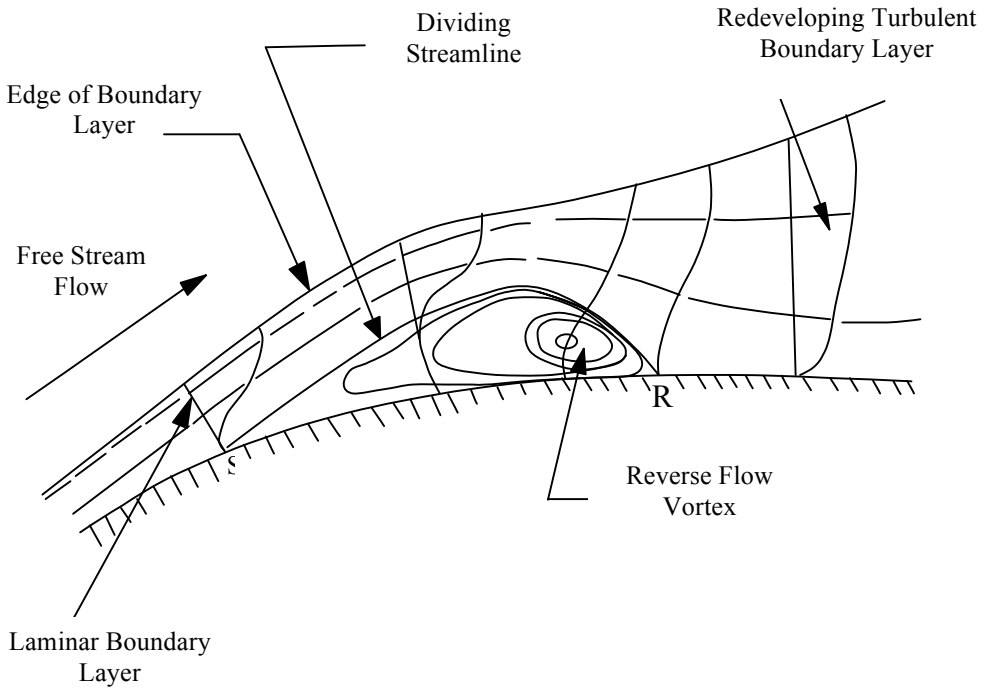

Figure 4.Visualization of Separation Bubble (Muti Lin, 1996).

This separation bubble can have a dramatic effect on the stalling characteristics of an airfoil as well as a decrease in lift and an increase in drag (Mueller, 2003). Studies by Lin and Pauley (1996) show that at low Reynolds numbers a separation is formed, and while still in oncoming flow, the separation bubble will move with the flow and shed at the end of the airfoil. Computational studies showed that as Reynolds number was increased, the formation of the separation bubble moved aft and reduced the size of the separation bubble. NASA has researched some fixed wing high altitude platforms like the APEX program. Basic simulations were conducted to discover the feasibility of a high altitude glider (Murray et. al, 1992). The research was continued by Greer et al. (1999) to continue with the design of a high altitude glider. Some major obstacles that needed to be overcome were the amount of lift needed to fly in such a low density environment, and also the lack of convective cooling for the instruments in such low densities (Greer et. al, 1999). Multiple other designs much like the APEX project were

researched and preliminary designs were developed (Martinez-Val et al., 1999 and Goraj et al., 2004).

There are some major concerns with a glider type high altitude platform. Size, speed, cooling and endurance are only a few of the concerns and challenges. A way to help solve some of these challenges is to research a different type of platform. Lighter than air platforms offer different solutions to some of the challenges presented by fixed wing flight. Brooke (2005) presents a brief overview of the current, publically known high altitude LTA projects. The first aircraft, and still only aircraft able to take payloads to very high altitudes are conventional zero pressure balloons. Although they are very simple in design, there are extreme limitations due to the inability to control the craft and limitations on flight duration. The Ultra Long Duration Balloon (Brooke, 2005) was developed to help solve the duration problem however did not address the control problem. Although with obvious limitations, tethered aerostats were also developed along with airships, but both provided significant challenges. In WWI the Zeppelin "Height Climber" ships, became the first manned airship to ever reach 25,000 feet in 1917. From this platform, other airships were developed to try to solve the problem of long duration flights at high altitudes, some successful and others not. With modern materials and technology, such extreme flight is more feasible but still presents great challenges (Brooke, 2005). There are some companies that have taken on the task of trying to accomplish high altitude LTA flight, government agencies including the DoD, Japanese National Aerospace Laboratory, and the Korean Research Institute, and commercial companies including, StratCom, Skystation, World Wide Aeros, JP Aerospace, as well as other (Brooke, 2005). There are many potential advantages to long endurance, high altitude platforms including increased communications, high altitude sensors for commercial and government use and so on, but with these advantages come

many challenges (Brooke, 2005). Thermal balance, or being able to keep the envelope from experiencing too much of a temperature rise due to the solar cells and waste heat from electronics is a major concern due to the potential of volume changes in the lifting gas due to the temperature rise (Brooke, 2005). Envelope design and construction is a significant problem for high altitude flight due to the long exposure to very cold temperatures. The envelope fabric needs to be able to withstand the increased potential for tears and rips, however still needs to be light enough to minimize weight and cost (Brooke, 2005). Controllability is possible for high altitude airships and has been accomplished in UAV's however designing a system for a large cumbersome aircraft in extreme temperatures and still keep a relatively low cost is a major challenge (Brooke, 2005). Reliability plays an important role due to the extreme environment at high altitudes and the time spent there. All systems play a major role and need to be able to do a specific task at any given moment (Brooke, 2005). There are also safety issues involved with high altitude aircraft. Station keeping capabilities pose a certain hazard to potential cities if the aircraft were to fail during flight (Brooke, 2005). Lastly cost and risk are a major challenge due to available technology.

Research conducted by Colozza (2005) shows that airships may be the only possibility thus far for long endurance, high altitude flight. There have been several aircraft that have achieved flight at altitudes greater than 18 km however all of them have been severely limited in the amount of payload they can carry and the duration at which they can stay aloft (Colozza, 2005). Aerostats are capable of lifting heavy payloads; however have a limited altitude of approximately 5 km due to the weight of the tether (Colozza, 2005). For high altitude flight, the most prominent fixed wing aircraft are the U2 and the SR-71. Both are capable of flight at altitudes greater than 21km, but due to the lower air density at altitude, the speed at which theses

aircraft must fly are extremely fast which severely limits the duration at which they can fly (Colozza, 2005). With the introduction of UAV's, an increase in the endurance of these high altitude aircraft has become a concern. Early solutions to and endurance concern were attained with the introduction of the Condor and the Global Hawk (Colozza, 2005). The Global Hawk is currently pushing the maximum for duration with an endurance of 35 hours (Colozza, 2005). None of these high altitude aircraft can carry large payloads and stay aloft for months at a time. The current concept of a high altitude airship came in the 1970's by the Navy (Colozza, 2005). The first Navy program was the High Altitude Super-Pressure Powered Aerostat (HASPA) and was followed by the High Surveillance Platform for Over-the-Horizon Targeting (HI-SPOT) program (Colozza, 2005). Because these programs were classified, very little is known about them, and since then, a number of other programs have been established to tackle the problem of high altitude flight. The main concern for high altitude airships is the ability to harness and store energy for a long duration flight. Currently the most popular method is using solar cells to harness power from the sun; however other methods like beaming power to the airship from the ground are also being researched (Colozza, 2005).

Miller and Stoia (2005) provide an analysis of the real world operational capability of a high altitude airship using solar regenerative power as well as conventional fuels. They present a solar collection model used to determine the amount of solar energy collected. This study extends the research to changing latitudes and show that at the equator, an airship during summer can collect almost nineteen times the amount of energy collected as the on the same day at the 60 deg N latitude. Schmidt (2007) also suggests the time of day (diurnal effects), vehicle geometry, and annual season must also be considered when determining available power. Using some basic assumptions to ease calculation, the solar energy incident to a surface normal to the sun's

rays was determined and used as the approximate peak solar energy available. A vehicle orientation study determined that a north-south orientation yielded slightly higher energy availability. Vehicle shape showed a very small effect on energy availability and it was concluded that it would have an insignificant effect on available energy. In concert with Miller and Stoia, Schmidt found that the available energy was at a maximum during the summer months.

Schmidt (2007) furthered his study to station keeping performance by focusing on the power available versus the power required. The power available is defined as the available motor shaft power generated by the solar cells, and the power required is defined as the shaft power required by the propulsion system necessary for station keeping the presence of winds. Using all the previous data found from the wind and solar analyses, it was determined that during the summer months there was enough power available for station keeping with very low power requirements, however, during the winter months there was not enough power available to overcome the amount of power required. It can be seen that there can be a large variation month to month in power requirements and a significant variation month to month in power available. Therefore a large conventional airship may be unable to meet the requirements necessary for station keeping performance during certain months of the year however, a design to lower the drag on an airship and thus the power required could result in the ability of an airship to stay aloft indefinitely.

The purpose of this research was to try to solve the challenge of decreasing the power required for station keeping performance. In order to do so, a conventional blimp was modified to reflect an avian tail in hopes that the drag reducing qualities of the avian tail would be used to reduce the power required for station keeping. Some changes in airship design have been

proposed but none documented heavily. This research could be an opening to future research in airship design for decreased power consumption in order to achieve indefinite flight time in near space.

CHAPTER 3

CONCEPTUAL VEHICLE DESIGN

The origins of this research began with the concept of a high altitude long endurance vehicle. From a review of previous research, there have been multiple studies and design analyses for high altitude gliders, but no actual tests have been completed.

An initial model was created to prove the ability and feasibility of the project. MathCAD and Excel spreadsheets were created for all calculations and verification for the feasibility of a high altitude glider. Due to the limitations of the facilities, the glider would have to be limited to roughly a 20 foot or 6 meter wingspan. The first design consideration was the airfoil shape to be used. The University of Illinois at Urbana-Champagne has a very thorough database of airfoil data (Selig, 2008). The database was searched and an average sailplane airfoil shape was chosen for the initial design. The data on the HQ 3/12 chosen for the initial design can be seen in Table 1.

Airfoil Parameters	
t/c	12%
camber	3%
c_{lmax}	1.177
α_{clmax} (deg)	11
α_{Lo} (deg)	-3.75
c_{Lo}	0.412
c_{Lm}	-0.073
$c_{L\alpha}$	6.033

Table 1. HQ 3/12 airfoil parameters (Selig, 2008).

The MathCAD model works off of initial inputs entered by the user, including but not limited to: atmospheric information, aircraft dimensions and airfoil data and can be found in full in Appendix 2.

In order to continue the design process, certain characteristics of the aircraft needed to be calculated. A major concern is the drag on the aircraft. Using the basic Reynolds number format shown by Crowe (2005) as seen Equation 3.1,

$$\mathrm{Re} = \frac{\rho V l}{\mu} \tag{3.1}$$

where the Reynolds number for different parts of the aircraft can be utilized with the derived drag formulation by Edward Lan (2003), to obtain the zero lift drag for the aircraft. The zero lift drag for each part of the aircraft can be seen in Equations 3.2 through 3.4,

$$cd_{o.w} = R_{w.t} c_{f.w} \left(1 + 2\frac{t}{c} + 100\left(\frac{t}{c}\right)^4\right)\frac{S_{wet}}{S_w} \tag{3.2}$$

$$cd_{o.t} = R_{LS.t} c_{f.t} \left(1 + 2\frac{t}{c} + 100\left(\frac{t}{c}\right)^4\right)\frac{S_{wet.tail}}{S_w} \tag{3.3}$$

$$cd_{o.f} = R_{w.f} c_{f.f} \left[1 + \left(\frac{60}{\left(l_f / d_f\right)^3}\right) + .25\left(l_f / d_f\right)\right]\frac{S_{wet.f}}{S_w} \tag{3.4}$$

where R_{wf} and R_{LS} are the wing/fuselage interference factor and lifting surface correction factor as defined by Equations 3.5 and 3.6.

$$R_{w.f} = (2.5523\times10^{-25})\mathrm{Re}_f^{\,3} - (1.3088\times10^{-16})\mathrm{Re}_f^{\,2} + (3.3404\times10^{-9})\mathrm{Re}_f + 1.0553 \tag{3.5}$$

$$R_{LS} = -1.8866\cos(\Lambda_{t\max})^3 + 3.3674\cos(\Lambda_{t\max})^2 - 1.2224\cos(\Lambda_{t\max}) + .8136 \tag{3.6}$$

c_{fx} is the turbulent friction coefficient on a given part of the aircraft and is defined by Equation 3.7,

$$c_{f.t} = \frac{.455}{(\log(\mathrm{Re}_t))^{2.58}\left[1+.0144M^2\right]^{0.65}} \tag{3.7}$$

and t/c is the thickness-to-chord ratio for either the wing or the tail, S_x is the area of the a part of the aircraft and l_f and d_f are the length and diameter of the fuselage respectively. The sum of the zero lift drag for the three separate parts is the total zero lift drag for the entire aircraft. Along with the drag, the lift coefficient of the aircraft was a very important factor to consider. Using Equation 3.8 (Anderson, 1999) to determine the lift coefficient, an excel spread sheet was created to predict the velocities necessary to fly at certain altitudes.

$$C_L = \frac{W}{qS_w} \tag{3.8}$$

For this project steady, level flight was the assumption made for determining flight performance. For steady, level flight the lift is equal to the weight of the aircraft. This is reflected in Equation 3.8. For our design, we know the lift coefficient, there for we can determine the velocity needed to attain steady, level flight at differing conditions. The excel spreadsheet that was created shows these calculations. A sample table from the spreadsheet reveals a major problem with this research. Table 2 shows the flight velocity needed for steady level flight increases drastically with increasing altitude. The full spreadsheet can be found in Appendix 1. For flight at a higher altitude, the velocity required increases due to the lowering density. Table 3 shows the velocities required to achieve steady level flight at near space altitudes. The cells shaded green in the following tables indicate parameters that will produce the amount of lift needed to successfully fly, while the cells shaded red indicated insufficient parameters.

	α	0	1	2	3	4	5	6	7
	C_l	0.446	0.561	0.679	0.795	0.912	1.032	1.137	1.242
V(mph)	V(ft/s)	Lift(lb)	Lift(lb)	Lift(lb)	Lift(lb)	Lift(lb)	Lift(lb)	Lift(lb)	Lift(lb)
30	44.00	13.60	17.11	20.70	24.24	27.81	31.47	34.67	37.87
35	51.33	18.51	23.28	28.18	32.99	37.85	42.83	47.19	51.54
40	58.67	24.18	30.41	36.81	43.09	49.44	55.94	61.63	67.32
45	66.00	30.60	38.49	46.58	54.54	62.57	70.80	78.00	85.21
50	73.33	37.77	47.51	57.51	67.33	77.24	87.41	96.30	105.19
55	80.67	45.71	57.49	69.59	81.47	93.46	105.76	116.52	127.28
60	88.00	54.39	68.42	82.81	96.96	111.23	125.86	138.67	151.48
65	95.33	63.84	80.30	97.19	113.79	130.54	147.72	162.75	177.77

Table 2. Lift generated at an altitude of 500ft.

	α	0	1	2	3	4	5	6	7
	C_l	0.418	0.526	0.633	0.739	0.844	0.941	0.972	1.039
V(mph)	V(ft/s)	Lift(lb)	Lift(lb)	Lift(lb)	Lift(lb)	Lift(lb)	Lift(lb)	Lift(lb)	Lift(lb)
30	44.00	0.18	0.23	0.27	0.32	0.36	0.40	0.42	0.45
35	51.33	0.24	0.31	0.37	0.43	0.49	0.55	0.57	0.61
---	---	---	---	---	---	---	---	---	---
365	535.33	26.57	33.44	40.24	46.98	53.65	59.82	61.79	66.05
370	542.67	27.31	34.36	41.35	48.27	55.13	61.47	63.49	67.87
375	550.00	28.05	35.29	42.47	49.59	56.63	63.14	65.22	69.72
380	557.33	28.80	36.24	43.61	50.92	58.15	64.84	66.97	71.59
385	564.67	29.56	37.20	44.77	52.27	59.69	66.55	68.75	73.49
390	572.00	30.34	38.17	45.94	53.63	61.25	68.29	70.54	75.41
395	579.33	31.12	39.16	47.13	55.02	62.83	70.06	72.36	77.35
400	586.67	31.91	40.16	48.33	56.42	64.44	71.84	74.21	79.32
405	594.00	32.72	41.17	49.54	57.84	66.06	73.65	76.07	81.32
410	601.33	33.53	42.19	50.77	59.28	67.70	75.48	77.96	83.34

Table 3. Lift generated at 100,000 ft.

As seen in Table 2, at low altitudes, a glider could easily posses the capabilities to fly steady and level at a zero angle of attack due to the relatively low velocities around 50 miles per hour. However, in near space, as seen in Table 3, the velocity at which the glider must fly to

maintain steady level flight at zero or a very low angle of attack, between 350 and 400 miles per hour, would be impossible for this project. Due to the extreme conditions the aircraft would have to operate in and the extreme performance capabilities the aircraft would have to possess, it was not feasible for a glider to fulfill the high altitude and long endurance problem. Other possibilities are available to achieve high altitude, long endurance flight. Lighter than air, along with hybrid airships that get a portion of their lift from a buoyant gas and the remainder from lifting surface technology, were considered. However, seeing the extreme velocities the glider would be required to fly at for extended periods of time, the research migrated toward a more feasible lighter than air approach with long endurance capabilities. There has been much research on lighter than air vehicles and the potential use in near space, however the same challenges arise in many of others research. The power needed to fly in near space for extended periods is very difficult. Instead of taking the approach of discovering newer regenerative power sources, the research shifted to modifying the design of the airship to decrease the drag, thus decreasing the overall power needed to station keep in near space. With this decrease in power required for station keeping, it was hypothesized that the feasibility of station keeping would be greater.

CHAPTER 4

MODEL AND VEHICLE DESIGN

4.1 Environmental Model

To create a model for the airship, and environmental model needed to be derived in order to accurately and efficiently determine atmospheric conditions for the airship model. With these equations derived and programmed into MathCAD, the drag and power models could be efficiently calculated.

4.1.1 Wind Model

The data used for the wind model was obtained from radiosonde soundings collected by the National Oceanic and Atmospheric Administration during the year 2004(Real Time Archive, 2004). The two locations considered for the modeling, Akron, OH and White Sands, NM, were chosen because of their differences in latitudes and weather patterns, and it is thought these two will be the most likely areas for lighter than air testing due to their previous involvement with LTA testing as well as facilities on site (Schmidt, 2007). The closest radiosonde launch sites to the locations of interest were the Pittsburgh National Weather Service weather station for Akron, and the Santa Teresa National Weather Service weather station for White Sands. Modeling the atmospheric wind profile from ground level into near space is very challenging. A Normal distribution or Gaussian distribution is typically used for statistically analyzing experimental data, however with wind data it has been seen that a Weibull or Rayleigh statistical distribution presents a very realistic representation of the wind distribution over longer periods of time (Manwell, 2009). A main reason for using a Weibull or Rayleigh distribution is that there is a

physical wind velocity minimum of 0 meters per second that a Normal or Gaussian distribution does not account for. This study assumes the Weibull distribution will be a good approximation for the data observations. The Weibull probability function is defined by Equation 4.1 (Manwell, 2009)

$$P(U) = \left(\frac{k}{c}\right)\left(\frac{U}{c}\right)^{k-1} \exp\left[-\left(\frac{U}{c}\right)^{k}\right] \tag{4.1}$$

with the cumulative distribution function being defined by Equation 4.2.

$$F(U) = 1 - \exp\left[-\left(\frac{U}{c}\right)^{k}\right] \tag{4.2}$$

The shape factor, k, and the scale factor, c are given by Equations 4.3 and 4.4 respectively (Manwell, 2009).

$$k = \left(\frac{\sigma_U}{\overline{U}}\right)^{-1.086} \tag{4.3}$$

$$c = \frac{\overline{U}}{\Gamma\left(1 + \frac{1}{k}\right)} \tag{4.4}$$

With the ability to determine the Weibull parameters from the observed data, the cumulative distribution function can be used to determine the estimated 99th and 1st percentile winds, $U_{99\%}$ and $U_{1\%}$ respectively, for a given altitude. Equations 4.5 and 4.6 show how $U_{99\%}$ and $U_{1\%}$ are found.

$$U_{99\%} = \left(-\left(c^{k}\right)\ln(.01)\right)^{1/k} \tag{4.5}$$

$$U_{99\%} = \left(-\left(c^k\right)\ln(.99)\right)^{1/k} \quad 4.6$$

$U_{99\%}$ means that 99% of the winds experienced will be less than this velocity, and the same for $U_{1\%}$, 1% of the winds experienced will be less than this velocity. For this study, the 99th and 1st percentile velocities, per altitude, for each month were averaged together. These two values create a range of wind velocities that one could potentially encounter at altitude. Table 4 and Figure 5 show these values and plots of the data obtained by solving for equations 4.5 and 4.6 for the region over Akron, OH,

Altitude (km AGL)	$\overline{U}$ **(knots)**	$U_{99\%}$ **(knots)**	$U_{1\%}$ **(knots)**
0	5.42	15.29	0.41
1	16.87	41.10	2.02
2	19.06	50.63	1.78
4	28.31	60.34	5.95
6	39.82	77.86	9.01
8	49.21	111.26	9.54
10	57.67	118.07	13.24
12	66.42	127.78	16.04
14	55.72	97.30	16.54
16	36.91	62.82	12.25
18	29.29	53.09	8.84
20	20.51	38.78	5.17
22	18.89	35.81	4.94
24	16.78	39.37	2.39
26	21.41	44.66	4.56

Table 4. Velocities obtained from Weibull distribution for Akron, OH.

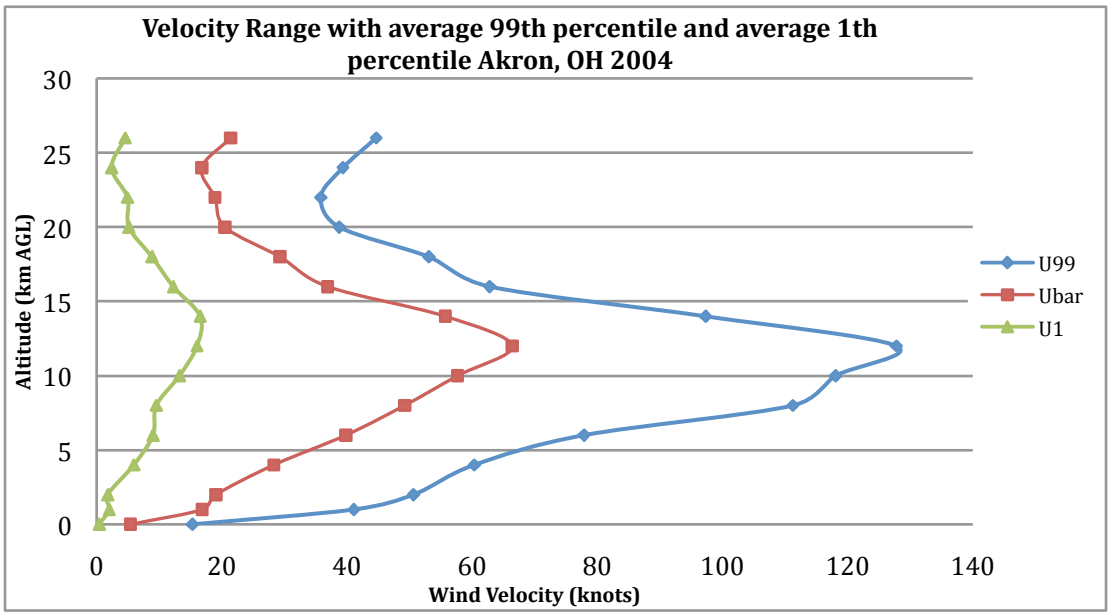

Figure 5. Wind profile for airspace above Akron, OH.

The data points for the 99th and 1st percentile velocities were then taken and a curve fit applied to obtain equations to model these velocities through the atmosphere. Equations 4.7 through 4.11 were used to determine the 99th and 1st percentile velocities in the given regions over Akron, OH, and are shown with its respective R^2 value,

$\underline{0km \le z < 6km}$

$$U_{99\%} = 0.79623226z^3 - 8.30063464z^2 + 31.51053206z + 15.72373244 \quad 4.7$$

$$R^2 = 0.99819073$$

$\underline{6km \le z < 16km}$

$$U_{99\%} = 0.03953700z^5 - 2.16584021z^4 + 46.16431211z^3 - 479.67673276z^2 + 2437.97717466z - 4753.63837232 \quad 4.8$$

$$R^2 = 1.00000000$$

$\underline{16km \le z < 26km}$

$$U_{99\%} = -0.02698388z^4 + 2.28655879z^3 - 71.26706811z^2 + 965.36077448z - 4735.83256639 \quad 4.9$$

$$R^2 = 0.99679672$$

While the following equations are used to model the 1st percentile curve,

$$\underline{0km \le z < 10km}$$

$$U_{1\%} = 0.00339807z^5 - 0.07437353z^4 + 0.52736950z^3 - 1.29904286z^2 + 1.91955613z + 0.51781450 \quad 4.10$$

$$R^2 = 0.99544961$$

$$\underline{10km \le z < 26km}$$

$$U_{1\%} = 0.00010253z^6 - 0.01102002z^5 + 0.48255658z^4 - 10.98302847z^3 + 136.52163886z^2 - 876.36218688z + 2281.63196219 \quad 4.11$$

$$R^2 = 0.99500328$$

This same methodology was used to model the atmosphere over White Sands, NM. Table 5 and Figure 6 show the values and plots for equations 4.5 and 4.6 for White Sands, NM.

Altitude (km AGL)	$\bar{U}$ (knots)	$U_{99\%}$ (knots)	$U_{1\%}$ (knots)
0	7.33	20.47	0.62
2	12.28	35.01	0.83
4	20.58	44.79	3.86
6	26.75	63.69	3.54
8	34.48	82.83	5.00
10	49.03	109.56	9.01
12	52.39	113.63	9.71
14	46.34	89.55	11.22
16	31.83	58.09	9.15
18	20.05	38.03	5.84
20	16.70	30.01	5.14
22	17.53	29.27	6.64
24	20.66	36.68	7.36
26	24.49	41.69	9.13

Table 5. Velocities obtained from Weibull distribution for White Sands, NM.

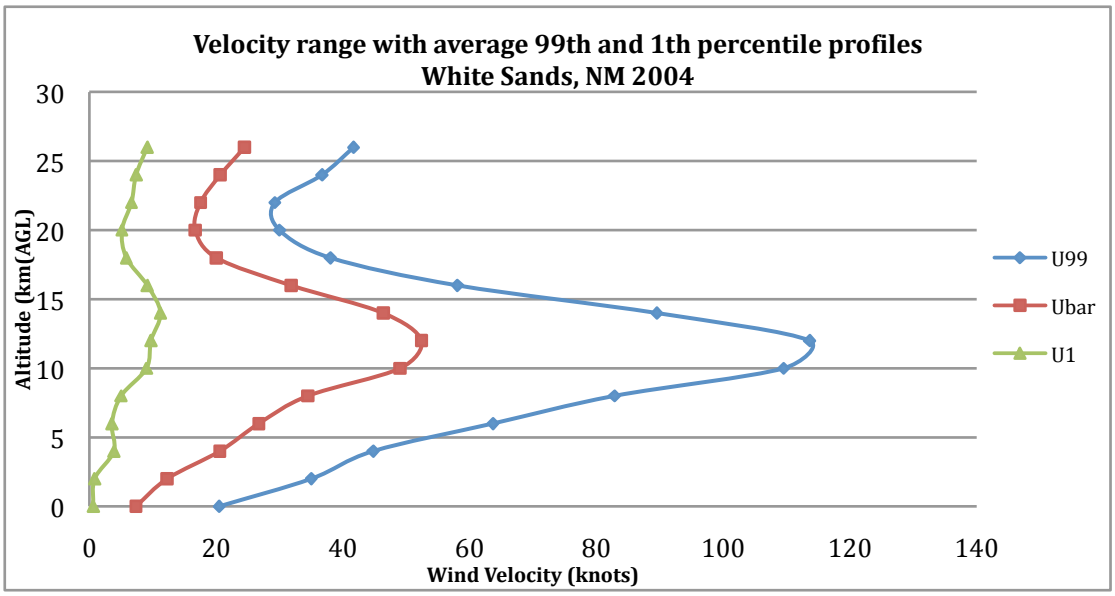

Figure 6. Wind profile for airspace above White Sands, NM.

A similar curve fitting analysis was used for the 99th and 1st percentile velocities as before. The following Equations 4.12 through 4.16 were used to model the wind profile above White Sands,

$\underline{0km \le z < 10km}$

$$U_{99\%} = 0.04057435z^3 - 0.16932701z^2 + 6.51338238z + 20.85908683 \qquad 4.12$$

$$R^2 = 0.99860314$$

$\underline{10km \le z < 26km}$

$$U_{99\%} = 0.00081275z^5 - 0.08897265z^4 + 3.77165072z^3 - 76.50348123z^2 + 729.54655527z - 2498.80996659 \qquad 4.13$$

$$R^2 = 0.99959379$$

$\underline{0km \le z < 4km}$

$$U_{1\%} = 0.35368099z^2 - 0.60463183z + 0.62377315 \qquad 4.14$$

$$R^2 = 1.00000000$$

$\underline{4km \le z < 14km}$

$$U_{1\%} = 0.00431715z^5 - 0.18992131z^4 + 3.17516732z^3 - 24.99080022z^2 + 92.61955937z - 125.77291277 \qquad 4.15$$

$$R^2 = 1.00000000$$

$\underline{14km \le z < 26km}$

$$U_{1\%} = 0.00117923z^5 - 0.12058143z^4 + 4.87068438z^3 - 96.95241205z^2 + 948.91263093z - 3638.01601144 \quad 4.16$$

$$R^2 = 0.99872502$$

4.1.2 Buoyancy Model

For this research, humidity was taken into account to more accurately reflect the atmospheric conditions needed to estimate the potential buoyancy of the LTA vehicle. The humidity ratio, or mixing ratio, was modeled using data retrieved from the U.S. Standard Atmosphere (US Standard Atmosphere, 2007). Data from sea level up to 80 km is shown in Table 6, and Figure 7 shows the plot of the data.

Altitude (km ASL)	**Mixing Ratio x 10^{-6}**	**Altitude (km ASL)**	**Mixing Ratio x 10^{-6}**
0	4686	26	18.6
1	3700	28	18.2
2	2843	30	17.6
4	1268	32	16.8
6	554	35	15.4
8	216	40	12.2
10	43.2	45	11.1
12	11.3	50	7.6
14	3.3	55	4.9
16	3.3	60	3.8
18	3.3	65	2.3
20	4.5	70	1.4
22	7.2	75	1.1
23	11.6	80	0.6

Table 6. U.S. Standard atmosphere mixing ratio at altitude.

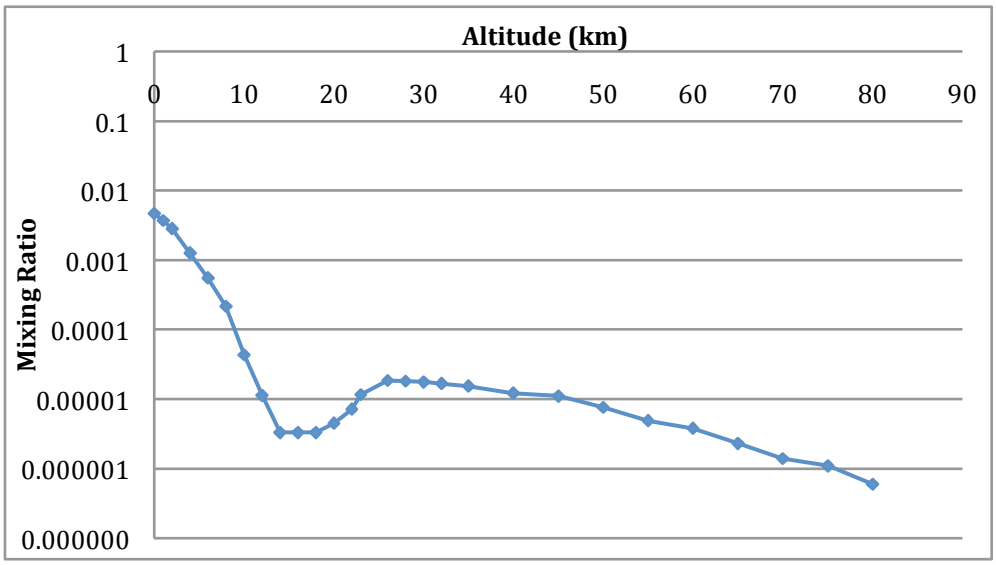

Figure 7. Plot of mixing ratio as a function of altitude.

The above data points were taken and a curve fit applied to obtain a model of the mixing ratio as a function of altitude. Equations 4.17 through 4.20 show the model for the mixing ratio, ω, and the corresponding R^2 value.

$0km \le z < 14km$

$$\log_{10}\omega = (-4.42789307x10^{-5}z^3 + 5.47755593x10^{-4}z^2 + 1.87339520x10^{-2}z - 0.429937881)^{-1} \quad 4.17$$

$$R^2 = 0.999178881$$

$14km \le z < 18km$

$$\omega = 3.30x10^{-6} \quad 4.18$$

$18km \le z < 26km$

$$\log_{10}\omega = (1.15470078x10^{-4}z^3 - 7.68205923x10^{-3}z^2 + 0.164889174z - 1.33503278)^{-1} \quad 4.19$$

$$R^2 = 0.991858085$$

$26km \le z < 80km$

$$\log_{10}\omega = (-2.69713488x10^{-7}z^3 + 5.04990009x10^{-5}z^2 - 1.95739140x10^{-3}z - 0.189770892)^{-1} \quad 4.20$$

$$R^2 = 0.997633441$$

The mixing ratio allows for a more accurate prediction of the density. When determining the moist air density, a few assumptions must be made: 1) Dry air and water vapor both behave as an ideal gas, 2) Both dry air and water vapor have the same temperature and occupy the same volume. By assumption 2, Dalton's Law (Moran, 2004) becomes valid, therefore the total atmospheric pressure can be assumed to be the sum of the partial pressures of dry air and water vapor. Using the definition of the mixing ratio, shown in Equation 4.21 (Ahrens, 2007),

$$\omega = \frac{M_w}{M_a} \tag{4.21}$$

the specific volume of moist air can be determined by Equation 4.22.

$$\nu = \frac{\nu_a}{1+\omega} \tag{4.22}$$

To find the moist air density at altitude, the pressure and temperature needed to be modeled. The US Standard Atmosphere data (1976) was used for these models. The standard atmosphere can be mathematically defined in six layers from sea level to 71 km. Equations 4.23 through 4.34 were used to model the 1976 Standard Atmosphere and are given below (US Standard Atmosphere, 1976).

$\underline{0km \le z < 11km}$

$$P = P_o\left(1 - \frac{z}{44.329km}\right)^{5.255876} \tag{4.23}$$

$$T = T_o\left(1 - \frac{z}{44.329km}\right) \tag{4.24}$$

$\underline{11km \le z < 20km}$

$$P = P_o(0.223361)e^{((10.999km - z)/16.3414km)} \tag{4.25}$$

$$T = T_o(0.751865) \tag{4.26}$$

$20km \le z < 32km$

$$P = P_o\left(0.988626 + \frac{z}{198.903km}\right)^{-34.16319} \quad 4.27$$

$$T = T_o\left(0.682457 + \frac{z}{288.136km}\right) \quad 4.28$$

$32km \le z < 47km$

$$P = P_o\left(0.808309 + \frac{z}{55.280km}\right)^{-12.20114} \quad 4.29$$

$$T = T_o\left(0.482561 + \frac{z}{102.906km}\right) \quad 4.30$$

$47km \le z < 51km$

$$P = P_o(0.00109456)e^{((46.998km - z)/7.922km)} \quad 4.31$$

$$T = T_o(0.939268) \quad 4.32$$

$51km \le z < 71km$

$$P = P_o\left(0.838263 - \frac{z}{176.142km}\right)^{12.20114} \quad 4.33$$

$$T = T_o\left(1.434843 - \frac{z}{102.906km}\right) \quad 4.34$$

P_o and T_o represent the standard air pressure and temperature at sea level. By using these equations, Equation 4.35 shows that by using the Ideal Gas Law for dry air and water vapor then combining the two and simplifying, the specific volume of dry air, ν_a, becomes

$$\nu_a = \left(1 + \frac{\omega R_w}{R_a}\right)\frac{TR_a}{P} \quad 4.35$$

Therefore the moist air density can now be shown by Equation 4.36.

$$\rho_a = \frac{(1+\omega)P}{\left(1+\frac{\omega R_w}{R_a}\right)R_a T} \tag{4.36}$$

With these equations and models used in a spreadsheet format, a working model of the atmosphere was created so a user can input an altitude and the standard environment at that altitude would be calculated. This model was the basis for the following drag and power models used to characterize the potential of an airship in the atmosphere.

4.2 Basic Blimp Model

The baseline blimp used for this project was a typical blimp shaped airship. The basic blimp was purchased from Southern BalloonWorks as a remote control kit. Dimensions of the basic blimp were taken using photos of the blimp and known distances to translate the curvature of the blimp into an electronic 3-Dimensional representation of itself. SolidWorks was used to create the blimp model to use for CFD analysis.

4.2.1 Dimensions

The blimps dimensions are shown in Table 7 and are as advertised for the blimp. The blimp has four fins used for stability with cables running between each fin to keep then rigid.

Length	13 ft.
Diameter	6 ft.
Volume	160 ft^3
# fins	4
Material	Polyurethane

Table 7. Basic Blimp dimensions.

Figure 8 is the SolidWorks drawing of the Basic Blimp used for modeling. The fins are oriented in a vertical cross style.

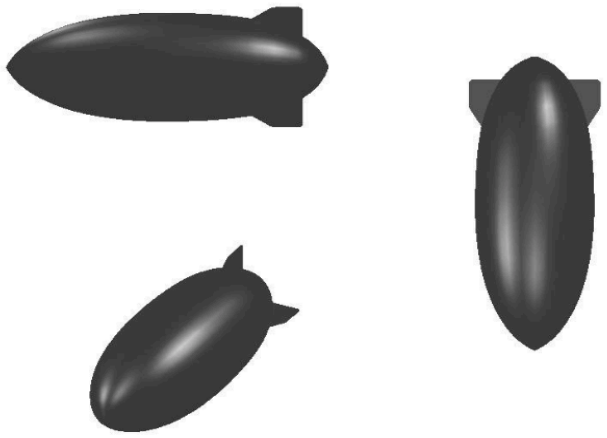

Figure 8. SolidWorks drawing of Basic Blimp.

The blimp used was a remote controlled blimp, but for this research none of the external motors or parts were used except the stabilizing fins.

4.2.2 Aerodynamic Analysis

The aerodynamic characteristics of the blimp can be found using basic principles of aerodynamics. Because a blimp does not have any wings to generate lift, all of the lift to fly is generated by a lifting gas, in this case helium. The lift generated by the helium will change with changing altitude due to the change in density of the surrounding atmosphere. As seen in Equation 4.37, as the air density decreases with altitude, the overall lift generated will decrease.

$$L_{LG} = g * vol(\rho_a - \rho_{LG}) \tag{4.37}$$

The density of the lifting gas can be is shown in Equation 4.38, and was found using the Ideal Gas Law while assuming constant a temperature between the two gases.

$$\rho_{LG} = \frac{\rho_a * R_a}{R_{LG}} \tag{4.38}$$

The drag of the airship was found using the volume of the given envelope and Equation 4.39,

$$D = \frac{1}{2}\rho_a V_\infty^2 C_{DV} Vol^{2/3} \tag{4.39}$$

where C_{DV} is the volumetric drag coefficient (Hoerner, 1958) and is shown in Equation 4.40.

$$C_{DV} = C_F\left[4\left(\frac{l}{d}\right)^{1/3} + 6\left(\frac{d}{l}\right)^{1.2} + 24\left(\frac{d}{l}\right)^{2.7}\right] \tag{4.40}$$

C_f represents the skin friction coefficient and was estimated using the flat plate theory. The equations for skin friction for a laminar and turbulent boundary layer (Nunn, 1989) are seen in Equations 4.41 and 4.42, respectively.

$$C_{fl} = \frac{1.328}{\sqrt{\mathrm{Re}_L}} \tag{4.41}$$

$$C_{ft} = \frac{0.072}{\sqrt[5]{\mathrm{Re}_L}} \tag{4.42}$$

For the case where the boundary layer transitions from laminar to turbulent at some length "x", Equation 4.43 shows that the combination friction coefficient can be found by understanding that the total drag with combination boundary layer is the drag from a totally turbulent boundary layer minus the turbulent drag to the transition point, then added to the laminar drag to the transition point.

$$D_c = D_{tt} - D_{tx} + D_{lx} \tag{4.43}$$

With the average skin fiction coefficient being defined by Equation 4.44,

$$C_f = \frac{F_s}{.5A\rho V_\infty^2} \tag{4.44}$$

the combination boundary layer friction coefficient can be proved to be Equation 4.45,

$$C_{fc} = \frac{0.072}{\sqrt[5]{\mathrm{Re}_L}} + \frac{\mathrm{Re}_{cr}}{\mathrm{Re}_L}\left[\frac{1.328}{\sqrt{\mathrm{Re}_{cr}}} - \frac{0.072}{\sqrt[5]{\mathrm{Re}_L}}\right] \tag{4.45}$$

where Re_{cr} is the Reynolds number at the transition point.

Using the method, previously shown (Hoerner, 1958) Figure 9 shows the drag coefficient for the basic blimp as a function of altitude, for the two different geo-locations studied.

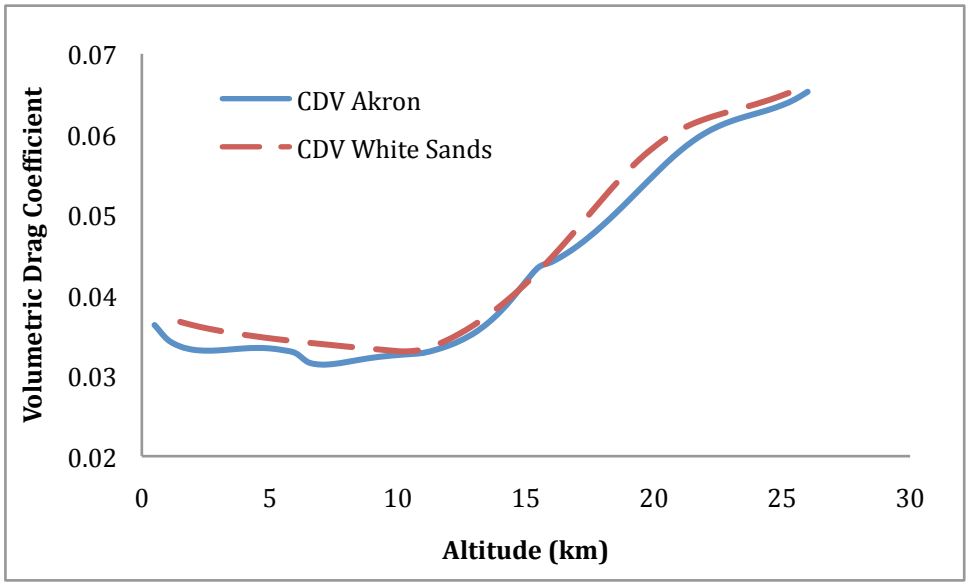

Figure 9. Volumetric Drag coefficient vs. altitude for Basic Blimp.

Due to the change in altitude, velocity, density and viscosity change as well which affects all aspects of flight including drag coefficient and power required for station keeping ability change as well.

Using this method, MathCAD was used to write a program that would calculate the theoretical drag acting on the blimp. The program allows a user to input basic data about the airship including length, width and volume, as well as the altitude the user wishes the data to be

computed for. Using all previously explained equations, the program will output all relevant data needed for further analysis including, wind velocities, pressure, temperature, density at the stated altitude. The aerodynamic data for the aircraft including Reynolds number, volumetric drag coefficient (CDV) and overall drag on the airship is also computed. The MathCAD model for the basic blimp can be found in Appendix 3. A CFD model was also created to estimate the drag requirements on the blimp.

For the CFD analysis, a mesh refinement analysis was performed to ensure accuracy of the CFD results. Basic conditions were used for the mesh refinement. The refinement was conducted at one atmosphere and at room temperature, with a free-stream velocity of 10 miles per hour. For the analysis, the mesh was continually refined until the change in calculated value, in this case drag, did not change. The refinement process was enacted close to the body where the flow would be most affected by the presence of the blimp. Table 8 shows the number of cells used for each calculation, the drag calculated for each run and the percent change in each consecutive run and Figure 10 shows the convergence of the data.

# cells	Avg. Force (lbf)	% change
63304	0.32479601	
92809	0.30072552	-8.0041391
168283	0.2681469	-12.14954
311671	0.26556131	-0.9736341

Table 8. Mesh refinement data for Basic Blimp.

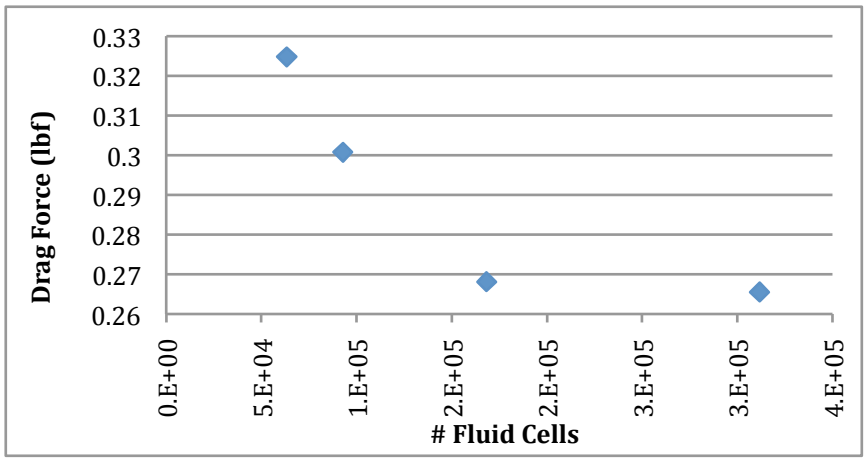

Figure 10. Mesh refinement convergence for Basic Blimp.

After the grid independence study, the theoretical values and the CFD results were compared to check for consistency. Table 9 shows a comparison between the theoretical values for drag obtained using the previously introduced equations from Hoerner (Hoerner, 1958) with the drag results obtained from the CFD model for both geo-locations, at multiple altitudes and at the 99th percentile velocity.

Location	CFD Drag at GL (N)	CFD Drag at 18.9 km (N)	CFD Drag at 20 km (N)	Theoretical Drag at GL (N)	Theoretical Drag at 18.9 km (N)	Theoretical Drag at 20 km (N)
Akron	9.706	3.453	2.724	10.697	4.167	2.745
White Sands	11.095	2.216	1.603	12.030	2.205	1.577

Table 9. Drag analysis results and comparison for Basic Blimp.

For the basic airship shape, Table 9 shows that the results from theoretical calculations and the results obtained from CFD modeling very closely resemble each other. This verifies the ability of the CFD model to accurately represent the drag obtained from theoretical equations. From the CFD model, velocity plots of the flow around the basic airship can be shown. Figure 11 shows a

side view of the basic blimp, and the change in the air velocity around it at the maximum wind velocity found at ground level in Akron, OH. The red color indicates a flow in the opposite direction than the oncoming flow.

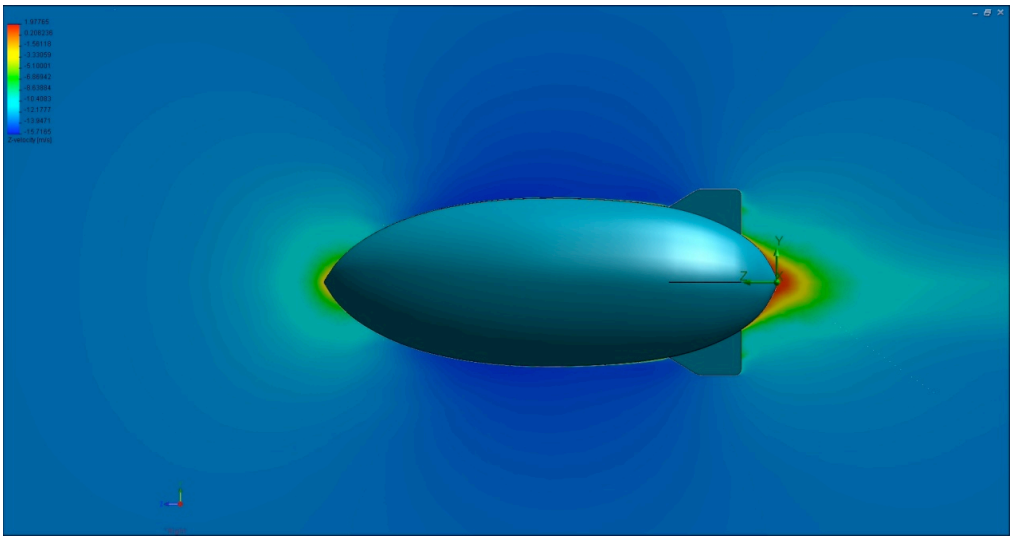

Figure 11. Velocity plot of Basic Blimp at ground level for Akron, OH.

The separation at the back of the blimp can clearly be seen in Figure 11 by the red color. Figure 12 shows a close up of the region of separation along with velocity vectors indicating the rotation of the flow in the wake of the blimp.

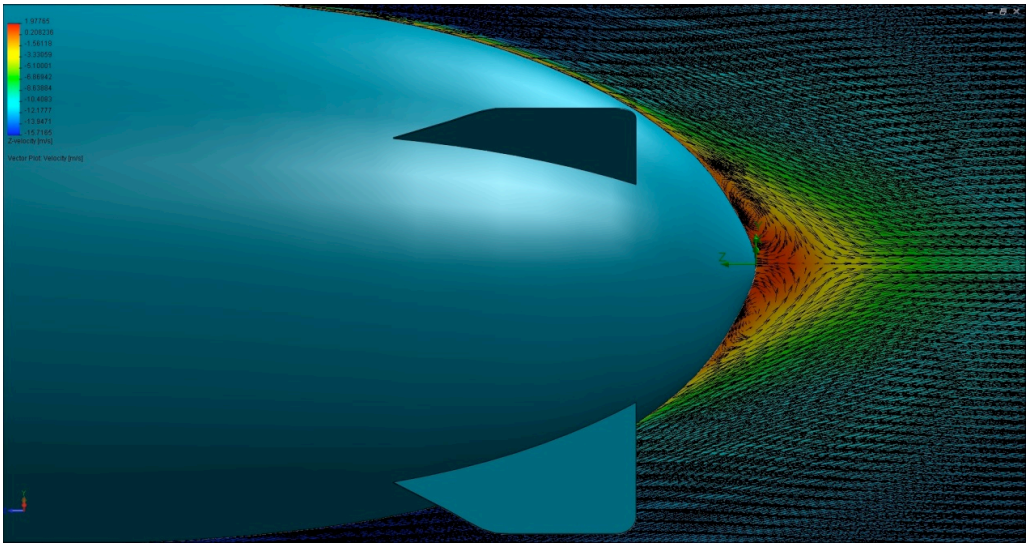

Figure 12. Velocity plot of separation region for Basic Blimp at ground level for Akron, OH.

In Figure 12, the location of the flow separation can be clearly seen as well as the growing boundary layer up to that point. From these figures it is seen that the flow stays attached to the blimp across most of the surface.

4.2.3 Basic Blimp Power Model

The total power required by the blimp can be considered to be the sum of the power required from key components including aerodynamic power, and the power required by the onboard electronics. This research deals only on the power needed for flight therefore the power needed for any onboard electronics will not be considered. The aerodynamic power required for steady level flight, that is the minimum amount of power needed to keep forward motion, is shown in Equation 4.46.

$$P_R = T_R * V_\infty \tag{4.46}$$

For this research, the focus is on the station keeping ability; therefore the power required for steady level flight will become the power required for station keeping performance. Thus the power required for station keeping can be assumed by Equation 4.47 (Dorrington 2006).

$$P_R = \frac{1}{2}\rho_a V_\infty^3 C_{DV} Vol^{2/3} \tag{4.47}$$

Using Equation 4.47, the environmental model previously derived and the 99% wind velocity for each geo-location, the power required for station keeping can be plotted against altitude. Figure 13 and Figure 14 show the relationship between the power required for station keeping and the altitude for Akron, Ohio and White Sands, NM respectively.

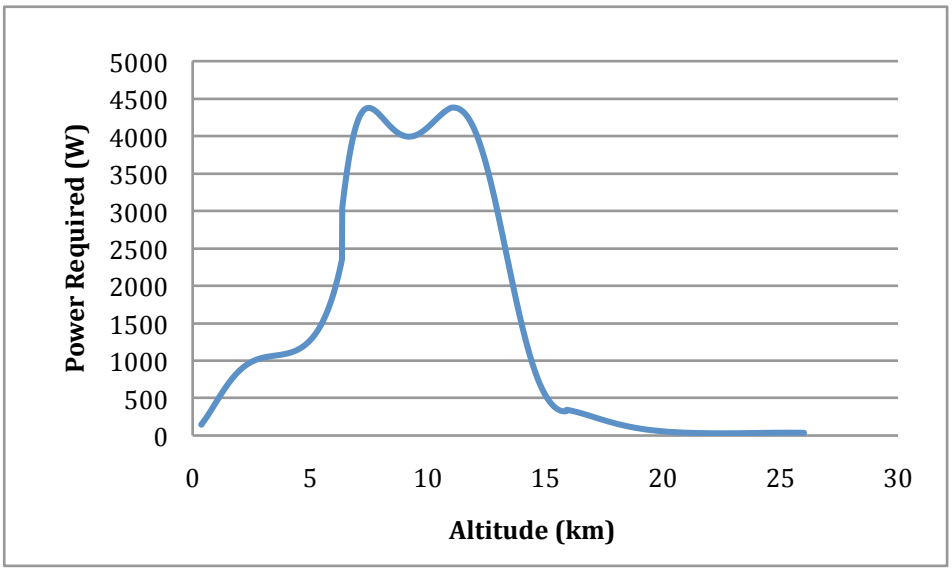

Figure 13. Power required vs. altitude for Basic Blimp over Akron, OH.

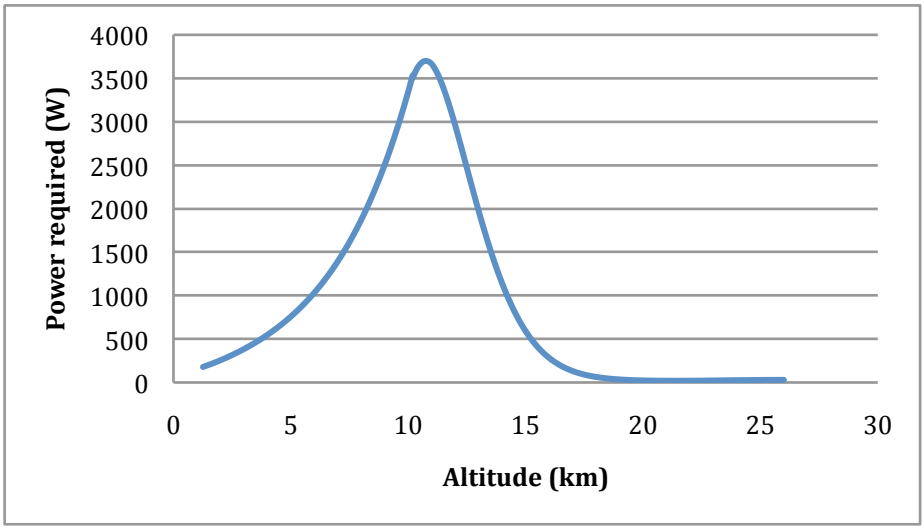

Figure 14. Power required vs. altitude for Basic Blimp over White Sands, NM.

As shown in the figures, a power maximum occurs over both geo-locations at around 10 km, at which point the power begins to decrease drastically. Table 10 shows the comparison of power required, using equation 4.35, between the theoretical values and the CFD values. The correlation between the drag values in Table 9 will be the same as the correlation between the power required values.

Location	CFD Power at GL (W)	CFD Power at 18.9 km (W)	CFD Power at 20 km (W)	Theoretical Power at GL (W)	Theoretical Power at 18.9 km (W)	Theoretical Power at 20 km (W)
Akron	129.533	82.129	55.511	142.750	99.106	55.931
White Sands	164.596	37.004	24.006	178.468	38.8264	23.620

Table 10. Power analysis and comparison for Basic Blimp.

The power required for station keeping performance is shown to have the same relation to that of the drag on the basic blimp as previously discussed. The power required for the computational result was determined by Equation 4.46 because the CFD analysis only resulted in a calculated drag value. The power required value for the theoretical results were computed using Equation 4.47. The relationship between the computational results and the theoretical results reveals a close resemblance between the two as expected.

4.2.4 Stability / Control

Stability and control was not a focus of this research, therefore a very brief view of the stability and control was conducted. The assumption was made that the remote control blimp that was purchased was already stable. Therefore the pitching and yawing moments were calculated and used to verify stability in the modified blimp. The pitching and yawing moments were calculated by Equations 4.48 and 4.49 respectively.

$$M_{BB} = F(CB_{blmp} - CP_{tail}) \quad 4.48$$

$$N_{BB} = F(CB_{blmp} - CP_{tail}) \quad 4.49$$

CB_{blmp} and CP_{tail} are the distances from the aft most point of the blimp to the location of the blimps center and buoyancy and the tails center of pressure, which for a flat plate it was assumed

was at the quarter chord location. For these equations, F represents the force acting on the tail and is found by equation 4.50.

$$F = \frac{1}{2}\rho V^2 C_D A_t \qquad 4.50$$

The value for C_d is the standard value for the drag coefficient for a flat plate at an angle of attack of 20 degrees, with A_t being the area of the tail. Because the basic blimp is symmetric about the longitudinal axis, the pitching and yawing moments are equal. For this study, only the pitching and yawing moments are considered for basic stability. Table 11 shows the values for determining the monents for the Basic Blimp.

	Tail Length (m)	Tail Area (m^2)	Tail Force (N)	Moment (N-m)
Basic Blimp	1.003	0.972	1869.577	1874.399

Table 11. Calculated moment for the Basic Blimp.

4.3 Modified Blimp Model

After analysis was done on the basic blimp, a modified blimp was designed in order to attempt to improve the drag and power required at near space altitudes. The design of the modified blimp was influenced by evolutions of nature. The long tail was added for the ability to increase stability and was thought to contribute to drag reduction much in the same way a bird's tail contributes to its reduction of drag. Tests were performed by Maybury and Rayner (2001) and have shown the tail of a bird decreases the drag of a bird. The tail acts as a splitter plate between the flow on top and below the bird and therefore decrease the wake height, as seen in Figure 15.

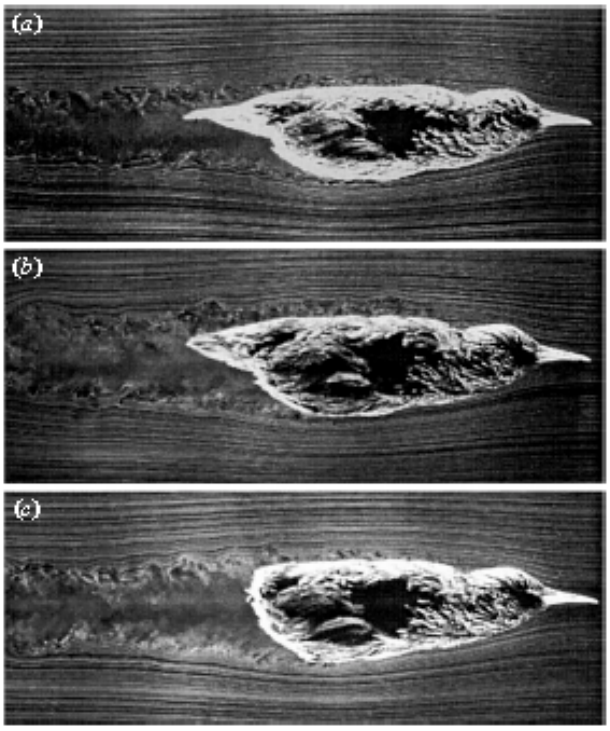

Figure 15. Visualization of the reduction in wake height due to presence of tail. a). Full tail, b). Tail wedge only, c). No tail (Maybury and Rayner, 2001).

4.3.1 Modified Blimp Dimensions

The modified blimp's basic dimensions are shown in Table 12. The major modification was the addition of a long tail to the basic blimp and can be seen in Figure 16, which is the SolidWorks drawing of the Modified Blimp used for modeling. The length of the tail was determined from references by approximate drawings of the early ancestors of avian flight.

Length	21.33 ft.
Diameter	6 ft.
Volume	169.15 ft^3
# fins	4

Table 12. Modified Blimp dimensions.

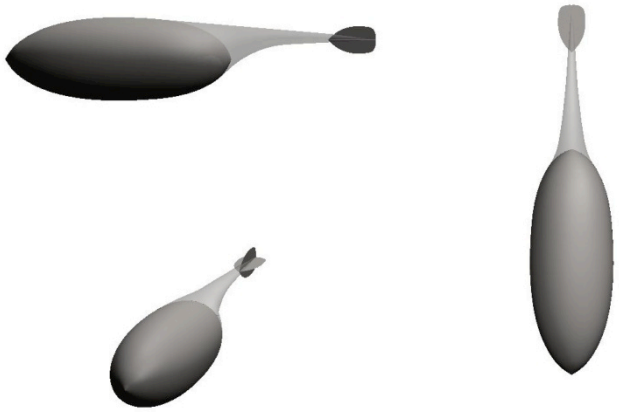

Figure 16. SolidWorks drawing of Modified Blimp.

4.3.2 Modified Blimp Aerodynamic Analysis

The aerodynamic characteristics of the modified blimp can be found using the same basic principles of aerodynamics that were utilized for analyzing the basic blimp using Equations 4.37 through 4.45. By repeating the method previously shown using equations from Hoerner (1958) for the modified blimp, the drag coefficients were found as functions of altitude for the two geo-locations and are shown in Figure 17.

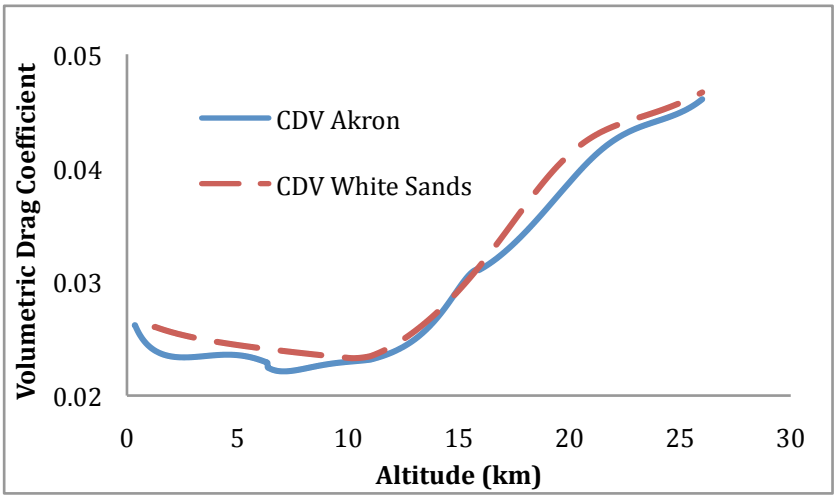

Figure 17. Drag coefficient vs. altitude for Modified Blimp.

As with the basic blimp, a MathCAD was used to write a program that would calculate the theoretical drag acting on the blimp. A CFD model was also created to estimate the drag requirements on the blimp.

To ensure accuracy, a mesh analysis was performed on the CFD model of the modified blimp. The refinement was conducted at the same conditions of one atmosphere and at room temperature, with a free-stream velocity of 10 miles per hour as the basic blimp mesh analysis. For the analysis, the mesh was continually refined until the change in calculated value, in this case drag, had a negligible change. The refinement process was enacted close to the body where the flow would be most affected by the presence of the blimp. Table 13 shows the number of cells used for each calculation, the drag calculated for each run and the percent change in each consecutive run and Figure 18 shows the convergence of the data.

# cells	Avg. Force (N)	% change
19943	0.911225	-----
33719	0..703586	-29.5115
82600	0.618999	-13.665
282583	0.624104	0.817869

Table 13. Mesh refinement data for Basic Blimp.

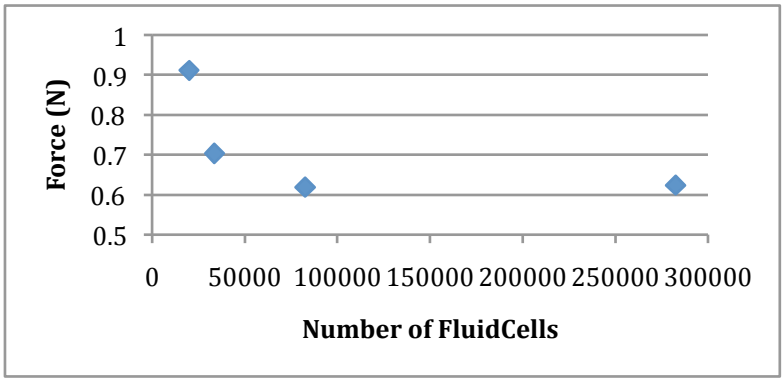

Figure 18. Mesh refinement convergence for Basic Blimp.

After the grid independence analysis, the theoretical values and the CFD results were compared. Table 14 shows a comparison between the theoretical values for drag with the drag results obtained from the CFD model for both geo-locations, multiple altitudes and at the 99th percentile velocity.

Location	CFD Drag at GL (N)	CFD Drag at 18.9 km (N)	CFD Drag at 20 km (N)	Theoretical Drag at GL (N)	Theoretical Drag at 18.9 km (N)	Theoretical Drag at 20 km (N)
Akron	10.396	3.473	2.246	7.836	3.052	2.011
White Sands	11.756	1.789	1.264	8.813	1.615	1.155

Table 14. Drag analysis results and comparison for Modified Blimp.

The drag results for the modified blimp show similar results to those of the basic blimp. The comparison between the computational results and those of the theoretical equations still show similar values. At the lower altitude, the difference between the computational value and the theoretical value is greater than the same relation for the basic blimp. As altitude increases, the relation between the computational result and the theoretical result begin to converge as with the basic blimp. This higher difference for the lower altitude could be attributed to the increased surface area of the modified blimp relative to the basic blimp. As altitude increases, the density decreases therefore the drag due to friction would also be decreasing which could account for the closer resemblance of the computational result to that of the theoretical result for the higher altitudes.

Figure 19 shows the velocity plot of the modified blimp at ground level in Akron, OH experiencing the maximum wind velocity from a profile view. As seen by the figure, the area that separation is most likely to occur has now been greatly diminished. The separation point can be described as the point in the boundary layer flow at which there is a change in the direction of

the flow away from the mainstream direction (Nunn, 1989). This separation occurs in a region of higher adverse pressure gradients. The combination of viscous forces and an adverse pressure gradient forces a flow to separate from a body (Nunn, 1989). With the flow separated, form drag greatly increases and greatly increases the overall drag acting on the body.

Figure 20 shows the area of interest magnified to reveal no separation or circulation. By The red color indicates flow in the opposite direction of the oncoming flow.

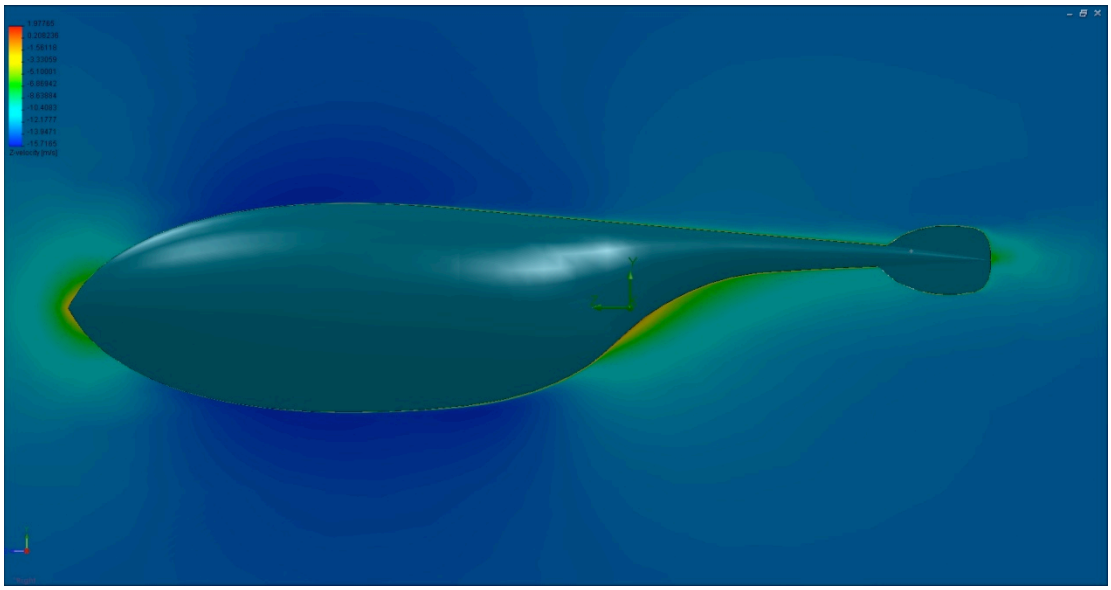

Figure 19. Profile view of velocity plot of the Modified Blimp for Akron, OH.

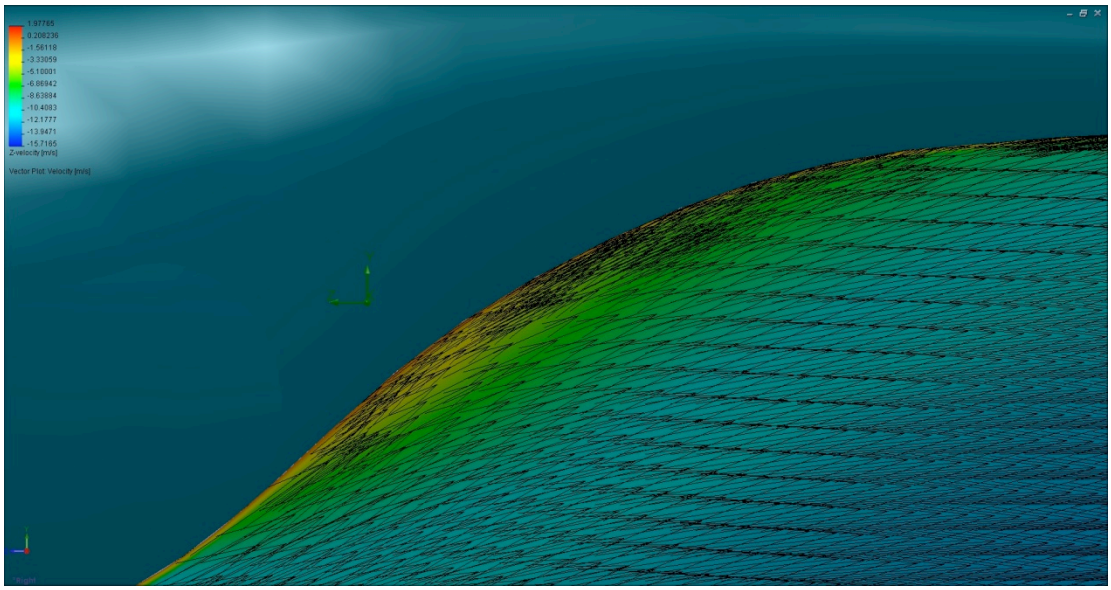

Figure 20. Magnified view of area of most likely separation.

Due to the longitudinal symmetry of the basic blimp, the separation seen in the profile view is the same for all profile views of the blimp. After the addition of the tail, the longitudianl symmetry was no longer present which created the potential for different separation locations.

4.3.3 Modified Blimp Power Model

The total power required by the modified blimp was calculated using the same process that was used for the basic blimp. The assumptions that were made for the basic blimp still hold for the modified blimp. Using Equation 4.47 to calculate the power required for the modified blimp, the power curves for the modified blimp through the atmosphere can be seen in Figure 21 and Figure 22.

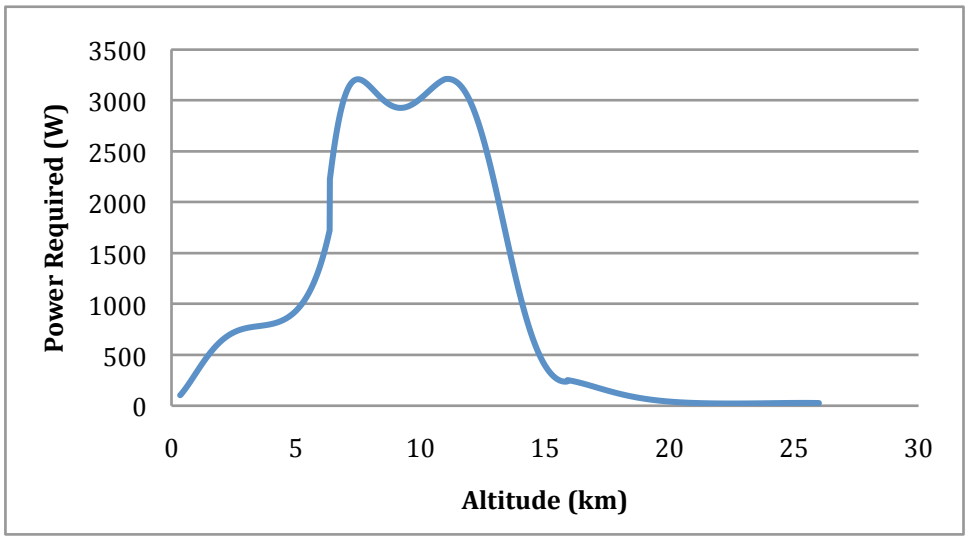

Figure 21. Power required vs. altitude for Modified Blimp over Akron, OH.

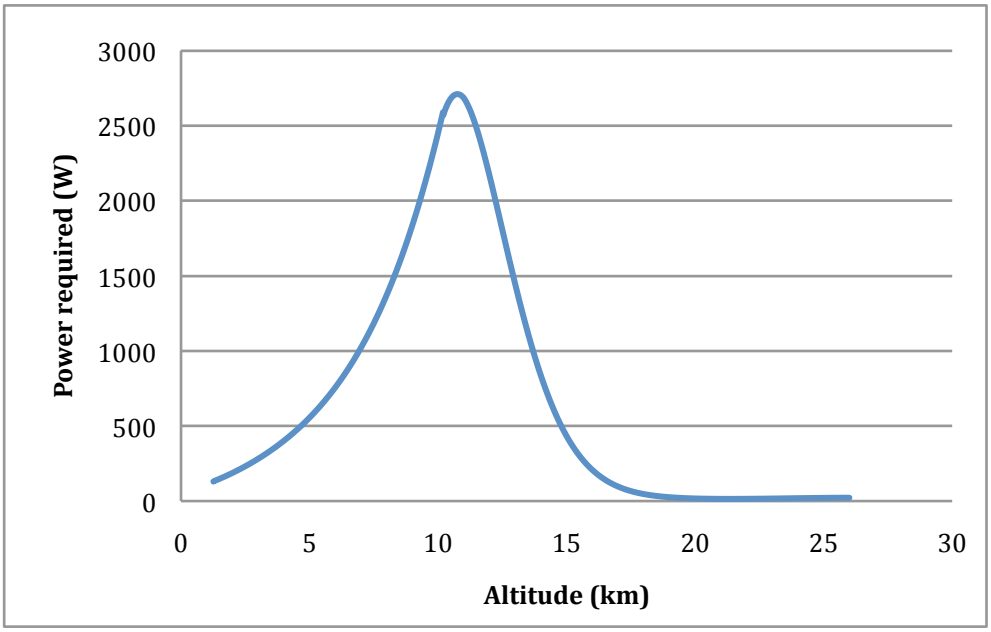

Figure 22. Power required vs. altitude for Modified Blimp over White Sands, NM.

Similarly to the basic blimp, the power required for station keeping for the modified blimp peaks around 10 kilometers then decreases drastically. Table 15 shows the comparison of power required, using equation 4.35, between the theoretical values and the CFD values and shows the same correlation between the drag values as shown in Table 14.

Location	CFD Power at GL (W)	CFD Power at 18.9 km (W)	CFD Power at 20 km (W)	Theoretical Power at GL (W)	Theoretical Power at 18.9 km (W)	Theoretical Power at 20 km (W)
Akron	138.736	82.615	45.762	104.574	72.601	40.973
White Sands	174.396	29.875	18.932	130.739	26.978	17.303

Table 15. Power analysis and comparison for Modified Blimp.

As with the results of the drag on the modified blimp, the power required for the modified blimp follows the same pattern due to the relationship between the drag and power as discussed earlier. Therefore it is expected that the power required follows the same trend as the resulting drag.

4.3.4 Stability / Control

Under the assumption that the basic blimp was stable, the stability of the modified blimp was determined by ensuring the same pitch and yaw moments existed between the two designs. Equations 4.48 and 4.49 were used to verify the yawing and pitching moments were consistent. Table 16 shows the pitching moments for each of the designs.

	Tail Length (m)	Tail Area (m^2)	Tail Force (N)	Moment (N-m)
Basic Blimp	1.003	0.972	1869.577	1874.399
Modified Blimp	3.619	0.300	577.268	2089.004

Table 16. Moment comparison between Basic Blimp and Modified Blimp.

Using the basic stability equations previously discussed, the stability of the modified blimp was determined. The calculated moment modified tail produces a greater moment than that of the basic tail, therefore satisfies the requirement to keep the modified airship stable. Because stability was not the purpose of this research this is sufficient information to conclude that the modified blimp would be stable.

CHAPTER 5

RESULTS AND DISCUSSION OF NEAR SPACE ANALYSIS

The previous models and methods were used to estimate the drag and power required when the tail modification is exposed to near space conditions. The following sections present the results of that analysis.

5.1 Basic Blimp Results for Near Space

After analysis and comparisons were completed with the lower atmospheric data, near space conditions were analyzed. It was determined using the MathCAD model that along with a wind lull in the lower portion of near space, there was also a power required lull that didn't necessarily correspond with the wind velocity lull. Figure 23 and Figure 24 show the theoretical relationship of the wind velocity and the power required in the near space region above Akron, OH experiencing the maximum wind velocity.

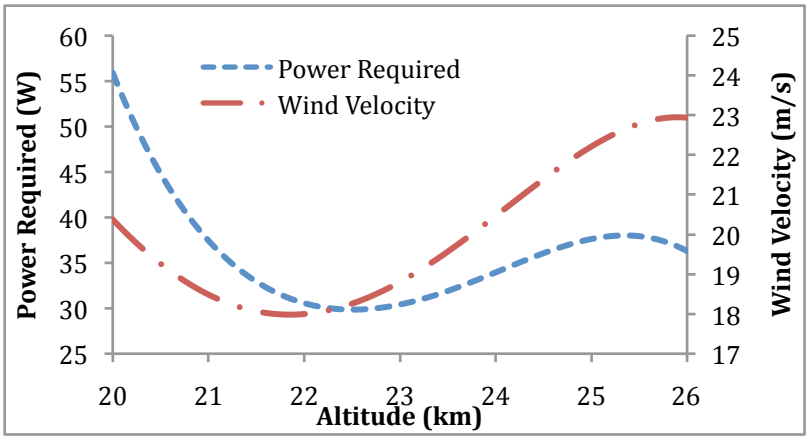

Figure 23. Relationship between power required and wind velocity for a basic airship over Akron, OH.

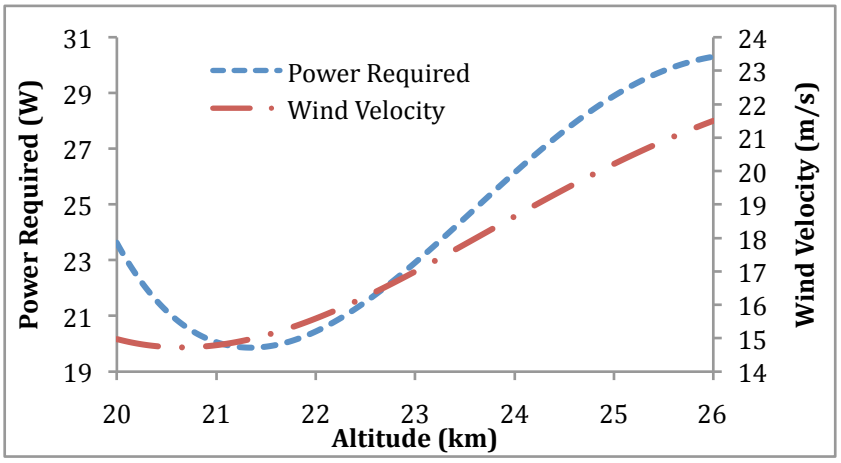

Figure 24. Relationship between power required and wind velocity for a basic airship over White Sands, NM.

These figures reveal that a minimum in power required exists separate from a minimum in the wind velocity. This relationship between minimum of the power required and wind velocity has not been previously determined or discussed in previous research. Although a minimum in wind velocity may seem to be most important to near space flight, the altitude of the minimum of power required should ultimately be considered most important. Because this research is centered on a decrease in drag and ultimately power required for station keeping, the conditions that occur at an altitude with the lowest power requirements, or the power knee region, were used for the computational analysis of the different airship configurations.

For the analysis in the near space region, the conditions were taken at the altitude that provided the lowest power required, not the altitude of the lowest wind velocity. For the near space region over Akron, OH, the altitude of the power knee region is experienced is 22.51km, while over White Sands, NM, the altitude is 21.35km. The altitudes of the wind knee regions are 21.85 km and 20.65 km for Akron, OH and White Sands, NM, respectively. Table 17 shows the calculated theoretical and computational values for the power required for multiple altitudes in the near space region, experiencing the maximum wind velocity.

Location	CFD Power at 20 km (W)	CFD Power at Wind Knee region (W)	CFD Power at Power Knee region (W)	Theoretical Power at 20 km (W)	Theoretical Power at Wind Knee region (W)	Theoretical Power at Power Knee region (W)
Akron	55.511	31.353	29.366	55.931	31.083	29.852
White Sands	24.006	20.669	19.726	23.620	20.724	19.862

Table 17. Power required for Basic Blimp in Near Space.

As seen in Table 17 the computational results mimic the theoretical results and also show that the power minimum actually occurs at a location different than that of the minimum wind velocity. Visualization of the basic blimp in the near space region over Akron, OH experiencing the maximum wind velocity can be seen in Figure 25. The area of flow separation, represented by the red, is larger than the area of flow separation behind the basic blimp at low altitudes.

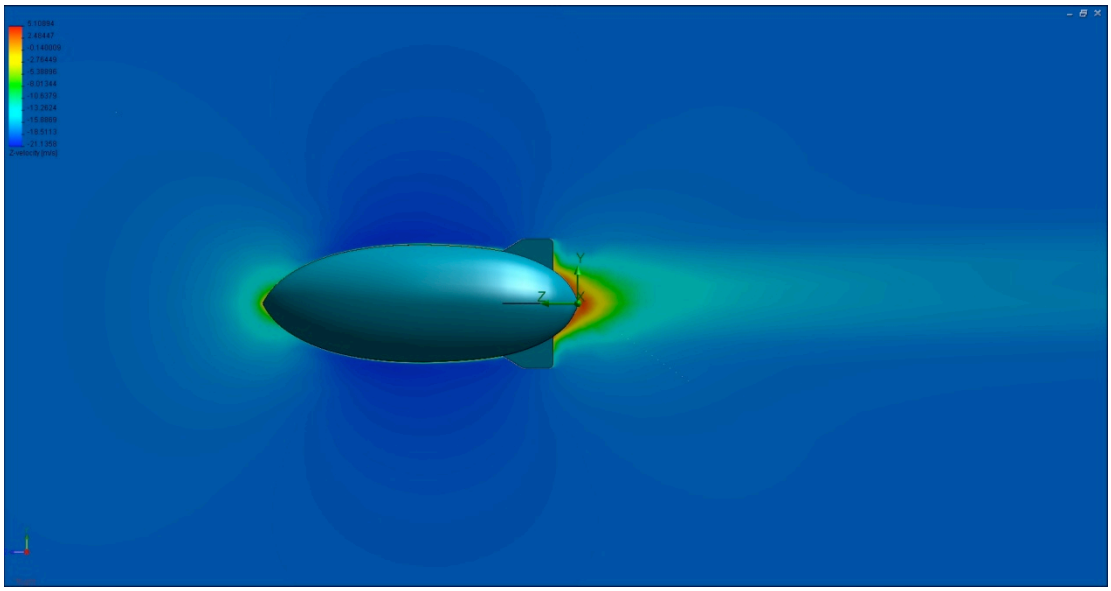

Figure 25. Visualization of wake for Basic Blimp at Power Knee Region.

5.2 Modified Blimp Results for Near Space

Analysis for the modified blimp follows exactly the same process as the basic blimp. As with the Basic blimp, the power required over both geo-locations reaches a minimum at an

altitude different than that of the minimum of the maximum wind velocity. Figure 26 and Figure 27 show the trends of the power required and the wind velocity.

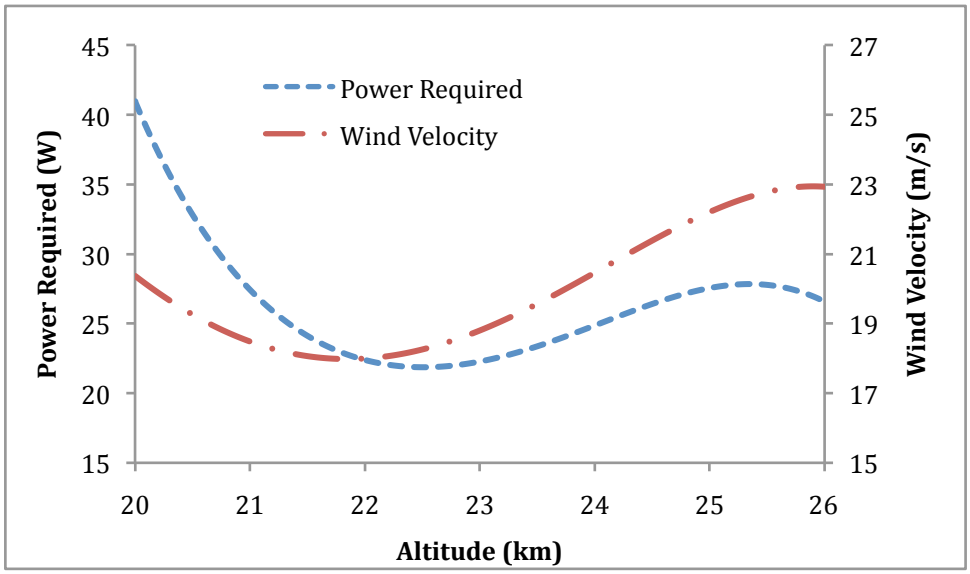

Figure 26. Relationship between power required and wind velocity for modified airship over Akron, OH.

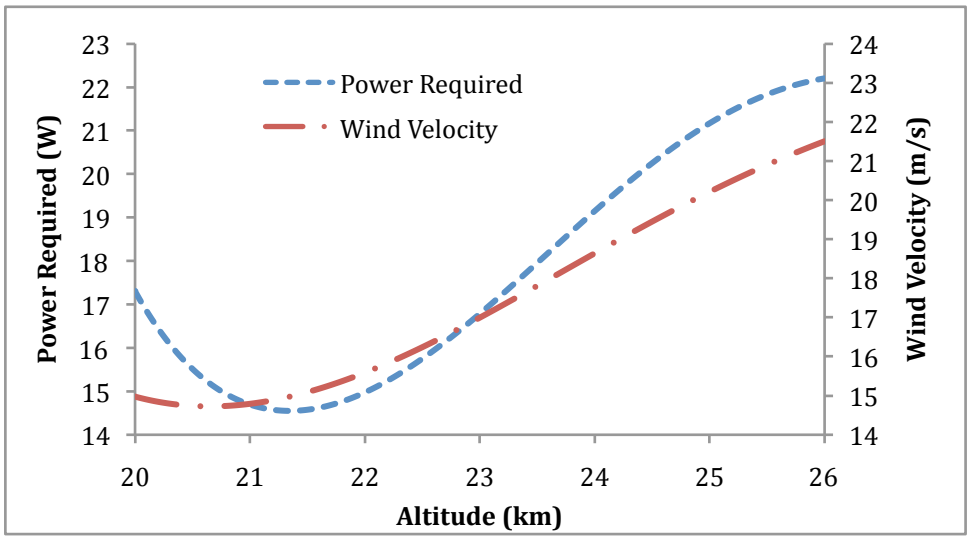

Figure 27. Relationship between power required and wind velocity for modified blimp over White Sands, NM.

The results for the power required for the Modified Blimp reflect the same trend as the Basic Blimp and can be seen in Table 18. The difference comes in the magnitude of the power required for the modified blimp while the wind velocity is the same. The power knee still occurs

at 22.51km and 21.35 km for Akron, OH and White Sands, NM respectively and the wind knee region still occurs at 21.85km and 20.65km for Akron, OH and White Sands, NM respectively.

Location	CFD Power at 20 km (W)	CFD Power at Wind Knee region (W)	CFD Power at Power Knee region (W)	Theoretical Power at 20 km (W)	Theoretical Power at Wind Knee region (W)	Theoretical Power at Power Knee region (W)
Akron	45.762	25.039	23.979	40.973	22.770	21.868
White Sands	18.932	16.659	15.937	17.303	15.182	14.550

Table 18. Power required for Modified Blimp in Near Space.

Table 18 shows the same trend present with the basic blimp. The altitude at which a power minimum actually occurs is separate from the altitude that the wind minimum occurs. A visualization of the modified blimp at the altitude that allows for the minimization of the power required in near space over Akron, OH is seen in Figure 28. As expected and seen in the figures, the modified blimp greatly reduces the area of separation and circulation, represented by the color red, which would help decrease the overall drag, and therefore power required for flight.

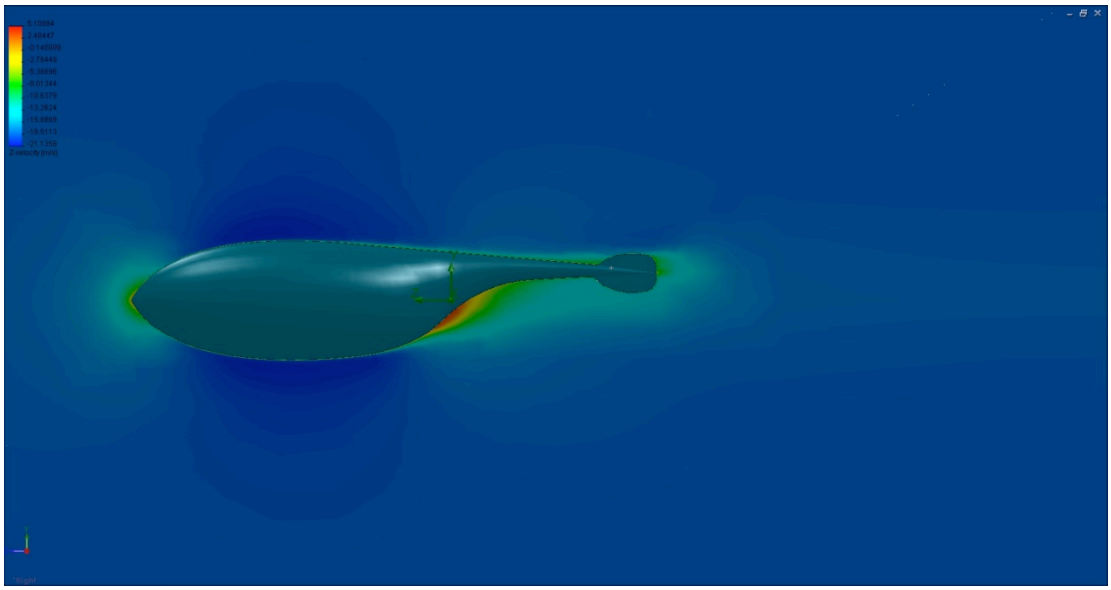

Figure 28. Visualization of wake for Modified Blimp at Power Knee Region.

5.3 Comparison of Results

The results of the analysis show that the addition of the tail can have a drag reduction effect to lower the amount of power required for station keeping performance. Table 19 shows the comparison of the power required values for the airspace over Akron, OH.

	CFD		Theoretical	
Altitude	Basic Blimp Power Required (W)	Modified Blimp Power Required (W)	Basic Blimp Power Required (W)	Modified Blimp Power Required (W)
GL	129.533	138.736	142.750	104.574
18.9 km	82.129	82.615	99.106	72.601
20 km	55.510	45.762	55.931	40.973
Wind Knee	31.353	25.039	31.083	22.770
Power Knee	29.366	23.979	29.852	21.868

Table 19. Comparison of power required for the Basic Blimp and Modified Blimp over Akron, OH.

Table 20 shows the comparison of the power required between the basic blimp and the modified blimp for the airspace over White Sands, NM experiencing the maximum wind velocity.

	CFD		Theoretical	
Altitude	Basic Blimp Power Required (W)	Modified Blimp Power Required (W)	Basic Blimp Power Required (W)	Modified Blimp Power Required (W)
GL	164.595	174.396	178.468	130.739
18.9 km	37.004	29.875	36.826	26.978
20 km	24.006	18.932	23.619	17.303
Wind Knee	20.669	16.659	20.724	15.182
Power Knee	19.726	15.937	19.862	14.550

Table 20. Comparison of power required for the Basic Blimp and Modified Blimp over White Sands, NM.

From these results, it can be seen that, although the modified blimp doesn't initially reduce the drag, and thus power required of the blimp at ground level, as the altitude increases, the amount of power required reduction increases to the point where the modified tail helps to reduce the drag, and therefore the power required for station keeping performance. The increase in the power required for station keeping at ground level may be attributed to the greater surface area of the modified blimp. As the altitude increases, the density in the air decreases along with the Reynolds number, which would decrease the overall drag due to friction. These results show that the model used for the theoretical calculations sufficiently approximated the drag and power required characteristics of the basic blimp, but with the change in the shape of the blimp, the ability of the model to closely estimate the drag diminished due to the lack in symmetry around the longitudinal axis. Although the decreases in power required may seem small, the size of a blimp needed to fly in near space would have to be very large in order to produce enough lift to carry all the equipment necessary for flight, therefore this small power required reduction may increase as the size of the blimp increases, further assisting in the potential ability to station keep for long periods of time.

CHAPTER 6

CONCLUSIONS AND FUTURE WORK

This research has shown that near space flight is in fact a very unforgiving regime of the atmosphere for flight and exploration. For long endurance expeditions, fixed wing aircraft do not have the ability for success. The atmosphere in near space is too thin for reasonable, fixed wing flight characteristics. The low density requires too much speed to be able to fly level and creates a low Reynolds number separation bubble that hinders the effectiveness of airfoils.

6.1 Models

With the addition of statistical atmospheric data, a complete profile of the atmosphere was created to simulate any altitude from sea level through near space. This environmental model was the foundation for the research conducted with high altitude airships. The model and the theoretical data derived from known equations were compared to show the close resemblance to each other and the verification that the computational analysis was correct.

6.2 Conclusions

Multiple conclusions can be drawn from the research and work that has been done:

- Near space is an unforgiving harsh environment for flight. Fixed wing flight is near impossible due to the excessive speeds and power requirements necessary for operation at such altitudes.

- Through history, birds have evolved to become more efficient and effective in flight. The adaptations of bird tails can be utilized to assist in the problems of near space flight by assisting in reducing the amount of drag and therefore power required for near space flight by acting as a splitter plate to assist in reducing the size of the wake behind the bird.
- Because fixed wing flight is nearly impossible in near space, lighter than air technology can be used to gain access to this region of our atmosphere. Although there was a lull in research and development of lighter than air technology, newer materials, structures and flight software are being researched and developed to aid in the ability of airships to successfully fly at high altitudes.
- Modifications to a basic blimp that include adapting a tail to resemble the tail of a bird can reduce the amount of drag experienced on an airship in near space. Using one of nature's examples of natural drag reduction, it has been shown computationally that the addition of the tail to an airship will reduce the drag in near space. Although the addition of the tail increased the drag at lower altitudes, most likely due to the increased surface area and therefore friction drag, it can decrease the drag at near space altitudes by potentially as much as 20%.

6.3 Potential Future Work

One possible area for future work regarding this research topic is the altering of theoretical equations to closely estimate the performance of a non-axisymmetric airship. The equations used were derived for an axis symmetric slender body of revolution. These derivations worked well for the basic airship however, theoretical results for the modified airship were skewed due to the nonsymmetrical shape. Another aspect of this research that could be

expanded upon is the optimization of the tail shape and design. There are many different types and shapes of tails that have the potential to reduce drag or create additional optimization. These possibilities could be expanded upon to more tailor the design of the tail to the flight goals.

REFERENCES

Ahrens, C.D., "Atmospheric Moisture," *Meterology Today: An Introduction to Weather, Climate, and the Environment*, 8th ed., Thomson Brooks/Cole, Belmont, CA, 2007, pp. 84-105.

Anderson, J. D., "Aerodynamics of the Airplane: The Drag Polar," *Aircraft Performance and Design*, 1st ed., WCB/McGraw-Hill, Boston, MA, 1999, pp. 51-142.

Anderson, J. D., "Airplane Performance: Steady Flight," *Aircraft Performance and Design*, 1st ed., WCB/McGraw-Hill, Boston, MA, 1999, pp. 199-317.

Beheshti, B.H., Soller, A., Wittmer, F., and Abhari, R.S.,"Experimental Investigation of the Aerodynamic Drag of a Hight Altitude Airship," AIAA Paper No. 2007-7894, AIAA 7th Aviation, Technology, Integration, and Operations Conference, 18-20 September 2007, Belfast, Northern Ireland.

Brandt, S. A., Stiles, R. J., Bertin, J. J., and Whitford, R., "Wing and Airplanes," *Introduction To Aeronautics: A Design Perspective*, 2nd ed., AIAA, Reston, VA, 2004, pp. 113-168.

Brooke, L., "High Altitude LTA Platforms: Capabilities and Possibilities," AIAA Paper No. 2005-7319, AIAA 5th Aviation, Technology, Integration, and Operations Conference, 26-28 September 2005, Arlington, VA.

Chatterjee, S., and Templin, R.J.,"Biplane wing planform and flight performance of the feathered dinosaur Microraptor gui," Copyright (2007) National Academy of Sciences, U.S.A., Vol. 104, No. 5, pp. 1576-1580.

Colozza, A., and Dolce, J.L.,"High-Altitude, Long-Endurance Airships for Coastal Surveillance," NASA TM-2005-213427, February 2005.

Crowe, C.T., Elger, D.F., Roberson, J.A., "Diminsionless Analysis and Similitude," *Engineering Fluid Mechanics*, 8th ed., Wiley, New Jersey, 2006, pp. 293.

Dorrington, G.E.,"Drag of a Spheroid-Cone Shaped Airship," J. Aircraft, 43:2, 2006, pp. 363-371.

Edward Lan, C.T., Roskam, J., "Airplane Drag," *Airplane Aerodynamics and Performance,* DARcorporation, Lawrence, Kansas, 2003, pp. 137-200.

Etkin, B., "Appendix B: Aerodynamic Data," *Dynamics of Flight: Stability and Control*, 2nd ed., John Wiley & Sons, New York, NY, 1982, p. 342-346.

Fernandez, S.S., “Presentation of the Karman Separation Line, used as the Boundary Separating Aeronautics and Astornautics,” International Aeronautics Federation, 21 June 2004.

Gatesy, S.M., and Dial, K.P.,"From Frond to Fan: Archaeopteryx and the Evolution of Short-Tailed Birds," Evolution, Vol. 50, No. 5, October 1996, pp. 2037-3048.

Goraj, Z., Frydrychiewicz, A., and Winiecki, J., “Design Cocept of a High-Altitude Long-Endurance Unmanned Aerial Vehicle,” *Aircraft Design*, Vol. 1, 1999, pp. 19-44.

Greer, D., Hamory, P., Krake, K., and Drela, M., “Design Predictions for a High-Altitude (Low-Reynolds-Number) Aerodynamic Flight Experiment,” NASA TM-1999-206579, July 1999.

Hedenstrom, A., "Aerodynamics, Evolution and Ecology of Avian Flight," Trends in Ecology & Evolution, 17:9, 2002, pp. 415-422.

Hoerner, S.F., “Drag of Streamlined Shapes,” *Fluid-Dynamics Drag*, Hoerner, Midland Park, NJ, 1958, pp. 6.1-6.20.

Huang, Y.M., and Chang, S.W.,"Practical Design of an Airship,"J. Aircraft, 32:6, November-December 1995, pp. 1294-1296.

Kantor, G., Wettergreen, D., Ostrowski, J.P., Singh, S.,"Collection of Environmental Data From an Airship Platform," Proceedings of the SPIE Conference on Sensor Fusion and Decentralized Control IV, Vol. 4571, 28-29 October 2001, pp. 76-83.

Knoedler, Andrew J. “Lowering the High Ground: Using Near-Space Vehicles for Persistent ISR.” Center for Strategy and Technology, Air War College, Air University, Maxwell AFB, Alabama, November 2005.

Liao, L., Pasternak, I., "A Review of Airship Structural Research and Development Progress in Aerospace Sciences," 2009.

Manwell, J.F., McGowan, J.G., and Rogers A.L., “Wind characteristics and resources,” *Wind Energy Explained, Theory, Design and Application*, 2nd ed., Wiley, New York, 2009, pp. 53-62.

Martinez-Val, R., Hernandez, C., “Preliminary design of a low speed, long endurance remote piloted vehicles (RPV) for civil applications,” Aircraft Design 2, 1999, pp. 167-182.

Maybury, W.J., and Rayner, J.M.V.,"The avian tail reduces body parasite drag by controlling flow separation and vortex shedding," Proc. R. Soc. Long. B., February 2001, pp. 1405-1410.

Miller, G.D., and Stoia, T.R.,"Operational Capability of High Altitude Solar Powered Airships," AIAA Paper No. 2005-7487, AIAA 5th Aviation, Technology, Integration, and Operations Conference, 26-28 September 2005, Arlington, VA.

Moran, M.J., Shapiro, H.N., "Ideal gas Mixture and Psychrometric Applications," *Fundamentals of Engineering Thermodynamics,* 5th ed., John Wiley & Sons, Hoboken, NJ, 2004, pp. 590-655.

Mueller, T.J., DeLaurier, J.D., "Aerodynamics of Small Vehicles," Annual Review of Fluid Mechanics, vol. 35, 2003, pp. 89-111.

Murray, J., Moes, T., Norlin, K., Bauer, J., Geenen, R., Moulton, B., and Hoang, S., "Piloted Simulation Study of a Balloon-Assisted Deployment of an Aircraft at High Altitude," NASA TM-104245, January 1992.

Muti Lin, J.C. and Pauley, L.L., "Low-Reynolds number separation on an airfoil." AIAA Journal. 34:8, August 1996, pp. 1570-1577.

Nakadate, M.,"Development and Flight Test of SPF-2 Low Altitude Stationary Flight Test Vehicle," AIAA Paper No. 2005-7408, AIAA 5th Aviation, Technology, Integration, and Operations Conference, 26-28 September 2005, Arlington, VA.

Nelson, R. C., "Static Stability and Control," *Flight Stability and Automatic Control*, 2nd ed., McGraw-Hill, Boston, MA, 1998, pp. 35-85.

Norberg, U.M.,"How a Long Tail and Changes in Mass and Wing Shape Affect the Cost for Flight in Animals," Functional Ecology, 9:1, February 1995, pp. 48-54.

Nunn, R.H., *Intermediate Fluid Dynamics,* Hemisphere, New York, 1989.

Raymer, D. P., "Thrust-to-Weight Ratio and Wing Loading," *Aircraft Design: A Conceptual Approach*, 4th ed., edited by Joseph A. Schetz, Education Series, AIAA, Reston, VA, 2006, pp. 87-110.

Raymer, D. P., "Initial Sizing," *Aircraft Design: A Conceptual Approach*, 4th ed., edited by Joseph A. Schetz, Education Series, AIAA, Reston, VA, 2006, pp. 111-126.

Raymer, D. P., "Aerodynamics," *Aircraft Design: A Conceptual Approach*, 4th ed., edited by Joseph A. Schetz, Education Series, AIAA, Reston, VA, 2006, pp. 303-364.

Raymer, D. P., "Performance and Flight Mechanics," *Aircraft Design: A Conceptual Approach*, 4th ed., edited by Joseph A. Schetz, Education Series, AIAA, Reston, VA, 2006, pp. 515-560.

Real-Time Archive, Radionsonde Database Access, Forecoast Systems Laboratory, NOAA, http://raob.fsl.noaa.gov, cited July-September 2009.

Roney, J.A.,"Statistical Wind Analysis for near-space applications," Journal of Atmospheric and Solar-Terrestrial Physics 69, 2007, pp. 1485-1501.

Sandlin, D.R.,"Flight Test of the HX-1 Radio-Controlled Hybrid Airship," AIAA Lighter Than Air Systems Technology Conference, 25-27 July 1983, pp. 132-136.

Savile, D.B.O.,"Adaptive Evolution of the Avian Wing," Evolution, 11:2 June 1957, pp. 212-224.

Schmidt, D.K., et al., "Near-Space Station-Keeping Performance of a Large High-Altitude Notional Airship," J. Aircraft, 44:2, March-April 2007, pp.611-615.

Selig, M., "UIUC Airfoil Coordinates Database." UIUC Airfoil Coordinates Database [online database], http://www.ae.uiuc.edu/m-selig/ads/coord_database.html [retrieved October, 2008].

Smith, J.M.,"The Importance of the Nervous System in the Evolution of Animal Flight," Evolution, Vol. 6, No. 1, March 1952, pp. 127-129.

Thomas. A.L.R.,"On the Aerodynamics of Birds' Tails," Philosophical Transactions: Biological Sciences, Vol. 340, No. 1294, 29 June 1993, pp. 361-380.

Tomme, Lt. Col. Edward B., "The Paradigm Shift to Effects-Based Space: Near-Space as a Combat Space Effects Enabler," Research paper 2005-01, CADRE, (Maxwell AFB, AL: Air University, 2005).

US Standard Atmosphere, NOAA, NSF, USAF. http://scipp.ucsc.edu/outreach/balloon/atmos/1976%20Standard%20Atmosphere.htm, accessed January, 2007.

APPENDIX 1

Lift genereated calculations for HQ 3/12 for multiple altitudes

This spreadsheet can be used to verify flight velocities calculated in the MathCad spreadsheet.
This spreadsheet shows the amount of lift generated for multiple velocity/lift coefficient combinations.
If a velocity and a lift coeffiecient are know, the lift genereated can be determined for steady level flight.
Given an initial weight input, the spreadsheet will show the velocity needed per lift coefficient.
Cells highlighted red show a velocity/lift coefficient combination that will not produce enough lift.
Cells highlighted green show a velocity/lift coefficient combination that will produce enough lift.
Each block of cells represents different altitudes ranging from 500ft ASL to 100,000ft ASL.

For steady level flight L=W | W = 15 kg = 33 lb | S = 1.25 m^2 = 13.44954 ft^2

500ft | ρ = 1.207 kg/m^3 = 0.002342 lb/ft^3

Re ≈ 300000

α	C_l	V(mph)	V(ft/s)	C_l 0.446 Lift(lb)	0.561 Lift(lb)	0.679 Lift(lb)	0.795 Lift(lb)	0.912 Lift(lb)	1.032 Lift(lb)	1.137 Lift(lb)	1.242 Lift(lb)	1.332 Lift(lb)	1.38 Lift(lb)	1.409 Lift(lb)	1.413 Lift(lb)	C_l Required
0	0.446	30	44.00001	13.60	17.11	20.70	24.24	27.81	31.47	34.67	37.87	40.61	42.08	42.96	43.08	1.082306772
1	0.561	35	51.33335	18.51	23.28	28.18	32.99	37.85	42.83	47.19	51.54	55.28	57.27	58.47	58.64	0.795164159
2	0.679	40	58.66668	24.18	30.41	36.81	43.09	49.44	55.94	61.63	67.32	72.20	74.80	76.38	76.59	0.608797559
3	0.795	45	66.00002	30.60	38.49	46.58	54.54	62.57	70.80	78.00	85.21	91.38	94.67	96.66	96.94	0.481025232
4	0.912	50	73.33335	37.77	47.51	57.51	67.33	77.24	87.41	96.30	105.19	112.81	116.88	119.34	119.67	0.389630438
5	1.032	55	80.66669	45.71	57.49	69.59	81.47	93.46	105.76	116.52	127.28	136.51	141.42	144.40	144.81	0.322008626
6	1.137	60	88.00002	54.39	68.42	82.81	96.96	111.23	125.86	138.67	151.48	162.45	168.31	171.84	172.33	0.270576693
7	1.242	65	95.33336	63.84	80.30	97.19	113.79	130.54	147.72	162.75	177.77	190.66	197.53	201.68	202.25	0.230550555
8	1.332	70	102.6667	74.04	93.13	112.72	131.97	151.40	171.32	188.75	206.18	221.12	229.08	233.90	234.56	0.19879104
9	1.38	75	110	84.99	106.91	129.39	151.50	173.80	196.66	216.67	236.68	253.83	262.98	268.51	269.27	0.173169083
10	1.409	80	117.3334	96.70	121.64	147.22	172.37	197.74	223.76	246.53	269.29	288.81	299.21	305.50	306.37	0.15219939
10.5	2	85	124.6667	109.17	137.32	166.20	194.59	223.23	252.60	278.30	304.00	326.03	337.78	344.88	345.86	0.134820221
		90	132	122.39	153.95	186.33	218.16	250.27	283.20	312.01	340.82	365.52	378.69	386.65	387.75	0.120256308
C_{l_max}	2	95	139.3334	136.37	171.53	207.61	243.07	278.85	315.54	347.64	379.74	407.26	421.94	430.80	432.03	0.107930869
		100	146.6667	151.10	190.06	230.03	269.33	308.97	349.62	385.20	420.77	451.26	467.52	477.34	478.70	0.097407609
		105	154	166.58	209.54	253.61	296.94	340.64	385.46	424.68	463.90	497.51	515.44	526.27	527.77	0.088351573
		110	161.3334	182.83	229.97	278.34	325.89	373.85	423.04	466.09	509.13	546.02	565.70	577.59	579.23	0.080502157
		115	168.6667	199.83	251.35	304.22	356.19	408.61	462.38	509.42	556.47	596.79	618.30	631.29	633.08	0.073654147
		120	176	217.58	273.68	331.25	387.84	444.92	503.46	554.68	605.91	649.81	673.23	687.38	689.33	0.067644173
		125	183.3334	236.09	296.96	359.43	420.83	482.77	546.29	601.87	657.45	705.09	730.50	745.85	747.97	0.06234087
		130	190.6667	255.35	321.20	388.76	455.17	522.16	590.86	650.98	711.10	762.63	790.11	806.71	809.00	0.057637639
		135	198.0001	275.37	346.38	419.24	490.86	563.10	637.19	702.02	766.85	822.42	852.06	869.96	872.43	0.053447248
		140	205.3334	296.15	372.51	450.87	527.89	605.58	685.26	754.98	824.71	884.47	916.34	935.60	938.25	0.04969776
		145	212.6667	317.68	399.59	483.65	566.27	649.61	735.08	809.87	884.66	948.77	982.96	1003.62	1006.47	0.046329422
		150	220.0001	339.97	427.63	517.58	606.00	695.18	786.65	866.69	946.73	1015.33	1051.92	1074.03	1077.07	0.043292271
		155	227.3334	363.01	456.61	552.66	647.07	742.30	839.97	925.43	1010.89	1084.15	1123.22	1146.82	1150.08	0.04054427
		160	234.6667	386.81	486.55	588.89	689.49	790.96	895.04	986.10	1077.17	1155.22	1196.85	1222.00	1225.47	0.038049847
		165	242.0001	411.36	517.43	626.27	733.26	841.17	951.85	1048.70	1145.54	1228.55	1272.82	1299.57	1303.26	0.035778736
		170	249.3334	436.67	549.26	664.80	778.37	892.92	1010.41	1113.22	1216.02	1304.14	1351.13	1379.53	1383.44	0.033705055
		175	256.6667	462.73	582.05	704.48	824.83	946.22	1070.72	1179.66	1288.60	1381.98	1431.78	1461.87	1466.02	0.031806566
		180	264.0001	489.55	615.78	745.31	872.64	1001.06	1132.78	1248.03	1363.29	1462.08	1514.76	1546.60	1550.99	0.030064077
		185	271.3334	517.13	650.47	787.29	921.79	1057.45	1196.59	1318.33	1440.08	1544.43	1600.09	1633.71	1638.35	0.028460952
		190	278.6667	545.46	686.11	830.42	972.29	1115.38	1262.14	1390.56	1518.97	1629.04	1687.75	1723.21	1728.11	0.026982717
		195	286.0001	574.55	722.69	874.70	1024.14	1174.86	1329.44	1464.71	1599.97	1715.91	1777.74	1815.10	1820.26	0.025616728
		200	293.3334	604.39	760.23	920.13	1077.33	1235.88	1398.49	1540.78	1683.07	1805.03	1870.08	1909.38	1914.80	0.024351902
		205	300.6667	634.99	798.71	966.72	1131.87	1298.45	1469.29	1618.79	1768.28	1896.41	1964.75	2006.04	2011.74	0.023178491
		210	308.0001	666.34	838.15	1014.45	1187.75	1362.56	1541.84	1698.71	1855.59	1990.05	2061.76	2105.09	2111.07	0.022087893
		215	315.3334	698.45	878.54	1063.33	1244.99	1428.21	1616.14	1780.57	1945.00	2085.94	2161.11	2206.53	2212.79	0.021072495
		220	322.6668	731.31	919.88	1113.36	1303.57	1495.41	1692.18	1864.35	2036.52	2184.09	2262.80	2310.35	2316.91	0.020125539
		225	330.0001	764.93	962.16	1164.54	1363.49	1564.16	1769.97	1950.05	2130.14	2284.50	2366.82	2416.56	2423.42	0.019241009
		230	337.3334	799.30	1005.40	1216.88	1424.77	1634.45	1849.51	2037.69	2225.86	2387.16	2473.18	2525.15	2532.32	0.018413537
		235	344.6668	834.43	1049.59	1270.36	1487.39	1706.29	1930.80	2127.24	2323.69	2492.07	2581.88	2636.14	2643.62	0.017638318
		240	352.0001	870.32	1094.73	1324.99	1551.35	1779.67	2013.83	2218.73	2423.62	2599.25	2692.91	2749.51	2757.31	0.016911043
		245	359.3334	906.96	1140.82	1380.78	1616.67	1854.59	2098.62	2312.14	2525.66	2708.68	2806.29	2865.26	2873.40	0.01622784
		250	366.6668	944.36	1187.86	1437.71	1683.33	1931.06	2185.15	2407.47	2629.80	2820.36	2922.00	2983.40	2991.87	0.015585218
		255	374.0001	982.51	1235.85	1495.79	1751.33	2009.08	2273.43	2504.74	2736.04	2934.31	3040.05	3103.93	3112.75	0.014980025
		260	381.3334	1021.42	1284.79	1555.03	1820.69	2088.64	2363.46	2603.92	2844.39	3050.51	3160.43	3226.85	3236.01	0.01440941
		265	388.6668	1061.08	1334.68	1615.41	1891.38	2169.74	2455.23	2705.04	2954.84	3168.96	3283.16	3352.15	3361.67	0.013870788
		270	396.0001	1101.50	1385.52	1676.94	1963.43	2252.39	2548.76	2808.08	3067.40	3289.67	3408.22	3479.84	3489.72	0.013361812
		275	403.3334	1142.67	1437.31	1739.63	2036.82	2336.58	2644.03	2913.04	3182.06	3412.64	3535.62	3609.92	3620.17	0.012880345
		280	410.6668	1184.60	1490.05	1803.46	2111.56	2422.32	2741.05	3019.93	3298.82	3537.87	3665.36	3742.38	3753.01	0.01242444
		285	418.0001	1227.29	1543.74	1868.45	2187.65	2509.61	2839.82	3128.75	3417.69	3665.35	3797.43	3877.23	3888.24	0.011992319
		290	425.3334	1270.73	1598.38	1934.58	2265.08	2598.44	2940.33	3239.50	3538.66	3795.08	3931.84	4014.47	4025.87	0.011582355
		295	432.6668	1314.92	1653.97	2001.87	2343.86	2688.81	3042.60	3352.17	3661.73	3927.08	4068.59	4154.09	4165.88	0.011193061
		300	440.0001	1359.87	1710.51	2070.30	2423.99	2780.73	3146.61	3466.76	3786.91	4061.33	4207.68	4296.10	4308.30	0.010823068

25000 ft			ρ	0.549 kg/m^3		0.001065 lb/ft^3										
Re ≈ 160000			C_l	0.446	0.56	0.677	0.794	0.91	1.024	1.133	1.237	1.318	1.371	1.399	1.401	C_l
α	C_l	V(mph)	V(ft/s)	Lift(lb)	Lift(lb)	Lift(lb)	Lift(lb)	Lift(lb)	Lift(lb)	Lift(lb)	Lift(lb)	Lift(lb)	Lift(lb)	Lift(lb)	Lift(lb)	Required
0	0.446	30	44.00001	6.19	7.77	9.39	11.01	12.62	14.20	15.71	17.16	18.28	19.01	19.40	19.43	2.379497766
1	0.56	35	51.33335	8.42	10.57	12.78	14.99	17.18	19.33	21.39	23.35	24.88	25.88	26.41	26.45	1.74820244
2	0.677	40	58.66668	11.00	13.81	16.69	19.58	22.44	25.25	27.93	30.50	32.50	33.80	34.49	34.54	1.338467493
3	0.794	45	66.00002	13.92	17.47	21.13	24.78	28.40	31.95	35.35	38.60	41.13	42.78	43.65	43.72	1.057554563
4	0.91	50	73.33335	17.18	21.57	26.08	30.59	35.06	39.45	43.65	47.65	50.77	52.82	53.89	53.97	0.856619196
5	1.024	55	80.66669	20.79	26.10	31.56	37.01	42.42	47.73	52.81	57.66	61.44	63.91	65.21	65.31	0.707949749
6	1.133	60	88.00002	24.74	31.07	37.56	44.05	50.48	56.81	62.85	68.62	73.11	76.05	77.61	77.72	0.594874442
7	1.237	65	95.33336	29.04	36.46	44.08	51.69	59.25	66.67	73.76	80.53	85.81	89.26	91.08	91.21	0.506875264
8	1.318	70	102.6667	33.68	42.28	51.12	59.95	68.71	77.32	85.55	93.40	99.52	103.52	105.63	105.78	0.43705061
9	1.371	75	110	38.66	48.54	58.68	68.82	78.88	88.76	98.21	107.22	114.24	118.84	121.26	121.44	0.380719643
10	1.399	80	117.3334	43.98	55.23	66.77	78.30	89.74	100.99	111.74	121.99	129.98	135.21	137.97	138.17	0.334616873
10.5	1.401	85	124.6667	49.65	62.35	75.37	88.40	101.31	114.01	126.14	137.72	146.74	152.64	155.75	155.98	0.296408026
		90	132	55.67	69.90	84.50	99.10	113.58	127.81	141.42	154.40	164.51	171.12	174.62	174.87	0.264388641
C_{l_max}	1.401	95	139.3334	62.03	77.88	94.15	110.42	126.55	142.41	157.57	172.03	183.29	190.66	194.56	194.84	0.237290636
		100	146.6667	68.73	86.29	104.32	122.35	140.23	157.79	174.59	190.61	203.10	211.26	215.58	215.89	0.214154799
		105	154	75.77	95.14	115.01	134.89	154.60	173.97	192.48	210.15	223.91	232.92	237.67	238.01	0.194244716
		110	161.3334	83.16	104.41	126.23	148.04	169.67	190.93	211.25	230.64	245.75	255.63	260.85	261.22	0.176987437
		115	168.6667	90.89	114.12	137.97	161.81	185.45	208.68	230.89	252.09	268.59	279.40	285.10	285.51	0.161931795
		120	176	98.97	124.26	150.22	176.19	201.92	227.22	251.41	274.48	292.46	304.22	310.43	310.88	0.14871861
		125	183.3334	107.38	134.83	163.00	191.17	219.10	246.55	272.79	297.84	317.34	330.10	336.84	337.32	0.137059071
		130	190.6667	116.15	145.83	176.30	206.77	236.98	266.67	295.05	322.14	343.23	357.03	364.33	364.85	0.126718816
		135	198.0001	125.25	157.27	190.13	222.98	255.56	287.58	318.19	347.39	370.14	385.03	392.89	393.45	0.117506063
		140	205.3334	134.70	169.13	204.47	239.81	274.84	309.27	342.19	373.60	398.07	414.08	422.53	423.14	0.109262653
		145	212.6667	144.50	181.43	219.34	257.24	294.82	331.76	367.07	400.77	427.01	444.18	453.25	453.90	0.101857217
		150	220.0001	154.63	194.16	234.72	275.29	315.51	355.03	392.82	428.88	456.97	475.34	485.05	485.74	0.095179911
		155	227.3334	165.11	207.32	250.63	293.95	336.89	379.10	419.45	457.95	487.94	507.56	517.93	518.67	0.089138314
		160	234.6667	175.94	220.91	267.06	313.22	358.98	403.95	446.95	487.97	519.93	540.83	551.88	552.67	0.083654218
		165	242.0001	187.11	234.93	284.02	333.10	381.76	429.59	475.32	518.95	552.93	575.16	586.91	587.75	0.078661083
		170	249.3334	198.62	249.39	301.49	353.59	405.25	456.02	504.56	550.88	586.95	610.55	623.02	623.91	0.074102007
		175	256.6667	210.47	264.27	319.49	374.70	429.44	483.24	534.68	583.76	621.98	646.99	660.21	661.15	0.069928098
		180	264.0001	222.67	279.59	338.00	396.42	454.33	511.25	565.67	617.59	658.03	684.49	698.47	699.47	0.06609716
		185	271.3334	235.21	295.34	357.04	418.75	479.92	540.04	597.53	652.38	695.10	723.05	737.81	738.87	0.062572622
		190	278.6667	248.10	311.52	376.60	441.69	506.21	569.63	630.27	688.12	733.18	762.66	778.24	779.35	0.059322659
		195	286.0001	261.33	328.13	396.68	465.24	533.21	600.01	663.87	724.81	772.27	803.33	819.73	820.91	0.056319474
		200	293.3334	274.90	345.17	417.29	489.40	560.90	631.17	698.35	762.46	812.38	845.05	862.31	863.54	0.0535387
		205	300.6667	288.82	362.65	438.41	514.18	589.30	663.12	733.71	801.06	853.51	887.83	905.97	907.26	0.050958905
		210	308.0001	303.08	380.55	460.06	539.57	618.40	695.86	769.94	840.61	895.65	931.67	950.70	952.06	0.048561179
		215	315.3334	317.69	398.89	482.23	565.57	648.19	729.40	807.04	881.12	938.81	976.56	996.51	997.93	0.046328783
		220	322.6668	332.63	417.66	504.92	592.18	678.69	763.72	845.01	922.57	982.99	1022.51	1043.40	1044.89	0.044246859
		225	330.0001	347.93	436.86	528.13	619.40	709.89	798.82	883.86	964.99	1028.17	1069.52	1091.36	1092.92	0.042302183
		230	337.3334	363.56	456.49	551.86	647.24	741.79	834.72	923.57	1008.35	1074.38	1117.58	1140.41	1142.04	0.040482949
		235	344.6668	379.54	476.55	576.12	675.68	774.40	871.41	964.17	1052.67	1121.60	1166.70	1190.53	1192.23	0.038778596
		240	352.0001	395.86	497.05	600.89	704.74	807.70	908.88	1005.63	1097.94	1169.83	1216.88	1241.73	1243.50	0.037179653
		245	359.3334	412.53	517.97	626.19	734.41	841.70	947.15	1047.97	1144.16	1219.08	1268.11	1294.01	1295.86	0.035677601
		250	366.6668	429.54	539.33	652.01	764.69	876.41	986.20	1091.18	1191.34	1269.35	1320.39	1347.36	1349.29	0.034264768
		255	374.0001	446.89	561.12	678.35	795.59	911.82	1026.05	1135.26	1239.47	1320.63	1373.74	1401.79	1403.80	0.032934225
		260	381.3334	464.59	583.34	705.21	827.09	947.93	1066.68	1180.22	1288.55	1372.93	1428.14	1457.31	1459.39	0.031679704
		265	388.6668	482.63	605.99	732.60	859.21	984.73	1108.10	1226.05	1338.59	1426.24	1483.59	1513.89	1516.06	0.030495521
		270	396.0001	501.01	629.07	760.51	891.94	1022.25	1150.31	1272.75	1389.58	1480.57	1540.11	1571.56	1573.81	0.029376516
		275	403.3334	519.74	652.59	788.93	925.28	1060.46	1193.31	1320.33	1441.52	1535.91	1597.68	1630.31	1632.64	0.02831799
		280	410.6668	538.81	676.53	817.88	959.23	1099.37	1237.09	1368.78	1494.42	1592.27	1656.30	1690.13	1692.55	0.027315663
		285	418.0001	558.23	700.91	847.35	993.79	1138.98	1281.67	1418.10	1548.27	1649.65	1715.98	1751.03	1753.53	0.026365626
		290	425.3334	577.99	725.72	877.35	1028.97	1179.30	1327.03	1468.29	1603.07	1708.04	1776.72	1813.01	1815.60	0.025464304
		295	432.6668	598.09	750.96	907.86	1064.76	1220.31	1373.19	1519.36	1658.82	1767.44	1838.52	1876.06	1878.75	0.024608423
		300	440.0001	618.53	776.63	938.90	1101.16	1262.03	1420.13	1571.30	1715.53	1827.86	1901.37	1940.20	1942.97	0.023794978

50000 ft			ρ	0.187 kg/m^3		0.000363 lb/ft^3										
Re ≈ 60000			C_l	0.446	0.552	0.665	0.779	0.898	1.018	1.122	1.219	1.298	1.357	1.165	1.16	C_l
α	C_l	V(mph)	V(ft/s)	Lift(lb)	Lift(lb)	Lift(lb)	Lift(lb)	Lift(lb)	Lift(lb)	Lift(lb)	Lift(lb)	Lift(lb)	Lift(lb)	Lift(lb)	Lift(lb)	Required
0	0.446	30	44.00	2.11	2.61	3.14	3.68	4.24	4.81	5.30	5.76	6.13	6.41	5.50	5.48	6.985798254
1	0.552	35	51.33	2.87	3.55	4.28	5.01	5.77	6.55	7.21	7.84	8.35	8.73	7.49	7.46	5.132423207
2	0.665	40	58.67	3.75	4.64	5.58	6.54	7.54	8.55	9.42	10.24	10.90	11.40	9.78	9.74	3.929511518
3	0.779	45	66.00	4.74	5.87	7.07	8.28	9.54	10.82	11.93	12.96	13.80	14.42	12.38	12.33	3.104799224
4	0.898	50	73.33	5.85	7.24	8.73	10.22	11.78	13.36	14.72	16.00	17.03	17.81	15.29	15.22	2.514887372
5	1.018	55	80.67	7.08	8.76	10.56	12.37	14.26	16.16	17.81	19.35	20.61	21.55	18.50	18.42	2.078419315
6	1.122	60	88.00	8.43	10.43	12.57	14.72	16.97	19.24	21.20	23.03	24.53	25.64	22.01	21.92	1.746449564
7	1.219	65	95.33	9.89	12.24	14.75	17.28	19.91	22.58	24.88	27.03	28.78	30.09	25.83	25.72	1.488099036
8	1.298	70	102.67	11.47	14.20	17.10	20.03	23.10	26.18	28.86	31.35	33.38	34.90	29.96	29.83	1.283105802
9	1.357	75	110.00	13.17	16.30	19.63	23.00	26.51	30.06	33.13	35.99	38.32	40.06	34.40	34.25	1.117727721
10	1.165	80	117.33	14.98	18.54	22.34	26.17	30.17	34.20	37.69	40.95	43.60	45.58	39.13	38.97	0.98237788
10.5	1.16	85	124.67	16.91	20.93	25.22	29.54	34.05	38.60	42.55	46.23	49.22	51.46	44.18	43.99	0.870203243
		90	132.00	18.96	23.47	28.27	33.12	38.18	43.28	47.70	51.83	55.18	57.69	49.53	49.32	0.776199806
C_{l_max}	1.357	95	139.33	21.13	26.15	31.50	36.90	42.54	48.22	53.15	57.74	61.49	64.28	55.19	54.95	0.696644701
		100	146.67	23.41	28.97	34.90	40.89	47.13	53.43	58.89	63.98	68.13	71.23	61.15	60.89	0.628721843
		105	154.00	25.81	31.94	38.48	45.08	51.96	58.91	64.93	70.54	75.11	78.53	67.42	67.13	0.570269245
		110	161.33	28.33	35.06	42.23	49.47	57.03	64.65	71.26	77.42	82.44	86.18	73.99	73.67	0.519604829
		115	168.67	30.96	38.32	46.16	54.07	62.33	70.66	77.88	84.62	90.10	94.20	80.87	80.52	0.47540404
		120	176.00	33.71	41.72	50.26	58.88	67.87	76.94	84.80	92.13	98.11	102.56	88.05	87.68	0.436612391
		125	183.33	36.58	45.27	54.54	63.89	73.65	83.49	92.02	99.97	106.45	111.29	95.54	95.13	0.402381979
		130	190.67	39.56	48.96	58.99	69.10	79.66	90.30	99.53	108.13	115.14	120.37	103.34	102.90	0.372024759
		135	198.00	42.66	52.80	63.61	74.52	85.90	97.38	107.33	116.61	124.16	129.81	111.44	110.96	0.344977692
		140	205.33	45.88	56.79	68.41	80.14	92.38	104.73	115.43	125.41	133.53	139.60	119.85	119.34	0.32077645
		145	212.67	49.22	60.92	73.39	85.97	99.10	112.34	123.82	134.52	143.24	149.75	128.56	128.01	0.299035359
		150	220.00	52.67	65.19	78.53	92.00	106.05	120.22	132.50	143.96	153.29	160.26	137.58	136.99	0.27943193
		155	227.3334	56.24	69.61	83.86	98.23	113.24	128.37	141.49	153.72	163.68	171.12	146.91	146.28	0.261694836
		160	234.6667	59.93	74.17	89.35	104.67	120.66	136.79	150.76	163.79	174.41	182.34	156.54	155.87	0.24559447
		165	242.0001	63.73	78.88	95.03	111.32	128.32	145.47	160.33	174.19	185.48	193.91	166.48	165.76	0.230935479
		170	249.3334	67.65	83.73	100.87	118.17	136.22	154.42	170.19	184.91	196.89	205.84	176.72	175.96	0.217550811
		175	256.6667	71.69	88.73	106.89	125.22	144.35	163.64	180.35	195.95	208.64	218.13	187.27	186.46	0.205296928
		180	264.0001	75.85	93.87	113.09	132.48	152.71	173.12	190.81	207.30	220.74	230.77	198.12	197.27	0.194049952
		185	271.3334	80.12	99.16	119.46	139.94	161.32	182.87	201.55	218.98	233.17	243.77	209.28	208.38	0.183702511
		190	278.6667	84.51	104.59	126.00	147.60	170.15	192.89	212.60	230.98	245.94	257.12	220.74	219.80	0.174161175
		195	286.0001	89.01	110.17	132.72	155.48	179.23	203.18	223.93	243.29	259.06	270.83	232.51	231.52	0.165344337
		200	293.3334	93.64	115.89	139.62	163.55	188.53	213.73	235.56	255.93	272.51	284.90	244.59	243.54	0.157180461
		205	300.6667	98.38	121.76	146.68	171.83	198.08	224.55	247.49	268.89	286.31	299.32	256.97	255.87	0.149606625
		210	308.0001	103.24	127.77	153.93	180.31	207.86	235.64	259.71	282.16	300.45	314.10	269.66	268.50	0.142567311
		215	315.3334	108.21	133.93	161.34	189.00	217.88	246.99	272.22	295.76	314.92	329.24	282.66	281.44	0.136013379
		220	322.6668	113.30	140.23	168.94	197.90	228.13	258.61	285.03	309.67	329.74	344.73	295.96	294.69	0.129901207
		225	330.0001	118.51	146.68	176.70	206.99	238.61	270.50	298.14	323.91	344.90	360.58	309.56	308.23	0.124191969
		230	337.3334	123.84	153.27	184.64	216.30	249.34	282.66	311.53	338.47	360.40	376.78	323.47	322.08	0.11885101
		235	344.6668	129.28	160.00	192.76	225.80	260.30	295.08	325.23	353.34	376.24	393.34	337.69	336.24	0.113847323
		240	352.0001	134.84	166.88	201.05	235.51	271.49	307.77	339.21	368.54	392.42	410.26	352.21	350.70	0.109153098
		245	359.3334	140.51	173.91	209.51	245.43	282.92	320.73	353.49	384.05	408.94	427.53	367.04	365.46	0.104743331
		250	366.6668	146.31	181.08	218.15	255.55	294.59	333.95	368.07	399.89	425.80	445.16	382.17	380.53	0.100595495
		255	374.0001	152.22	188.40	226.96	265.87	306.49	347.44	382.94	416.04	443.01	463.14	397.61	395.91	0.096689249
		260	381.3334	158.25	195.86	235.95	276.40	318.62	361.20	398.10	432.52	460.55	481.48	413.36	411.59	0.09300619
		265	388.6668	164.39	203.46	245.11	287.13	331.00	375.23	413.56	449.31	478.43	500.18	429.41	427.57	0.089529632
		270	396.0001	170.65	211.21	254.45	298.07	343.60	389.52	429.31	466.43	496.66	519.23	445.77	443.85	0.086244423
		275	403.3334	177.03	219.11	263.96	309.21	356.45	404.08	445.36	483.87	515.22	538.64	462.43	460.45	0.083136773
		280	410.6668	183.53	227.15	273.65	320.56	369.53	418.91	461.70	501.62	534.13	558.41	479.40	477.34	0.080194113
		285	418.0001	190.14	235.33	283.51	332.11	382.84	434.00	478.34	519.70	553.38	578.53	496.67	494.54	0.077404967
		290	425.3334	196.87	243.66	293.54	343.87	396.39	449.36	495.27	538.09	572.96	599.01	514.25	512.05	0.07475884
		295	432.6668	203.72	252.14	303.75	355.83	410.18	464.99	512.50	556.81	592.89	619.84	532.14	529.86	0.072246118
		300	440.0001	210.68	260.76	314.14	367.99	424.20	480.89	530.02	575.84	613.16	641.03	550.33	547.97	0.069857983

75000 ft			ρ	0.027 kg/m^3	0.000108 lb/ft^3											
Re ≈ 17600			C_l	0.419	0.534	0.644	0.752	0.865	0.99	1.09	1.169	1.18	1.2	1.165	1.177	C_l
α	C_l	V(mph)	V(ft/s)	Lift(lb)	Lift(lb)	Lift(lb)	Lift(lb)	Lift(lb)	Lift(lb)	Lift(lb)	Lift(lb)	Lift(lb)	Lift(lb)	Lift(lb)	Lift(lb)	Required
0	0.419	30	44.00001	0.59	0.75	0.90	1.05	1.21	1.39	1.53	1.64	1.65	1.68	1.63	1.65	23.53505962
1	0.534	35	51.33335	0.80	1.02	1.23	1.44	1.65	1.89	2.08	2.23	2.25	2.29	2.22	2.25	17.29106421
2	0.644	40	58.66668	1.04	1.33	1.61	1.87	2.16	2.47	2.72	2.91	2.94	2.99	2.90	2.93	13.23847104
3	0.752	45	66.00002	1.32	1.68	2.03	2.37	2.73	3.12	3.44	3.69	3.72	3.79	3.68	3.71	10.4600265
4	0.865	50	73.33335	1.63	2.08	2.51	2.93	3.37	3.86	4.25	4.55	4.60	4.67	4.54	4.58	8.472621463
5	0.99	55	80.66669	1.97	2.52	3.04	3.54	4.08	4.67	5.14	5.51	5.56	5.66	5.49	5.55	7.002166498
6	1.09	60	88.00002	2.35	3.00	3.61	4.22	4.85	5.55	6.11	6.56	6.62	6.73	6.53	6.60	5.883764905
7	1.169	65	95.33336	2.76	3.51	4.24	4.95	5.69	6.52	7.17	7.69	7.77	7.90	7.67	7.75	5.013385481
8	1.18	70	102.6667	3.20	4.08	4.92	5.74	6.60	7.56	8.32	8.92	9.01	9.16	8.89	8.99	4.322766052
9	1.2	75	110	3.67	4.68	5.64	6.59	7.58	8.68	9.55	10.24	10.34	10.52	10.21	10.31	3.765609539
10	1.165	80	117.3334	4.18	5.32	6.42	7.50	8.62	9.87	10.87	11.66	11.77	11.97	11.62	11.74	3.309617759
10.5	1.177	85	124.6667	4.72	6.01	7.25	8.46	9.74	11.14	12.27	13.16	13.28	13.51	13.11	13.25	2.931702928
		90	132	5.29	6.74	8.13	9.49	10.92	12.49	13.76	14.75	14.89	15.14	14.70	14.85	2.615006624
C_{l_max}	1.2	95	139.3334	5.89	7.51	9.06	10.57	12.16	13.92	15.33	16.44	16.59	16.87	16.38	16.55	2.346986555
		100	146.6667	6.53	8.32	10.03	11.72	13.48	15.42	16.98	18.21	18.38	18.70	18.15	18.34	2.118155366
		105	154	7.20	9.17	11.06	12.92	14.86	17.00	18.72	20.08	20.27	20.61	20.01	20.22	1.921229357
		110	161.3334	7.90	10.07	12.14	14.18	16.31	18.66	20.55	22.04	22.24	22.62	21.96	22.19	1.750541624
		115	168.6667	8.63	11.00	13.27	15.49	17.82	20.40	22.46	24.09	24.31	24.72	24.00	24.25	1.601629766
		120	176	9.40	11.98	14.45	16.87	19.41	22.21	24.45	26.23	26.47	26.92	26.14	26.41	1.470941226
		125	183.3334	10.20	13.00	15.68	18.31	21.06	24.10	26.53	28.46	28.72	29.21	28.36	28.65	1.355619434
		130	190.6667	11.03	14.06	16.96	19.80	22.78	26.07	28.70	30.78	31.07	31.60	30.67	30.99	1.25334637
		135	198.0001	11.90	15.16	18.29	21.35	24.56	28.11	30.95	33.19	33.50	34.07	33.08	33.42	1.162225166
		140	205.3334	12.79	16.31	19.67	22.96	26.41	30.23	33.28	35.70	36.03	36.64	35.57	35.94	1.080691513
		145	212.6667	13.72	17.49	21.09	24.63	28.33	32.43	35.70	38.29	38.65	39.31	38.16	38.55	1.007446072
		150	220.0001	14.69	18.72	22.57	26.36	30.32	34.70	38.21	40.98	41.36	42.06	40.84	41.26	0.941402385
		155	227.3334	15.68	19.99	24.10	28.15	32.38	37.06	40.80	43.76	44.17	44.92	43.61	44.06	0.881646354
		160	234.6667	16.71	21.30	25.69	29.99	34.50	39.48	43.47	46.62	47.06	47.86	46.46	46.94	0.82740444
		165	242.0001	17.77	22.65	27.32	31.90	36.69	41.99	46.23	49.58	50.05	50.90	49.41	49.92	0.7780185
		170	249.3334	18.87	24.04	29.00	33.86	38.95	44.57	49.08	52.63	53.13	54.03	52.45	52.99	0.732925732
		175	256.6667	19.99	25.48	30.73	35.88	41.27	47.24	52.01	55.78	56.30	57.26	55.59	56.16	0.691642568
		180	264.0001	21.15	26.96	32.51	37.96	43.66	49.97	55.02	59.01	59.56	60.57	58.81	59.41	0.653751656
		185	271.3334	22.34	28.47	34.34	40.10	46.12	52.79	58.12	62.33	62.92	63.99	62.12	62.76	0.618891268
		190	278.6667	23.57	30.03	36.22	42.29	48.65	55.68	61.30	65.75	66.37	67.49	65.52	66.20	0.586746639
		195	286.0001	24.82	31.63	38.15	44.55	51.24	58.65	64.57	69.25	69.90	71.09	69.02	69.73	0.557042831
		200	293.3334	26.11	33.28	40.13	46.86	53.91	61.70	67.93	72.85	73.54	74.78	72.60	73.35	0.529538841
		205	300.6667	27.43	34.96	42.16	49.24	56.63	64.82	71.37	76.54	77.26	78.57	76.28	77.06	0.504022693
		210	308.0001	28.79	36.69	44.25	51.67	59.43	68.02	74.89	80.32	81.07	82.45	80.04	80.87	0.480307339
		215	315.3334	30.17	38.46	46.38	54.16	62.29	71.30	78.50	84.19	84.98	86.42	83.90	84.76	0.458227229
		220	322.6668	31.59	40.27	48.56	56.70	65.23	74.65	82.19	88.15	88.98	90.49	87.85	88.75	0.437635406
		225	330.0001	33.05	42.12	50.79	59.31	68.22	78.08	85.97	92.20	93.07	94.65	91.89	92.83	0.41840106
		230	337.3334	34.53	44.01	53.08	61.98	71.29	81.59	89.83	96.34	97.25	98.90	96.01	97.00	0.400407442
		235	344.6668	36.05	45.94	55.41	64.70	74.42	85.18	93.78	100.58	101.53	103.25	100.23	101.27	0.383550089
		240	352.0001	37.60	47.92	57.79	67.48	77.62	88.84	97.81	104.90	105.89	107.69	104.55	105.62	0.367735307
		245	359.3334	39.18	49.94	60.22	70.32	80.89	92.58	101.93	109.32	110.35	112.22	108.95	110.07	0.352878861
		250	366.6668	40.80	52.00	62.71	73.22	84.23	96.40	106.14	113.83	114.90	116.85	113.44	114.61	0.338904859
		255	374.0001	42.45	54.10	65.24	76.18	87.63	100.29	110.42	118.43	119.54	121.57	118.02	119.24	0.32574477
		260	381.3334	44.13	56.24	67.82	79.20	91.10	104.26	114.80	123.12	124.28	126.38	122.70	123.96	0.313336593
		265	388.6668	45.84	58.42	70.46	82.27	94.64	108.31	119.25	127.90	129.10	131.29	127.46	128.77	0.301624118
		270	396.0001	47.59	60.65	73.14	85.41	98.24	112.44	123.80	132.77	134.02	136.29	132.32	133.68	0.290556292
		275	403.3334	49.37	62.92	75.88	88.60	101.91	116.64	128.42	137.73	139.03	141.38	137.26	138.67	0.28008666
		280	410.6668	51.18	65.22	78.66	91.85	105.65	120.92	133.14	142.79	144.13	146.57	142.30	143.76	0.270172878
		285	418.0001	53.02	67.58	81.50	95.16	109.46	125.28	137.93	147.93	149.32	151.85	147.43	148.94	0.260776284
		290	425.3334	54.90	69.97	84.38	98.53	113.34	129.71	142.82	153.17	154.61	157.23	152.64	154.22	0.251861518
		295	432.6668	56.81	72.40	87.31	101.96	117.28	134.23	147.78	158.49	159.99	162.70	157.95	159.58	0.243396193
		300	440.0001	58.75	74.88	90.30	105.44	121.29	138.81	152.84	163.91	165.46	168.26	163.35	165.03	0.235350596

100000ft			ρ	0.017 kg/m³		0.000033 lb/ft³										
Re ≈ 4000			C_l	0.418	0.526	0.633	0.739	0.844	0.941	0.972	1.039	1.103	1.136	1.165	1.174	C_l
α	C_l	V(mph)	V(ft/s)	Lift(lb)	Lift(lb)	Lift(lb)	Lift(lb)	Lift(lb)	Lift(lb)	Lift(lb)	Lift(lb)	Lift(lb)	Lift(lb)	Lift(lb)	Lift(lb)	Required
0	0.418	30	44.00	0.18	0.23	0.27	0.32	0.36	0.40	0.42	0.45	0.47	0.49	0.50	0.50	76.8437808
1	0.526	35	51.33	0.24	0.31	0.37	0.43	0.49	0.55	0.57	0.61	0.64	0.66	0.68	0.69	56.45665528
2	0.633	40	58.67	0.32	0.40	0.48	0.56	0.64	0.72	0.74	0.79	0.84	0.87	0.89	0.90	43.2246267
3	0.739	45	66.00	0.40	0.51	0.61	0.71	0.82	0.91	0.94	1.00	1.07	1.10	1.13	1.13	34.15279147
4	0.844	50	73.33	0.50	0.63	0.76	0.88	1.01	1.12	1.16	1.24	1.32	1.36	1.39	1.40	27.66376109
5	0.941	55	80.67	0.60	0.76	0.91	1.07	1.22	1.36	1.40	1.50	1.59	1.64	1.68	1.69	22.86261247
6	0.972	60	88.00	0.72	0.90	1.09	1.27	1.45	1.62	1.67	1.78	1.89	1.95	2.00	2.02	19.2109452
7	1.039	65	95.33	0.84	1.06	1.28	1.49	1.70	1.90	1.96	2.09	2.22	2.29	2.35	2.37	16.3690894
8	1.103	70	102.67	0.98	1.23	1.48	1.73	1.97	2.20	2.27	2.43	2.58	2.66	2.72	2.74	14.11416382
9	1.136	75	110.00	1.12	1.41	1.70	1.98	2.27	2.53	2.61	2.79	2.96	3.05	3.13	3.15	12.29500493
10	1.165	80	117.33	1.28	1.61	1.93	2.26	2.58	2.87	2.97	3.17	3.37	3.47	3.56	3.59	10.80615667
10.5	1.174	85	124.67	1.44	1.81	2.18	2.55	2.91	3.24	3.35	3.58	3.80	3.92	4.02	4.05	9.57223567
		90	132.00	1.62	2.03	2.45	2.86	3.26	3.64	3.76	4.02	4.26	4.39	4.50	4.54	8.538197866
C_{l_max}	1.174	95	139.33	1.80	2.27	2.73	3.18	3.63	4.05	4.19	4.47	4.75	4.89	5.02	5.06	7.663091714
		100	146.67	1.99	2.51	3.02	3.53	4.03	4.49	4.64	4.96	5.26	5.42	5.56	5.60	6.915940272
		105	154.00	2.20	2.77	3.33	3.89	4.44	4.95	5.11	5.47	5.80	5.98	6.13	6.18	6.272961698
		110	161.33	2.41	3.04	3.65	4.27	4.87	5.43	5.61	6.00	6.37	6.56	6.73	6.78	5.715653117
		115	168.67	2.64	3.32	3.99	4.66	5.33	5.94	6.13	6.56	6.96	7.17	7.35	7.41	5.22944444
		120	176.00	2.87	3.61	4.35	5.08	5.80	6.47	6.68	7.14	7.58	7.81	8.00	8.07	4.8027363
		125	183.33	3.12	3.92	4.72	5.51	6.29	7.02	7.25	7.75	8.22	8.47	8.69	8.75	4.426201774
		130	190.67	3.37	4.24	5.10	5.96	6.81	7.59	7.84	8.38	8.89	9.16	9.39	9.47	4.09227235
		135	198.00	3.64	4.57	5.50	6.43	7.34	8.18	8.45	9.04	9.59	9.88	10.13	10.21	3.794754607
		140	205.33	3.91	4.92	5.92	6.91	7.89	8.80	9.09	9.72	10.32	10.62	10.90	10.98	3.528540955
		145	212.67	4.19	5.28	6.35	7.41	8.47	9.44	9.75	10.42	11.07	11.40	11.69	11.78	3.289388952
		150	220.00	4.49	5.65	6.80	7.93	9.06	10.10	10.44	11.15	11.84	12.20	12.51	12.60	3.073751232
		155	227.33	4.79	6.03	7.26	8.47	9.68	10.79	11.14	11.91	12.64	13.02	13.36	13.46	2.878643193
		160	234.67	5.11	6.43	7.73	9.03	10.31	11.49	11.87	12.69	13.47	13.88	14.23	14.34	2.701539169
		165	242.00	5.43	6.83	8.22	9.60	10.96	12.22	12.63	13.50	14.33	14.76	15.13	15.25	2.540290274
		170	249.33	5.76	7.25	8.73	10.19	11.64	12.98	13.40	14.33	15.21	15.67	16.07	16.19	2.393058918
		175	256.67	6.11	7.69	9.25	10.80	12.33	13.75	14.20	15.18	16.12	16.60	17.02	17.16	2.258266211
		180	264.00	6.46	8.13	9.79	11.42	13.05	14.55	15.03	16.06	17.05	17.56	18.01	18.15	2.134549467
		185	271.33	6.83	8.59	10.34	12.07	13.78	15.37	15.87	16.97	18.01	18.55	19.03	19.17	2.020727618
		190	278.67	7.20	9.06	10.90	12.73	14.54	16.21	16.74	17.90	19.00	19.57	20.07	20.22	1.915772928
		195	286.00	7.58	9.54	11.49	13.41	15.31	17.07	17.64	18.85	20.01	20.61	21.14	21.30	1.818787711
		200	293.33	7.98	10.04	12.08	14.10	16.11	17.96	18.55	19.83	21.05	21.68	22.24	22.41	1.728985068
		205	300.67	8.38	10.55	12.69	14.82	16.92	18.87	19.49	20.83	22.12	22.78	23.36	23.54	1.645672878
		210	308.00	8.80	11.07	13.32	15.55	17.76	19.80	20.45	21.86	23.21	23.90	24.51	24.70	1.568240424
		215	315.33	9.22	11.60	13.96	16.30	18.62	20.76	21.44	22.92	24.33	25.06	25.70	25.89	1.496147165
		220	322.67	9.65	12.15	14.62	17.07	19.49	21.73	22.45	24.00	25.47	26.24	26.91	27.11	1.428913279
		225	330.00	10.10	12.71	15.29	17.85	20.39	22.73	23.48	25.10	26.64	27.44	28.14	28.36	1.366111659
		230	337.33	10.55	13.28	15.98	18.65	21.30	23.75	24.53	26.23	27.84	28.67	29.41	29.63	1.30736111
		235	344.67	11.01	13.86	16.68	19.47	22.24	24.80	25.61	27.38	29.07	29.93	30.70	30.94	1.252320556
		240	352.00	11.49	14.46	17.40	20.31	23.20	25.86	26.71	28.56	30.32	31.22	32.02	32.27	1.200684075
		245	359.33	11.97	15.07	18.13	21.17	24.17	26.95	27.84	29.76	31.59	32.54	33.37	33.63	1.152176638
		250	366.67	12.47	15.69	18.88	22.04	25.17	28.06	28.99	30.99	32.89	33.88	34.74	35.01	1.106550443
		255	374.00	12.97	16.32	19.64	22.93	26.19	29.20	30.16	32.24	34.22	35.25	36.15	36.43	1.063581741
		260	381.33	13.48	16.97	20.42	23.84	27.22	30.35	31.35	33.51	35.58	36.64	37.58	37.87	1.023068088
		265	388.67	14.01	17.63	21.21	24.76	28.28	31.53	32.57	34.82	36.96	38.07	39.04	39.34	0.984825955
		270	396.00	14.54	18.30	22.02	25.71	29.36	32.73	33.81	36.14	38.37	39.52	40.52	40.84	0.948688652
		275	403.33	15.08	18.98	22.84	26.67	30.46	33.96	35.07	37.49	39.80	40.99	42.04	42.36	0.914504499
		280	410.67	15.64	19.68	23.68	27.65	31.57	35.20	36.36	38.87	41.26	42.50	43.58	43.92	0.882135239
		285	418.00	16.20	20.39	24.53	28.64	32.71	36.47	37.67	40.27	42.75	44.03	45.15	45.50	0.851454635
		290	425.33	16.77	21.11	25.40	29.66	33.87	37.76	39.01	41.69	44.26	45.59	46.75	47.11	0.822347238
		295	432.67	17.36	21.84	26.29	30.69	35.05	39.07	40.36	43.14	45.80	47.17	48.38	48.75	0.794707299
		300	440.00	17.95	22.59	27.18	31.74	36.24	40.41	41.74	44.62	47.37	48.78	50.03	50.42	0.768437808
		305	447.33	18.55	23.35	28.10	32.80	37.46	41.77	43.14	46.12	48.96	50.42	51.71	52.11	0.74344964
		310	454.67	19.17	24.12	29.03	33.89	38.70	43.15	44.57	47.64	50.58	52.09	53.42	53.83	0.719660798
		315	462.00	19.79	24.90	29.97	34.99	39.96	44.55	46.02	49.19	52.22	53.79	55.16	55.58	0.696995744
		320	469.33	20.42	25.70	30.93	36.11	41.24	45.98	47.49	50.77	53.89	55.51	56.92	57.36	0.675384792
		325	476.67	21.07	26.51	31.90	37.25	42.54	47.43	48.99	52.37	55.59	57.25	58.72	59.17	0.654763576
		330	484.00	21.72	27.33	32.89	38.40	43.86	48.90	50.51	53.99	57.31	59.03	60.54	61.00	0.635072569
		335	491.33	22.38	28.17	33.90	39.57	45.20	50.39	52.05	55.64	59.06	60.83	62.38	62.87	0.616256652
		340	498.67	23.06	29.01	34.92	40.76	46.55	51.91	53.62	57.31	60.84	62.66	64.26	64.76	0.598264729
		345	506.00	23.74	29.87	35.95	41.97	47.93	53.44	55.20	59.01	62.64	64.52	66.16	66.68	0.581049382
		350	513.33	24.43	30.75	37.00	43.20	49.33	55.00	56.82	60.73	64.47	66.40	68.10	68.62	0.564566553
		355	520.67	25.14	31.63	38.06	44.44	50.75	56.59	58.45	62.48	66.33	68.31	70.06	70.60	0.548775265
		360	528.00	25.85	32.53	39.14	45.70	52.19	58.19	60.11	64.25	68.21	70.25	72.04	72.60	0.533637367
		365	535.33	26.57	33.44	40.24	46.98	53.65	59.82	61.79	66.05	70.12	72.21	74.06	74.63	0.519117303
		370	542.67	27.31	34.36	41.35	48.27	55.13	61.47	63.49	67.87	72.05	74.21	76.10	76.69	0.505181904
		375	550.00	28.05	35.29	42.47	49.59	56.63	63.14	65.22	69.72	74.01	76.23	78.17	78.78	0.491800197
		380	557.33	28.80	36.24	43.61	50.92	58.15	64.84	66.97	71.59	76.00	78.27	80.27	80.89	0.478943232
		385	564.67	29.56	37.20	44.77	52.27	59.69	66.55	68.75	73.49	78.01	80.35	82.40	83.03	0.466583928
		390	572.00	30.34	38.17	45.94	53.63	61.25	68.29	70.54	75.41	80.05	82.45	84.55	85.20	0.454696928
		395	579.33	31.12	39.16	47.13	55.02	62.83	70.06	72.36	77.35	82.12	84.57	86.73	87.40	0.44325847
		400	586.67	31.91	40.16	48.33	56.42	64.44	71.84	74.21	79.32	84.21	86.73	88.94	89.63	0.432246267
		405	594.00	32.72	41.17	49.54	57.84	66.06	73.65	76.07	81.32	86.33	88.91	91.18	91.88	0.421639401
		410	601.33	33.53	42.19	50.77	59.28	67.70	75.48	77.96	83.34	88.47	91.12	93.45	94.17	0.41141822

APPENDIX 2

MathCAD spreadsheet calculating environment, aerodynamic, performance and stability characteristics

The Following calculations are environmental, aerodynamic, performance, and stability calculations for a glider style aircraft. The original idea to have a glider that could fly at altitudes up to 100K ft is pursued in this spreadsheet. Part of the requirements was that the plane needed to fly straight and level at altitudes up to 100K ft. In the performance section of each spreadsheet the highlighted velocity for the higher altitudes is the reason for abandoning the idea of a small glider. The velocities that the glider needed to fly at to be able to create enough lift to fly level were too high to be reasonable for this project.

Definitions :

$\gamma := 1.4$

ratio of specific heats

$h := 500ft$

altitude

$T_o := 288.15K = 518.67 \cdot R$

standard temperature

$\rho_o := 1.225 \frac{kg}{m^3} = 2.376892 \times 10^{-3} \cdot \frac{slug}{ft^3}$

standard density

$\lambda_T := -6.5 \frac{K}{km}$

temperature lapse rate

$R := 8.31432 \frac{J}{mol \cdot K}$

Gas constant

$MM_{air} := 0.0289644 \frac{kg}{mol}$

Molar Mass of Dry Air

$\mu_o := 1.78938 \cdot 10^{-5} \frac{kg}{m \cdot s}$

Standard Viscosity

$C := 110.4K$

Sutherland's Constant

$Mass := 15kg$

Mass of plane

$W := Mass \cdot g = 33.069 \cdot lbf$

Weight of plane

flight velocity

$b := 236in$

Wing Span

$\lambda_w := 1$

Taper Ratio of wing

$\Lambda := 0deg$

Wing sweep

$\Lambda quarter_chord := 0deg$

Sweep at 1/4 chord

$\Lambda half_chord := 0deg$

Sweep at 1/2 chord

$\Gamma_{tip} := 0$

Wing Dihedral(Γ.tip used if polyhedral wing)

$\Gamma_{root} := 2deg$

$S_w := 1.25m^2$

Wing Area

Distance in the z direction from the wing root quarter chord point to the fuselage centerline

$z_w := 3in$

$t := 14in$

Maximum Fuselage thickness

$t1 := 12in$

Thickness 1/4 down the fuselage

$t2 := 4in$

Thickness 3/4 down the fuselage

$l_f := 89in$

Fuselage Length

$d_f := 14in$

Diameter of fuselage

$w_f := d_f$

Width of Fuselage

$S_{fs} := t \cdot l_f = 1.246 \times 10^3 \cdot in^2$

Side planform area of fuselage

Incidence of the fueslage camber line to the fuselage reference line

$icl := 0$

$c_{HT} := .5$

Tail Volume Coefficients; Raymer p.122

$c_{VT} := .02$

$w_t := 12in$

Width of tail

$h_v := 16in$

Vertical height of tail

$b_h := 30in$

Horizontal length of half of tail

$cbar_t := 12in$

tail mean chord

$S_{HT} := b_h \cdot cbar_t = 360 \cdot in^2$

Horizontal Tail Area

$S_{VT} := h_v \cdot cbar_t = 192 \cdot in^2$

Vertical Tail Area

$$AR_h := \frac{b_h^2}{S_{HT}} = 2.5$$

Aspect Ratio of Tail

$\lambda_t := .8$

Taper ratio of Tail

$x_{cg} := 24in$

Distance from nose to CG

$\eta := 1$

Ratio of dynamic pressures.

Note : For these basic calculations, we assume unity, however, η could be greater or less than unity if the tail surfaces were located in a wake region or if it were in the slip stream of a prop, or exhaust wake of a jet engine.

Aerodynamics :

Wing:

HG 3/12

$toverc_w := 12\%$

Thickness to chord ratio

$x_{tmax} := 35\%$

X position at maximum thickness

$\Lambda_{tmax} := 0$

Sweep at maximum thickness location

$camber := 3\%$

Amount of camber

$x_{cmax} := 50\%$

X position at maximum camber

$c_{lmax} := 1.177$

Maximum lift coefficient

$\alpha_{clmax} := 11deg$

Angle of attack at maximum lift coefficient

$\alpha_{Lo} := -3.75deg$

Angle of attack at zero lift

$c_{lo} := .412$

Lift coefficient at zero angle of attack

$c_{lm} := -.073$

Moment coefficient at zero angle of attack

$c_{l\alpha} := 6.033$

Lift Curve Slope

$i_w := 0rad$

Incidence Angle

$C_{Mac} := -.073$

Tail :

HG 3/12

$toverc_t := 12\%$

Thickness to chord ratio

$x_{tmax.t} := 35\%$

X position at maximum thickness

$\Lambda_{tmax.t} := 0$

Sweep at maximum thickness location

$camber_{t.} := 3\%$

Amount of camber

$x_{cmax.t} := 50\%$

X position at maximum camber

$c_{lmax.t} := 1.177$

Maximum lift coefficient

$\alpha_{clmax.t} := 11deg$

Angle of attack at maximum lift coefficient

$\alpha_{Lo.t} := -3.75deg$

Angle of attack at zero lift

$c_{lo.t} := .412$

Lift coefficient at zero angle of attack

$c_{lm.t} := -.073$

Moment coefficient at zero angle of attack

$c_{l\alpha.t} := 6.033$

Lift Curve Slope

$i_t := 0rad$

Incidence Angle

Calculations :

Conversion Factors_____

$kmol := 1000 \cdot mol$
$kJ := 1000 \cdot J$

Input Variables_____

NSV altitude

Functions_____

$$k_{air}(T) := 0.0241 \cdot \frac{W}{m \cdot K} \cdot \left(\frac{T}{273 \cdot K}\right)^{\frac{3}{2}} \cdot \frac{273 \cdot K + 194 \cdot K}{T + 194 \cdot K}$$

$$\mu_{air}(T) := 1.716 \cdot 10^{-5} \cdot \frac{N \cdot s}{m^2} \cdot \left(\frac{T}{273 \cdot K}\right)^{\frac{3}{2}} \cdot \frac{273 \cdot K + 110.4 \cdot K}{T + 110.4 \cdot K}$$

data :=

	0	1	2	3	4
0	0	288.15	$1.013 \cdot 10^5$	1.225	340.294
1	250	286.525	$9.836 \cdot 10^4$	1.196	339.333
2	500	284.9	$9.546 \cdot 10^4$	1.167	338.37
3	750	283.275	$9.263 \cdot 10^4$	1.139	337.403
4	$1 \cdot 10^3$	281.65	$8.987 \cdot 10^4$	1.112	336.434
5	$1.25 \cdot 10^3$	280.025	$8.718 \cdot 10^4$	1.085	335.462

$data_A := csort(data, 0)$

$X := data_A^{\langle 0 \rangle}$

$Y := data_A^{\langle 1 \rangle}$

$Z := data_A^{\langle 2 \rangle}$

$ZZ := data_A^{\langle 3 \rangle}$

$YZ := data_A^{\langle 4 \rangle}$

$Z_Z := \frac{h}{1m}$

$Z_{Z2} := \frac{h}{1 \cdot km}$

$Z_Z = 152.4$

$\rho_{inf} := linterp(X, ZZ, Z_Z) \frac{kg}{m^3}$

$\rho_{inf} = 2.342 \times 10^{-3} \cdot \frac{slug}{ft^3}$

Density of air at altitude.

$p_{inf} := linterp(X, Z, Z_Z) Pa$

$p_{inf} = 9.952 \times 10^4 Pa$

Pressure of atmosphere at altitude.

$T_{inf} := linterp(X, Y, Z_Z) K$

$T_{inf} = 287.159 K$

Temperature at altitude.

$$a_{inf} := \text{linterp}(X, YZ, Z_Z) \cdot \frac{m}{s}$$

$$a_{inf} = 339.708 \frac{m}{s}$$

Speed of sound at altitude

$$R_{inf} := \frac{p_{inf}}{\rho_{inf} \cdot T_{inf}}$$

$$R_{inf} = 0.287 \cdot \frac{kJ}{kg \cdot K}$$

$$U_{inf} := \left(4.708 \cdot 10^{-7} \cdot Z_{Z2}^{\ 6} - 7.138 \cdot 10^{-5} \cdot Z_{Z2}^{\ 5} + 3.891 \cdot 10^{-3} \cdot Z_{Z2}^{\ 4} - 8.809 \cdot 10^{-2} \cdot Z_{Z2}^{\ 3} + 0.6504 \cdot Z_{Z2}^{\ 2} + 1.571 \cdot Z_{Z2}\right) \cdot \frac{m}{s}$$

$$U_{inf} = 0.254 \frac{m}{s}$$

$$\mu_{air}(T_{inf}) = 1.785 \times 10^{-5} \frac{kg}{m \cdot s}$$

Orginal planned flight velocity used for drag calculations. Higher values here result in higher drag estimates

$$V := 15 \frac{m}{s}$$

Chord Length

$$l := 12in$$

Reynolds Number

$$Re := \frac{(\rho_{inf} \cdot V \cdot l)}{\mu_{air}(T_{inf})} = 3.092 \times 10^{5}$$

$$a_{inf} = 339.708 \cdot \frac{m}{s}$$

Mach Number

$$M := \frac{V}{a_{inf}} = 0.044$$

$$q := .5 \cdot \rho_{inf} \cdot V^2 = 135.817\,Pa$$

Dynamic Pressure

$$cbar_w := \frac{S_w}{b} = 8.21 \cdot in$$

wing Mean Chord

$$c_R := cbar_w = 0.209 \cdot m$$

wing Root Chord

$$AR := \frac{b^2}{S_w} = 28.746$$

Aspect Ratio

$$MAC := \frac{2}{3} \cdot c_R \cdot \frac{1 + \lambda_w + \lambda_w^2}{1 + \lambda_w} = 0.209\,m$$

Mean Aerodynamic Chord and position;

Brandt p. 302

$$y_{MAC} := \frac{b}{6} \cdot \frac{1 + 2\lambda_w}{1 + \lambda_w} = 4.917 \cdot ft$$

$$x_{ac} := y_{MAC} \cdot \tan(\Lambda) + .25MAC = 0.052\,m$$

$$e_o := \frac{2}{2 - AR + \left(4 + AR^2 + \tan(\Lambda)^2\right)^{.5}} = 0.9664$$

Span Efficiency Factor; Brandt p 151 (Wing Only!)

$$k_o := \frac{1}{AR \cdot \pi \cdot e_o} = 0.01146$$

Drag due to lift factor; Brandt p. 130

(Wing Only!)

Length from Wing 1/4 chord to

HT 1/4 chord, same for vertical tail; Raymer p.121

$$l_t := \frac{c_{HT} \cdot cbar_w \cdot S_w}{S_{HT}} = 22.092 \cdot in$$

$$V_H := \frac{l_t \cdot S_{HT}}{S_w \cdot cbar_w} = 0.5$$

Horizontal tail volume ratio; Nelson p. 48

$$V_V := \frac{l_t \cdot S_{VT}}{S_w \cdot b} = 9.277 \times 10^{-3}$$

Vertical tail volume ratio; Nelson p. 76

$$S_{wet} := S_w \cdot 2 = 2.5\,m^2$$

Wet surface area of wing

$$S_{wet.tail} := 2 \cdot (b_h \cdot cbar_t) + 2 \cdot (h_v \cdot cbar_t) = 0.712 \cdot m^2$$

Wet surface area of Tail

$$S_{wet.f} := \pi \cdot d_f \cdot l_f = 2.525\,m^2$$

Wet surface area of the fuselage

$$Re_f := \frac{\rho_{inf} \cdot V \cdot l_f}{\mu_{air}(T_{inf})} = 2.293 \times 10^6$$

Reynolds number of fuselage

Oswald Efficiency Factor; Raymer p. 347

(Entrire Aircraft)

$$e_1 := 1.78(1 - .045 \cdot AR^{.68}) - .64 = 0.354$$

Drag due to lift factor; Raymer p. 347

(Entire Aircraft)

$$k_1 := \frac{1}{(AR \cdot \pi \cdot e_1)} = 0.031$$

Drag calculations

Wing:

From Edward Lan (1997)

$$Re_w := \frac{\rho_{inf} \cdot V \cdot cbar_w}{\mu_{air}(T_{inf})} = 2.115 \times 10^5$$

$$R_{w.f} := (2.5523 \cdot 10^{-25}) \cdot Re_f^{\,3} - 1.3088 \cdot 10^{-16} \cdot Re_f^{\,2} + 3.3404 \cdot 10^{-9} \cdot Re_f + 1.0553 = 1.062$$

$$R_{LS} := -1.8866 \cdot \cos(\Lambda_{tmax})^3 + 3.3674 \cdot \cos(\Lambda_{tmax})^2 - 1.2224 \cdot \cos(\Lambda_{tmax}) + .8136 = 1.072$$

$$c_{fw} := \frac{.455}{(\log(Re_w))^{2.58} \cdot [1 + .0144 \cdot (M)^2]^{.65}} = 6.082 \times 10^{-3}$$

$$cd_{o.w} := R_{w.f} \cdot R_{LS} \cdot c_{fw} \cdot \left(1 + 2 \cdot toverc_w + 100 \cdot toverc_w^{\,4}\right) \cdot \frac{S_{wet}}{S_w} = 0.017$$

Tail:

$$Re_t := \frac{\rho_{inf} \cdot V \cdot cbar_t}{\mu_{air}(T_{inf})} = 3.092 \times 10^5$$

$$R_{LS.t} := -1.8866 \cdot \cos(\Lambda_{tmax})^3 + 3.3674 \cdot \cos(\Lambda_{tmax})^2 - 1.2224 \cdot \cos(\Lambda_{tmax}) + .8136 = 1.072$$

$$c_{f.t} := \frac{.455}{(\log(Re_t))^{2.58} \cdot [1 + .0144 \cdot (M)^2]^{.65}} = 5.622 \times 10^{-3}$$

$$cd_{o.t} := R_{LS.t} \cdot c_{f.t} \cdot \left(1 + 2 \cdot toverc_t + 100 \cdot toverc_t^{\,4}\right) \cdot \frac{S_{wet.tail}}{S_w} = 4.329 \times 10^{-3}$$

Fuselage:

$$c_{f.f} := \frac{.455}{(\log(Re_f))^{2.58} \cdot [1 + .0144 \cdot (M)^2]^{.65}} = 3.846 \times 10^{-3}$$

$$cd_{o.f} := R_{w.f} \cdot c_{f.f} \cdot \left[1 + \left[\frac{60}{\left(\frac{l_f}{d_f}\right)^3}\right] + .025 \cdot \left(\frac{l_f}{d_f}\right)\right] \cdot \frac{S_{wet.f}}{S_w} = 0.011$$

Total zero lift drag

$$Cd_o := cd_{o.w} + cd_{o.t} + cd_{o.f}$$

$$Cd_o = 0.033$$

Performance Power Required

Oswald Efficiency Factor

$$e_1 := 1.78\left(1 - .045 \cdot AR^{.68}\right) - .64 = 0.354$$

Drag due to lift factor

$$k_1 := \frac{1}{AR \cdot \pi \cdot e_1} = 0.031$$

Minimum Power required; Raymer p.518

$$P_R := Cd_o \cdot .5 \cdot \rho_{inf} \cdot V^3 \cdot S_w + \frac{W^2}{\pi \cdot AR \cdot e_1 \cdot .5 \cdot \rho_{inf} \cdot V \cdot S_w} = 0.194 \cdot hp$$

$$S_w = 13.455 \cdot ft^2$$

Velocity for minimum power required; Anderson p.238

$$V_{min} := \sqrt{\left(\frac{2}{\rho_{inf}}\right) \cdot \sqrt{\left(\frac{k_1}{3 \cdot Cd_o}\right)} \cdot \frac{W}{S_w}} = 23.368 \cdot mph$$

Velocity required for minimum drag;Anderson p.214

$$V_{mind} := \sqrt{\frac{\sqrt{4 \cdot Cd_o \cdot k_1}}{\rho_{inf} \cdot Cd_o} \cdot \frac{W}{S_w}} = 30.754 \cdot mph$$

Minimum Thrust/Drag required;Anderson p.214

$$T_{rmin} := W \cdot \sqrt{4 \cdot Cd_o \cdot k_1} = 2.134 \cdot lbf$$

Plot data

$$v := 1mph, 2mph .. 200mph$$

Power required w.r.t. velocity where altitude(ρ) and weight are constant; Raymer p.518

$$p(v) := Cd_o \cdot .5 \cdot \rho_{inf} \cdot v^3 \cdot S_w + \frac{W^2}{\pi \cdot AR \cdot e_1 \cdot .5 \cdot \rho_{inf} \cdot v \cdot S_w}$$

Drag/Thrust required w.r.t. velocity where altitude(ρ) and weight are constant; Anderson p.212

$$d(v) := \frac{1}{2}\cdot\rho_{inf}\cdot v^2\cdot S_w\cdot Cd_o + \frac{2\cdot k_1\cdot W^2}{\rho_{inf}\cdot v^2\cdot S_w}$$

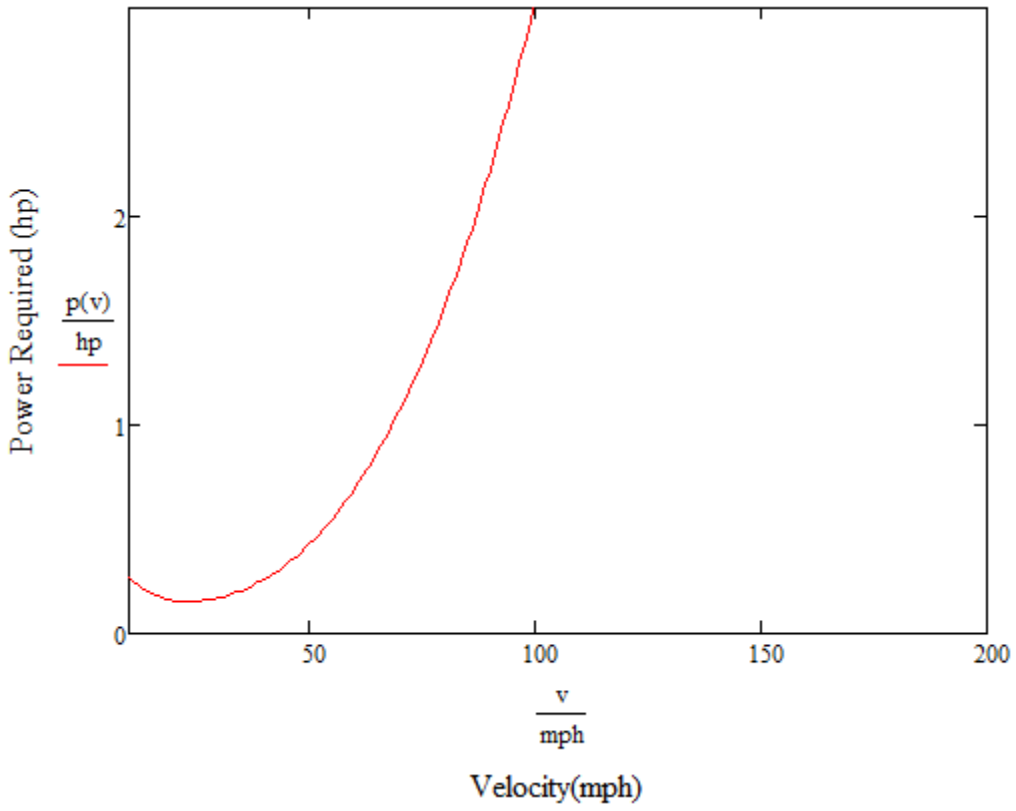

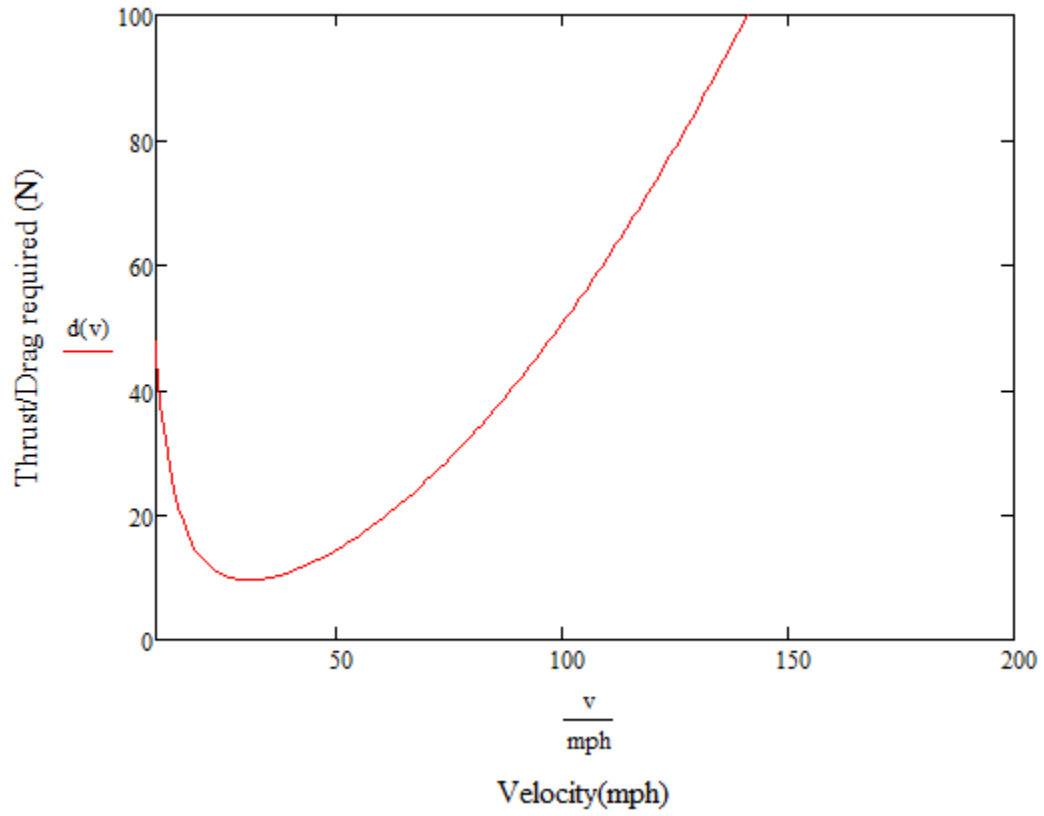

$L := W = 33.069 \cdot lbf$

For Steady level flight, Lift = Weight

$$V_{L_W} := \sqrt{\frac{(2 \cdot L)}{\rho_{inf} \cdot c_{lo} \cdot S_w}} = 48.66 \cdot mph$$

Velocity required for Steady level flight

Aerodynamics

Maximum lift coefficient for aircraft;

Raymer p. 96

$$C_{Lmax.w} := .9 \cdot c_{lmax} = 1.059$$

$$V_{stall} := \sqrt{2 \cdot \frac{W}{\rho_{inf} \cdot S_w \cdot C_{Lmax.w}}} = 30.347 \cdot mph$$

Stall velocity; Anderson p. 254

$$C_L := \frac{W}{q \cdot S_w} = 0.866$$

Lift Coefficient at given flight conditions;

Anderson p. 58

The Following from Raymer p. 311

$$\beta := \sqrt{1 - \left(\frac{V_{min}}{a_{inf}}\right)^2} = 1$$

$$c_{l\alpha r.M} := \frac{c_{l\alpha}}{\beta} = 6.036$$

$$\eta := \frac{c_{l\alpha}}{\left(\frac{2\cdot\pi}{\beta}\right)} = 0.96$$

$$C_{Low} := \frac{2\cdot\pi\, AR}{2 + \sqrt{\frac{\left(AR^2\cdot\beta^2\right)}{\eta^2}\cdot\left(1 + \frac{\tan\left(\Lambda_{tmax}\right)^2}{\beta^2}\right) + 4}} = 5.643\cdot\frac{1}{rad}$$

Wing lift curve slope

or ...

from Brandt p.122

$$C_{l\alpha w} := \frac{c_{l\alpha}}{1 + \frac{c_{l\alpha}}{\pi\cdot e_o\cdot AR}} = 0.098\cdot\frac{1}{deg}$$

Horizontal Tail Lift

The following from Raymer p. 311 with β the same as above

$$\kappa_h := \frac{c_{l\alpha.t}}{\left(\frac{2\cdot\pi}{\beta}\right)} = 0.96$$

$$C_{Lot} := 2\cdot\pi\cdot\frac{AR_h}{2 + \sqrt{AR_h{}^2\cdot\frac{\beta^2}{\kappa_h{}^2}\cdot\left(1 + \frac{\tan\left(\Lambda_{tmax.t}\right)^2}{\beta^2}\right) + 4}} = 2.973\cdot\frac{1}{rad}$$

or ...

from Brandt p.122

$$C_{l\alpha t} := \frac{c_{l\alpha,t}}{1 + \frac{c_{l\alpha,t}}{\pi \cdot e_o \cdot AR_h}} = 3.361 \cdot \frac{1}{rad}$$

Vertical Tail Lift

$$C_{L\alpha v} := 2 \cdot \pi = 6.283$$

Stability Analysis

$$d\varepsilon overd\alpha 1 := \frac{2 \cdot C_{L\alpha w}}{\pi \cdot AR} = 0.125$$

Change in Downwash angle; Nelson p.48

from USAF Stability and Control Datcom

$$h_H := 3.087in$$

$$K_A := \frac{1}{AR} - \frac{1}{1 + AR^{1.7}}$$

$$K_\lambda := \frac{10 - 3 \cdot \lambda_w}{7} = 1$$

$$K_H := \frac{1 - \frac{h_H}{b}}{\left(2 \cdot \frac{l_t}{b}\right)^{\frac{1}{3}}} = 1.725$$

$$d\varepsilon overd\alpha 2 := 4.44\left(K_A \cdot K_\lambda \cdot K_H \cdot \sqrt{\cos(\Lambda quarter_chord)}\right)^{1.19} = 0.139$$

or ...

from Brandt p.154

$$d\varepsilon overd\alpha 3 := \frac{21deg \cdot C_{L\alpha w}}{AR^{.725}} \left(\frac{cbar_w}{l_t}\right)^{.25} \cdot \left(\frac{10 - 3 \cdot \lambda_w}{7}\right) \cdot \left(1 - \frac{4in}{b}\right) = 0.139$$

$$delC_{L\alpha t} := C_{l\alpha t} \cdot (1 - d\varepsilon overd\alpha 3) \cdot \frac{S_{HT}}{S_w}$$

$$C_{L\alpha whole} := C_{L\alpha w} + delC_{L\alpha t} = 6.181$$

Note : The first change in downwash angle is inaccurate due to the fact that it does not take into account the position of the tail plane relative to the wing.

Note : The differences in downwash angle for the second and third method vary because the last is calculated using test results rather than theory which is the method used second

Fuselage Contribution

$\alpha_{0w} := \alpha_{Lo}$

$FR := \frac{l_f}{d_f} = 6.357$

Body fineness ratio

Correction factor for body fineness ratio;

Nelson p.53-54

k2minusk1 := .95

Exact Solutions

$C_{mof} := \frac{1}{36.5 \cdot S_w \cdot cbar_w} \cdot \int_0^{l_f} w_f^2 \cdot (d\varepsilon \text{ overd} \alpha 3)\, dx = 4.179 \times 10^{-3} \cdot \frac{1}{rad}$

Slop of the Pitching Moment Curve; Nelson p.53

$C_{mof} := \frac{k2minusk1}{36.5 \cdot S_w \cdot cbar_w} \cdot \int_0^{l_f} w_f^2 \cdot (\alpha_{0w} + icl)\, dx = -1.868 \times 10^{-3} \cdot \frac{1}{rad}$

Pitching Moment at zero angle of attack; Nelson p.53

.

Approximate solutions using method in Nelson p.53

$$iclsum := \begin{pmatrix} 0 \\ 0 \\ 0 \\ 0 \\ 0 \\ 0 \\ 0 \\ 0 \\ 0 \\ 0 \\ 0 \end{pmatrix}$$

$$xsum := \begin{pmatrix} 3.81818in \\ 3.81818in \\ 3.81818in \\ 3.81818in \\ 3.81818in \\ 3.81818in \\ 3.81818in \\ 3.81818in \\ 3.81818in \\ 3.81818in \\ 3.81818in \end{pmatrix}$$

$\Delta xsum := xsum$

$$C_{mofsum} := \frac{k2minusk1}{36.5 \cdot S_w \cdot cbar_w} \cdot \sum_{a=0}^{10} \left[w_f^{\,2} \cdot \left(\alpha_{0w} + iclsum_a \right) \cdot \Delta xsum_a \right] = -1.539 \times 10^{-5} \cdot \frac{1}{deg}$$

$$C_{mofsum} := \frac{1}{36.5 \cdot S_w \cdot cbar_w} \cdot \left[\sum_{a=0}^{10} \left[w_f^{\,2} \cdot (d\varepsilon \text{ overd}\alpha 3) \cdot \Delta xsum_a \right] \right] = 1.972 \times 10^{-3}$$

Tail Contribution

$$\alpha_w := \frac{C_L \cdot deg}{C_{L\alpha w}} = 2.68 \times 10^{-3}$$

$$\varepsilon_t := d\varepsilon \text{ overd}\alpha 3 \cdot \alpha_w = 3.727 \times 10^{-4}$$

$$C_{L.t} := C_{L\alpha t} \cdot \left(\alpha_w - i_w + i_t - \varepsilon_t \right) = 6.859 \times 10^{-3}$$

Lift coefficient of the tail; Nelson p.48

$$\varepsilon_o := \frac{2 \cdot c_{lo}}{\pi \, AR} = 9.124 \times 10^{-3} \cdot rad$$

$$C_{mot} := V_H \cdot C_{L\alpha t} \cdot (\varepsilon_o + i_w - i_t) = 0.014$$

$$C_{m\alpha t} := -V_H \cdot C_{L\alpha t} \cdot (1 - d\varepsilon \, overd\alpha 3) = -1.28 \cdot \frac{1}{rad}$$

Longitudinal Static Stability

Stick fixed Neutral Point; Nelson p.56

$$x_{np} := \left[\frac{x_{ac}}{cbar_w} - \frac{C_{m\alpha f}}{C_{L\alpha w}} + V_H \cdot \frac{C_{L\alpha t}}{C_{L\alpha w}} \cdot (1 - d\varepsilon \, overd\alpha 3) \right] cbar_w = 3.908 \cdot in$$

$$xbar_{np} := \frac{x_{np}}{cbar_w} = 0.476$$

$$xbar_{ac} := \frac{x_{ac}}{cbar_w} = 0.25$$

$$xbar_{cg} := .25$$

$$SM := (xbar_{np} - xbar_{cg}) = 0.226$$

Static Margin

$$C_{mow} := C_{Mac} + c_{lo} \cdot (xbar_{cg} - xbar_{ac}) = -0.073$$

Total Cmα must be negative to maintain stability, therefore CG must always be ahead of the AC; Nelson p.43

$$C_{M\alpha} := (xbar_{cg} - xbar_{ac}) \cdot C_{L\alpha w} + C_{m\alpha f} - C_{L\alpha t} \cdot (1 - d\varepsilon \, overd\alpha 3) \cdot V_H = -1.276$$

Nelson p.56

$$C_{Mo} := C_{mow} + C_{mof} + \eta \cdot V_H \cdot C_{L\alpha t} \cdot (\varepsilon_o + i_w - i_t) = -0.062$$

Directional Stability

The following from section 2.6 of Nelson

$$\frac{x_{cg}}{l_f} = 0.27$$

$$\frac{l_f^2}{S_{fs}} = 6.357$$

$$\sqrt{\frac{t1}{t2}} = 1.732$$

$$\frac{t}{w_f} = 1$$

$$K_{N1} := .0035$$

From graph on p 75 Nelson

$$Re_f = 2.293 \times 10^6$$

$$K_{R1} := 1.05$$

From graph on p 75 Nelson

$$C_{n\beta_BWtry} := -K_{N1} \cdot K_{R1} \cdot \frac{S_{fs}}{S_w} \cdot \frac{l_f}{b} = -8.913 \times 10^{-4}$$

$$\left(\eta_v(1 + d\sigma overd\beta)\right) := \sigma over\beta$$

η.v = ratio of dynamic pressures Qv/Qw

$$\sigma over\beta := .724 + \frac{3.06 \cdot \frac{S_{VT}}{S_w}}{1 + \cos(\Lambda quarter_chord)} + \frac{.4 \cdot z_w}{d_f} + .009 \cdot AR = 1.22$$

$$C_{n\beta_Vtry} := V_V \cdot c_{l\alpha.t} \cdot \sigma over\beta = 0.068$$

$$C_{n\beta try} := C_{n\beta_Vtry} + C_{n\beta_BWtry} = 0.067$$

For Stability Cnβ msut be positve

Lateral Stability

The following from section B.11 in appendix B; Etkin p.342

$$cl\beta\Gamma_{\Lambda 0} := -.013$$

Fig B.11,3; Etkin p.346

$$cl\beta\Gamma_{partial_full} := 0$$

Fig B.11,3; Etkin p.346

$$cl\beta\Gamma := \frac{AR + 4 \cdot \cos(\Lambda quarter_chord)}{(AR + 4) \cdot \cos(\Lambda quarter_chord)} \cdot cl\beta\Gamma_{\Lambda 0} = -0.013$$

$$cl\beta := cl\beta\Gamma \cdot \left(\Gamma_{root} + cl\beta\Gamma_{partial_full} \cdot \Gamma_{tip}\right) = -4.538 \times 10^{-4}$$

APPENDIX 3

MathCAD spreadsheet to determine environmental model and drag characteristics

Enter Altitude(ASL) for "h" in kilometers

$h := 21.85$

$R_{lifting.gas} := 2077 \frac{J}{kg \cdot K}$

$volume := 159.8ft^3$

$C_{DV} := .004998$

$velocity := 10mph = 4.4704 \frac{m}{s}$

$d := 6ft$

$l := 13ft = 3.9624\,m$

$doverl := \frac{d}{l} = 0.46154$

$T_o := 288.15K$

$P_o := 101325Pa$

$R_w := 461.5 \frac{J}{kg \cdot K}$

$R_a := 287.03 \frac{J}{kg \cdot K}$

$\Delta := 1knot$

$\mu_o := 1.78938 \cdot 10^{-5} \frac{kg}{m \cdot s}$

$\rho_o := \frac{P_o}{R_a \cdot T_o} = 1.2251 \frac{kg}{m^3}$

$\nu := \frac{\mu_o}{\rho_o} = 1.4606 \times 10^{-5} \frac{m^2}{s}$

Sutherland's Constant from Engineering Fluid Mechanics Book

$S := 111K$

$Re_{crit} := 3 \cdot 10^5$

$$\text{mixingratio}(z) := \begin{cases} 10^{\left[\left(\begin{array}{l} -4.42789307\cdot10^{-5}\cdot z^3+5.47755593\cdot10^{-4}\cdot z^2 \ldots \\ +1.87339520\cdot10^{-2}\cdot z-0.429937881 \end{array}\right)^{-1}\right]} & \text{if } 0 \le z < 14 \\ 3.30\cdot10^{-6} & \text{if } 14 \le z \le 18 \\ 10^{\left[\left(\begin{array}{l} 1.15470078\cdot10^{-4}\cdot z^3-7.68205923\cdot10^{-3}\cdot z^2 \ldots \\ +0.164889174\cdot z-1.33503278 \end{array}\right)^{-1}\right]} & \text{if } 18 < z \le 26 \\ 10^{\left[\left(\begin{array}{l} -2.69713488\cdot10^{-7}\cdot z^3 \ldots \\ +5.04990009\cdot10^{-5}\cdot z^2-1.95739140\cdot10^{-3}\cdot z-0.189770892 \end{array}\right)^{-1}\right]} & \text{if } 26 < z \le 80 \end{cases}$$

$$\text{temperature}(z) := \begin{bmatrix} T_o\cdot\left[1-\left(\frac{z}{44.329}\right)\right] & \text{if } 0 \le z < 11 \\ T_o\cdot(0.751865) & \text{if } 11 \le z < 20 \\ T_o\cdot\left(0.682457+\frac{z}{288.136}\right) & \text{if } 20 \le z < 32 \\ T_o\cdot\left(0.482561+\frac{z}{102.906}\right) & \text{if } 32 \le z < 47 \\ T_o\cdot(0.939268) & \text{if } 47 \le z < 51 \\ T_o\cdot\left(1.434843-\frac{z}{102.906}\right) & \text{if } 51 \le z \le 71 \\ \text{"no data"} & \text{otherwise} \end{bmatrix}$$

$$\text{pressure}(z) := \begin{bmatrix} P_o\cdot\left[1-\left(\frac{z}{44.329}\right)\right]^{5.255876} & \text{if } 0 \le z < 11 \\ P_o\cdot(0.223361)\,e^{\left[\frac{(10.999-z)}{6.3414}\right]} & \text{if } 11 \le z < 20 \\ P_o\cdot\left(0.988626+\frac{z}{198.903}\right)^{-34.16319} & \text{if } 20 \le z < 32 \\ P_o\cdot\left(0.898309+\frac{z}{55.280}\right)^{-12.20114} & \text{if } 32 \le z < 47 \\ P_o\cdot(0.00109456)\,e^{\left[\frac{(46.998-z)}{7.922}\right]} & \text{if } 47 \le z < 51 \\ P_o\cdot\left(0.838263-\frac{z}{176.142}\right)^{12.20114} & \text{if } 51 \le z \le 71 \\ \text{"no data"} & \text{otherwise} \end{bmatrix}$$

$$U_{avg.akron}(z) := \begin{cases} \Delta\cdot(0.01782131\cdot z^3 - 0.35733085z^2 \ldots + 6.88269975\cdot z + 7.12532034) & \text{if } .356616 \le z \le 10.356616 \\ \Delta\cdot(0.00086669\cdot z^5 - 0.08523235\cdot z^4 \ldots + 3.30851461\cdot z^3 - 62.87569373\cdot z^2 \ldots + 576.51359007\cdot z - 1962.80017872) & \text{if } 10.356616 < z \le 26.356616 \\ \text{"no data"} & \text{otherwise} \end{cases}$$

$$U_{99\%.akron}(z) := \begin{cases} \Delta\cdot(0.79623226\cdot z^3 - 8.30063464\cdot z^2 \ldots + 31.51053206\cdot z + 15.72373244) & \text{if } 0.356616 \le z \le 6.356616 \\ \Delta\cdot(0.03953700\cdot z^5 - 2.16584021\cdot z^4 \ldots + 46.16431211\cdot z^3 - 479.67673276\cdot z^2 \ldots + 2437.97717466\cdot z - 4753.63837232) & \text{if } 6.356616 < z \le 15.9 \\ \Delta\cdot(-0.02698388\cdot z^4 + 2.28655879\cdot z^3 - 71.26706811\cdot z^2 \ldots + 965.36077448\cdot z - 4735.83256639) & \text{if } 15.9 < z \le 26.356616 \\ \text{"no data"} & \text{otherwise} \end{cases}$$

$$U_{1\%.akron}(z) := \begin{cases} \Delta\cdot(0.00339807\cdot z^5 - 0.07437353\cdot z^4 \ldots + 0.52736950\cdot z^3 - 1.29904286\cdot z^2 \ldots + 1.91955613\cdot z + 0.51781450) & \text{if } 0.356616 \le z \le 10.356616 \\ \Delta\cdot(0.00010253\cdot z^6 - 0.01102002\cdot z^5 \ldots + 0.48255658\cdot z^4 - 10.98302847\cdot z^3 \ldots + 136.52163886\cdot z^2 - 876.36218688\cdot z \ldots + 2281.63196219) & \text{if } 10.356616 < z \le 26.356616 \\ \text{"no data"} & \text{otherwise} \end{cases}$$

$$U_{avg.WS}(z) := \begin{cases} \Delta\cdot(-0.00049959\cdot z^5 + 0.01021943\cdot z^4 - 0.05699801\cdot z^3 \ldots + .16664812\cdot z^2 + 2.77166583\cdot z + 7.16298899) & \text{if } 1.253337 \le z \le 15.253337 \\ \Delta\cdot(0.00134021\cdot z^5 - 0.13807129\cdot z^4 \ldots + 5.59399286\cdot z^3 - 110.81025444\cdot z^2 \ldots + 1065.44818118\cdot z - 3917.67176849) & \text{if } 15.253337 < z \le 27.253337 \\ \text{"no data"} & \text{otherwise} \end{cases}$$

$$U_{99\%.WS}(z) := \begin{cases} \Delta\cdot(0.04057435\cdot z^3 - 0.16932701\cdot z^2 \ldots + 6.51338238\cdot z + 20.85908683) & \text{if } 1.253337 \le z \le 10.2 \\ \Delta\cdot(0.00081275\cdot z^5 - 0.08897265\cdot z^4 \ldots + 3.77165072\cdot z^3 - 76.50348123\cdot z^2 \ldots + 729.54655527\cdot z - 2498.80996659) & \text{if } 10.2 < z \le 27.253337 \\ \text{"no data"} & \text{otherwise} \end{cases}$$

$$U_{1\%.WS}(z) := \begin{cases} \Delta\cdot\left(0.35368099\cdot z^2 - 0.60463183\cdot z + 0.62377315\right) & \text{if } 1.253337 \le z \le 5.253337 \\ \Delta\cdot\left(\begin{array}{l} 0.00431715\cdot z^5 - 0.18992131\cdot z^4 \ldots \\ +3.17516732\cdot z^3 - 24.99080022\cdot z^2 \ldots \\ +92.61955937\cdot z - 125.77291278 \end{array}\right) & \text{if } 5.253337 < z \le 15.253337 \\ \Delta\cdot\left(\begin{array}{l} 0.00117923\cdot z^5 - 0.12058143\cdot z^4 \ldots \\ +4.87068438\cdot z^3 - 96.95241205\cdot z^2 \ldots \\ +948.91263093\cdot z - 3638.01601144 \end{array}\right) & \text{if } 15.253337 < z \le 27.253337 \\ \text{"no data"} & \text{otherwise} \end{cases}$$

$$\rho_{moist.air}(h) := \frac{[(1 + mixingratio(h))\cdot pressure(h)]}{\left[\left(1 + mixingratio(h)\cdot\frac{R_w}{R_a}\right)\cdot R_a\cdot temperature(h)\right]}$$

Assuming constant temperature between air and lifting gas and utilizing the Ideal Gas Law

$$\rho_{lifting.gas}(h) := \frac{\rho_{moist.air}(h)\cdot R_a}{R_{lifting.gas}}$$

Sutherlands Formula

$$\mu(temp) := \mu_o\cdot\left(\frac{T_o + S}{temp + S}\right)\cdot\left(\frac{temp}{T_o}\right)^{\frac{3}{2}}$$

$$\mu(temperature(h)) = 1.43131 \times 10^{-5}\ \frac{kg}{m\cdot s}$$

Generic drag calculation

$$Reynolds(\rho, v, l, \mu) := \frac{\rho\cdot v\cdot l}{\mu}$$

$$Re_{hull} := Reynolds\left(\rho_{moist.air}(h), velocity, 1, \mu(temperature(h))\right) = 8.07856 \times 10^4$$

The following program and graph verify the program works correctly

the graph can be compared with plot in Nunn (pg. 260) and Crowe (pg. 353)

$$C_{f.fa}(xper, Re) := \begin{cases} \text{if } 0 < Re < Re_{crit} \\ \quad C_{f.fa} \leftarrow \dfrac{1.328}{\sqrt{Re}} \\ \quad C_{f.fa} \\ \text{otherwise} \\ \quad xper \leftarrow xper \\ \quad C_{f.fa} \leftarrow \dfrac{.072}{\sqrt[5]{Re}} \quad \text{if } xper \le 0.01 \\ \quad C_{f.fa} \leftarrow \dfrac{1.328}{\sqrt{Re}} \quad \text{if } (xper \ge 0.99) \\ \quad C_{f.fa} \leftarrow \dfrac{.072}{\sqrt[5]{Re}} + \dfrac{Re_{crit}}{Re} \cdot \left(\dfrac{1.328}{\sqrt{Re_{crit}}} - \dfrac{.072}{\sqrt[5]{Re}} \right) \quad \text{if } .01 < xper < .99 \\ \quad C_{f.fa} \end{cases}$$

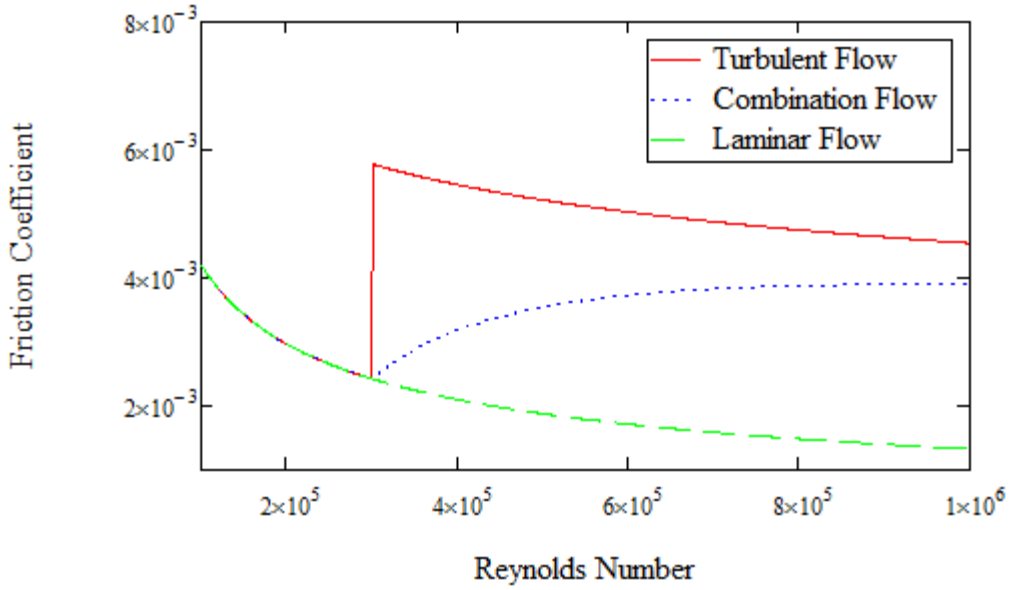

Figure 1. Friction Coefficient vs. Reynolds number

$$C_{f.f}(Re_{hull}) := \begin{cases} \text{if } 0 < Re_{hull} < Re_{crit} \\ \quad \begin{cases} C_{f.f} \leftarrow \dfrac{1.328}{\sqrt{Re_{hull}}} \\ C_{f.f} \end{cases} \\ \text{otherwise} \\ \quad \begin{cases} xper \leftarrow \dfrac{\left[\dfrac{(Re_{crit}\cdot\nu)}{velocity}\right]}{1} \\ C_{f.f} \leftarrow \dfrac{.072}{\sqrt[5]{Re_{hull}}} \quad \text{if } xper < 0.01 \\ C_{f.f} \leftarrow \dfrac{1.328}{\sqrt{Re_{hull}}} \quad \text{if } (xper > 0.99) \\ C_{f.f} \leftarrow \dfrac{.072}{\sqrt[5]{Re_{hull}}} + \dfrac{Re_{crit}}{Re_{hull}}\cdot\left(\dfrac{1.328}{\sqrt{Re_{crit}}} - \dfrac{.072}{\sqrt[5]{Re_{hull}}}\right) \quad \text{if } .01 < xper < .99 \\ C_{f.f} \end{cases} \end{cases}$$

$$c_{fturb}(REY) := \frac{.072}{\sqrt[5]{REY}}$$

$$c_f := C_{f.f}(Re_{hull}) = 0.004672305$$

$$cfturb := c_{fturb}\left(Reynolds\left(\rho_{moist.air}(h), velocity, 1, \mu(temperature(h))\right)\right) = 7.51391 \times 10^{-3}$$

$$c_dv(cft, d_1) := cft\cdot\left[4\cdot\left(\frac{1}{d_1}\right)^{\left(\frac{1}{3}\right)} + 6\cdot(d_1)^{1.2} + 24\cdot(d_1)^{2.7}\right]$$

$$d_1 := 0.000000001, .01 .. 1$$

$$CDV(c_{f1}, d_1) := c_{f1}\cdot\left[4\cdot\left(\frac{1}{d_1}\right)^{\left(\frac{1}{3}\right)} + 6\cdot(d_1)^{1.2} + 24\cdot(d_1)^{2.7}\right]$$

$$Lift(h) := g\cdot volume\cdot\left(\rho_{moist.air}(h) - \rho_{lifting.gas}(h)\right)$$

$$Drag_{user}(h) := .5\cdot\rho_{moist.air}(h)\cdot velocity^2\cdot c_dv(cfturb, doverl)\cdot(volume)^{\frac{2}{3}}$$

$$Re_{h.99\%.a} := \frac{\rho_{moist.air}(h)\cdot U_{99\%.akron}(h)\cdot 1}{\mu(temperature(h))} = 3.24969 \times 10^5$$

$$C_{f.f.99\%.a}\left(Re_{h.99\%.a}\right) := \begin{cases} \text{if } 0 < Re_{h.99\%.a} < Re_{crit} \\ \quad C_{f.f} \leftarrow \dfrac{1.328}{\sqrt{Re_{h.99\%.a}}} \\ \quad C_{f.f} \\ \text{otherwise} \\ \quad xper \leftarrow \dfrac{\left[\dfrac{\left(Re_{crit}\cdot\nu\right)}{U_{99\%.akron}(h)}\right]}{1} \\ \quad C_{f.f} \leftarrow \dfrac{.072}{\sqrt[5]{Re_{h.99\%.a}}} \quad \text{if } xper < 0.01 \\ \quad C_{f.f} \leftarrow \dfrac{1.328}{\sqrt{Re_{h.99\%.a}}} \quad \text{if } (xper > 0.99) \\ \quad C_{f.f} \leftarrow \dfrac{.072}{\sqrt[5]{Re_{h.99\%.a}}} - \dots \quad \text{if } .01 < xper < .99 \\ \qquad + \dfrac{Re_{crit}}{Re_{h.99\%.a}}\cdot\left(\dfrac{1.328}{\sqrt{Re_{crit}}} - \dfrac{.072}{\sqrt[5]{Re_{h.99\%.a}}}\right) \\ \quad C_{f.f} \end{cases}$$

$$c_{fturb.99\%.akron} := \frac{.072}{\sqrt[5]{Re_{h.99\%.a}}}$$

$$c_{f.99\%.akron} := C_{f.f.99\%.a}\left(Re_{h.99\%.a}\right) = 0.002675334$$

$$c_dv_{99\%.akron}(d_1) := c_{fturb.99\%.akron}\cdot\left[4\cdot\left(\frac{1}{d_1}\right)^{\left(\frac{1}{3}\right)} + 6\cdot(d_1)^{1.2} + 24\cdot(d_1)^{2.7}\right]$$

$$c_dv_{99\%.akron}(.46154) = 0.05986$$

$$Lift_{99\%.akron}(h) := g\cdot volume\cdot\left(\rho_{moist.air}(h) - \rho_{lifting.gas}(h)\right)$$

$$Drag_{99\%.akron}(h) := .5\cdot\rho_{moist.air}(h)\cdot U_{99\%.akron}(h)^2\cdot c_dv_{99\%.akron}(.461538)\cdot(volume)^{\frac{2}{3}}$$

Akron 99% Wind Velocity

$$Re_{h.avg.a} := \frac{\rho_{moist.air}(h)\cdot U_{avg.akron}(h)\cdot 1}{\mu(temperature(h))} = 1.70261\times 10^5$$

$$C_{f.f.avg.a}(Re_{h.avg.a}) := \begin{cases} \text{if } 0 < Re_{h.avg.a} < Re_{crit} \\ \quad C_{f.f} \leftarrow \dfrac{1.328}{\sqrt{Re_{h.avg.a}}} \\ \quad C_{f.f} \\ \text{otherwise} \\ \quad xper \leftarrow \dfrac{\left[\dfrac{(Re_{crit}\cdot\nu)}{U_{avg.akron}(h)}\right]}{1} \\ \quad C_{f.f} \leftarrow \dfrac{.072}{\sqrt[5]{Re_{h.avg.a}}} \quad \text{if } xper < 0.01 \\ \quad C_{f.f} \leftarrow \dfrac{1.328}{\sqrt{Re_{h.avg.a}}} \quad \text{if } (xper > 0.99) \\ \quad C_{f.f} \leftarrow \dfrac{.072}{\sqrt[5]{Re_{h.avg.a}}} - \dfrac{Re_{crit}}{Re_{h.avg.a}}\cdot\left(\dfrac{1.328}{\sqrt{Re_{crit}}} - \dfrac{.072}{\sqrt[5]{Re_{h.avg.a}}}\right) \quad \text{if } .01 < xper < .99 \\ \quad C_{f.f} \end{cases}$$

$$c_{fturb.avg.akron} := \frac{.072}{\sqrt[5]{Re_{h.avg.a}}}$$

$$c_{f.avg.akron} := C_{f.f.avg.a}(Re_{h.avg.a}) = 0.003218399$$

$$c_dv_{avg.akron}(d_1) := c_{fturb.avg.akron}\cdot\left[4\cdot\left(\frac{1}{d_1}\right)^{\left(\frac{1}{3}\right)} + 6\cdot(d_1)^{1.2} + 24\cdot(d_1)^{2.7}\right]$$

$$c_dv_{avg.akron}(.46154) = 0.06812$$

$$Drag_{avg.akron}(h) := .5\cdot\rho_{moist.air}(h)\cdot U_{avg.akron}(h)^2\cdot c_dv_{avg.akron}(.461538)\cdot(volume)^{\frac{2}{3}}$$

Akron Average Wind Velocity

$$Re_{h.1\%.a} := \frac{\rho_{moist.air}(h)\cdot U_{1\%.akron}(h)\cdot 1}{\mu(temperature(h))} = 4.14622\times 10^4$$

$$C_{f.f.1\%.a}\left(Re_{h.1\%.akron}\right) := \begin{cases} \text{if } 0 < Re_{h.1\%.a} < Re_{crit} \\ \quad C_{f.f} \leftarrow \dfrac{1.328}{\sqrt{Re_{h.1\%.a}}} \\ \quad C_{f.f} \\ \text{otherwise} \\ \quad xper \leftarrow \dfrac{\left[\dfrac{\left(Re_{crit}\cdot\nu\right)}{U_{1\%.akron}(h)}\right]}{1} \\ \quad C_{f.f} \leftarrow \dfrac{.072}{\sqrt[5]{Re_{h.1\%.a}}} \quad \text{if } xper < 0.01 \\ \quad C_{f.f} \leftarrow \dfrac{1.328}{\sqrt{Re_{h.1\%.a}}} \quad \text{if } (xper > 0.99) \\ \quad C_{f.f} \leftarrow \dfrac{.072}{\sqrt[5]{Re_{h.1\%.a}}} - \ldots \quad \text{if } .01 < xper < .99 \\ \qquad + \dfrac{Re_{crit}}{Re_{h.1\%.a}}\cdot\left(\dfrac{1.328}{\sqrt{Re_{crit}}} - \dfrac{.072}{\sqrt[5]{\sqrt{Re_{h.1\%.a}}}}\right) \\ \quad C_{f.f} \end{cases}$$

$$c_{f.1\%.akron} := C_{f.f}\left(Re_{h.1\%.a}\right) = 0.006521868$$

$$c_{fturb.1\%.akron} := \frac{.072}{\sqrt[5]{Re_{h.1\%.a}}}$$

$$c_dv_{1\%.akron}(d_l) := c_{fturb.1\%.akron}\cdot\left[4\cdot\left(\frac{1}{d_l}\right)^{\left(\frac{1}{3}\right)} + 6\cdot(d_l)^{1.2} + 24\cdot(d_l)^{2.7}\right]$$

$$c_dv_{1\%.akron}(.46154) = 0.09036$$

$$Drag_{1\%.akron}(h) := .5\cdot\rho_{moist.air}(h)\cdot U_{1\%.akron}(h)^2\cdot c_dv_{1\%.akron}(.461538)\cdot(volume)^{\frac{2}{3}}$$

Akron 1% Wind Velocity

$$Re_{h.99.ws} := \frac{\rho_{moist.air}(h)\cdot U_{99\%.WS}(h)\cdot 1}{\mu(temperature(h))} = 2.7869\times 10^5$$

$$C_{f.f.99.ws}(Re_{h.99.ws}) := \begin{cases} \text{if } 0 < Re_{h.99.ws} < Re_{crit} \\ \quad C_{f.f} \leftarrow \dfrac{1.328}{\sqrt{Re_{h.99.ws}}} \\ \quad C_{f.f} \\ \text{otherwise} \\ \quad xper \leftarrow \dfrac{\left[\dfrac{(Re_{crit}\cdot\nu)}{U_{99\%.WS}(h)}\right]}{1} \\ \quad C_{f.f} \leftarrow \dfrac{.072}{\sqrt[5]{Re_{h.99.ws}}} \quad \text{if } xper < 0.01 \\ \quad C_{f.f} \leftarrow \dfrac{1.328}{\sqrt{Re_{h.99.ws}}} \quad \text{if } (xper > 0.99) \\ \quad C_{f.f} \leftarrow \dfrac{.072}{\sqrt[5]{Re_{h.99.ws}}} - \dots \quad \text{if } .01 < xper < .99 \\ \qquad + \dfrac{Re_{crit}}{Re_{h.99.ws}}\cdot\left(\dfrac{1.328}{\sqrt{Re_{crit}}} - \dfrac{.072}{\sqrt[5]{Re_{h.99.ws}}}\right) \\ \quad C_{f.f} \end{cases}$$

$$c_{fturb.99\%.WS} := \frac{.072}{\sqrt[5]{Re_{h.99.ws}}}$$

$$c_{f.99\%.WS} := C_{f.f}(Re_{h.99.ws}) = 0.002515577$$

$$c_dv_{99\%.WS}(d_1) := c_{fturb.99\%.WS}\cdot\left[4\cdot\left(\frac{1}{d_1}\right)^{\left(\frac{1}{3}\right)} + 6\cdot(d_1)^{1.2} + 24\cdot(d_1)^{2.7}\right]$$

$$c_dv_{99\%.WS}(.46154) = 0.06173$$

$$Drag_{99\%.WS}(h) := .5\cdot\rho_{moist.air}(h)\cdot U_{99\%.WS}(h)^2\cdot c_dv_{99\%.WS}(.461538)\cdot(volume)^{\frac{2}{3}}$$

White Sands 99% Wind Velocity

White Sands Average Wind Velocity

$$Re_{h.a.ws} := \frac{\rho_{moist.air}(h)\cdot U_{avg.WS}(h)\cdot 1}{\mu(temperature(h))} = 1.63527\times 10^5$$

$$C_{f.f.avg.WS}(Re_{h.a.ws}) := \begin{cases} \text{if } 0 < Re_{h.a.ws} < Re_{crit} \\ \quad C_{f.f} \leftarrow \dfrac{1.328}{\sqrt{Re_{h.a.ws}}} \\ \quad C_{f.f} \\ \text{otherwise} \\ \quad xper \leftarrow \dfrac{\left[\dfrac{(Re_{crit}\cdot\nu)}{U_{avg.WS}(h)}\right]}{1} \\ \quad C_{f.f} \leftarrow \dfrac{.072}{\sqrt[5]{Re_{h.a.ws}}} \quad \text{if } xper < 0.01 \\ \quad C_{f.f} \leftarrow \dfrac{1.328}{\sqrt{Re_{h.a.ws}}} \quad \text{if } (xper > 0.99) \\ \quad C_{f.f} \leftarrow \dfrac{.072}{\sqrt[5]{Re_{h.a.ws}}} - \dots \quad \text{if } .01 < xper < .99 \\ \qquad + \dfrac{Re_{crit}}{Re_{h.a.ws}} \cdot \left(\dfrac{1.328}{\sqrt{Re_{crit}}} - \dfrac{.072}{\sqrt[5]{Re_{h.a.ws}}} \right) \\ \quad C_{f.f} \end{cases}$$

$$c_{f.avg.WS} := C_{f.f.avg.WS}(Re_{h.a.ws}) = 0.003283997$$

$$c_{fturb.avg.WS} := \frac{.072}{\sqrt[5]{Re_{h.a.ws}}}$$

$$c_dv_{avg.WS}(d_1) := c_{fturb.avg.WS}\cdot\left[4\cdot\left(\frac{1}{d_1}\right)^{\left(\frac{1}{3}\right)} + 6\cdot(d_1)^{1.2} + 24\cdot(d_1)^{2.7}\right]$$

$$c_dv_{avg.WS}(.46154) = 0.06867$$

$$Drag_{avg.WS}(h) := .5\cdot\rho_{moist.air}(h)\cdot U_{avg.WS}(h)^2\cdot c_dv_{avg.WS}(.461538)\cdot(volume)^{\frac{2}{3}}$$

White Sands 1% Wind Velocity

$$Re_{h.1.ws} := \frac{\rho_{moist.air}(h)\cdot U_{1\%.WS}(h)\cdot 1}{\mu(temperature(h))} = 5.98434 \times 10^4$$

$$C_{f.f.1\%.WS}(Re_{h.1.ws}) := \begin{cases} \text{if } 0 < Re_{h.1.ws} < Re_{crit} \\ \quad C_{f.f} \leftarrow \dfrac{1.328}{\sqrt{Re_{h.1.ws}}} \\ \quad C_{f.f} \\ \text{otherwise} \\ \quad xper \leftarrow \dfrac{\left[\dfrac{(Re_{crit}\cdot\nu)}{U_{1\%.WS}(h)}\right]}{1} \\ \quad C_{f.f} \leftarrow \dfrac{.072}{\sqrt[5]{Re_{h.1.ws}}} \quad \text{if } xper < 0.01 \\ \quad C_{f.f} \leftarrow \dfrac{1.328}{\sqrt{Re_{h.1.ws}}} \quad \text{if } (xper > 0.99) \\ \quad C_{f.f} \leftarrow \dfrac{.072}{\sqrt[5]{Re_{h.1.ws}}} - \dots \quad \text{if } .01 < xper < .99 \\ \qquad + \dfrac{Re_{crit}}{Re_{h.1.ws}}\cdot\left(\dfrac{1.328}{\sqrt{Re_{crit}}} - \dfrac{.072}{\sqrt[5]{Re_{h.1.ws}}}\right) \\ \quad C_{f.f} \end{cases}$$

$$c_{f.1\%.WS} := C_{f.f.1\%.WS}(Re_{h.1.ws}) = 0.005428625$$

$$c_{fturb.1\%.WS} := \frac{.072}{\sqrt[5]{Re_{h.1.ws}}}$$

$$c_dv_{1\%.WS}(d_1) := c_{fturb.1\%.WS}\cdot\left[4\cdot\left(\frac{1}{d_1}\right)^{\left(\frac{1}{3}\right)} + 6\cdot(d_1)^{1.2} + 24\cdot(d_1)^{2.7}\right]$$

$$c_dv_{1\%.WS}(.46154) = 0.08397$$

$$Drag_{1\%.WS}(h) := .5\cdot\rho_{moist.air}(h)\cdot U_{1\%.WS}(h)^2\cdot c_dv_{1\%.WS}(.461538)\cdot(volume)^{\frac{2}{3}}$$

$$Drag_{user}(h) = 0.03172\cdot lbf$$

$$Drag_{99\%.akron}(h) = 1.7284969\cdot N$$

$$Drag_{avg.akron}(h) = 0.5399614\cdot N$$

$$Drag_{1\%.akron}(h) = 0.0424744\cdot N$$

$$Drag_{99\%.WS}(h) = 1.3109041\cdot N$$

$$Drag_{avg.WS}(h) = 0.5021299\cdot N$$

$$Drag_{1\%.WS}(h) = 0.082221\cdot N$$

$$\mu(temperature(h)) = 1.43131\times 10^{-5}\ \frac{kg}{m\cdot s}$$

$\omega := \text{mixingratio}(h) = 7.55499 \times 10^{-6}$

$\text{temperature}(h) = 218.50105 \cdot K$

$\text{pressure}(h) = 4.09398 \times 10^{3}\ Pa$

$\rho_{moist.air}(h) = 0.06528 \frac{kg}{m^3}$

$\rho_{lifting.gas}(h) = 9.02099 \times 10^{-3} \frac{kg}{m^3}$

$U_{avg.akron}(h) = 9.42169 \cdot \frac{m}{s}$

$U_{99\%.akron}(h) = 17.98268 \cdot \frac{m}{s}$

$U_{1\%.akron}(h) = 2.29438 \cdot \frac{m}{s}$

$U_{avg.WS}(h) = 9.04905 \cdot \frac{m}{s}$

$U_{99\%.WS}(h) = 15.42175 \cdot \frac{m}{s}$

$U_{1\%.WS}(h) = 3.31153 \cdot \frac{m}{s}$

$\text{Lift}(h) = 0.56121 \cdot lbf$

$\text{Drag}_{user}(h) = 0.03172 \cdot lbf$

$\text{Power} := \text{Drag}_{user}(h) \cdot \text{velocity} = 0.63081\ W$

$v := 0mph, 1mph .. 135mph$

$c := 0.1, .011 .. .03$

for equation see paper by Dorrington

and performance book by Anderson

$$p_{cdv}(v,c) := \frac{1}{2} \cdot \rho_{moist.air}(h) \cdot v^3 \cdot c \cdot \left[\text{volume}\left(\frac{2}{3}\right) \right]$$

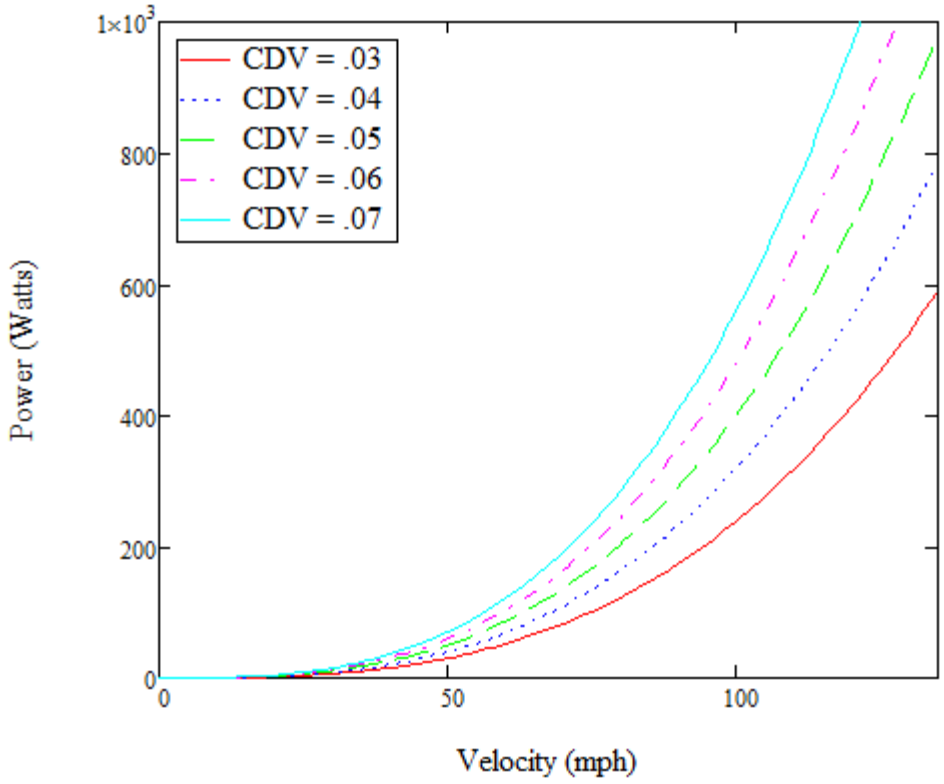

Figure 2. Power as a function of Velocity

alt := 0, .01.. 70

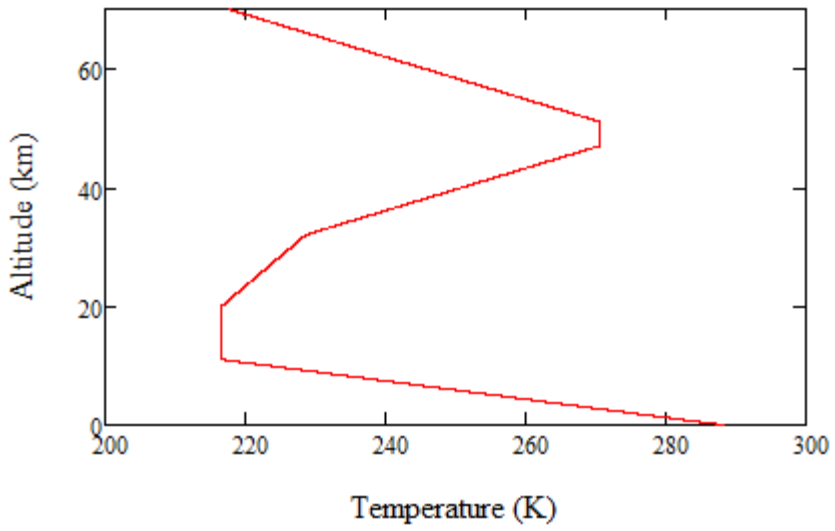

Figure 3.Temperature as a function of altitude

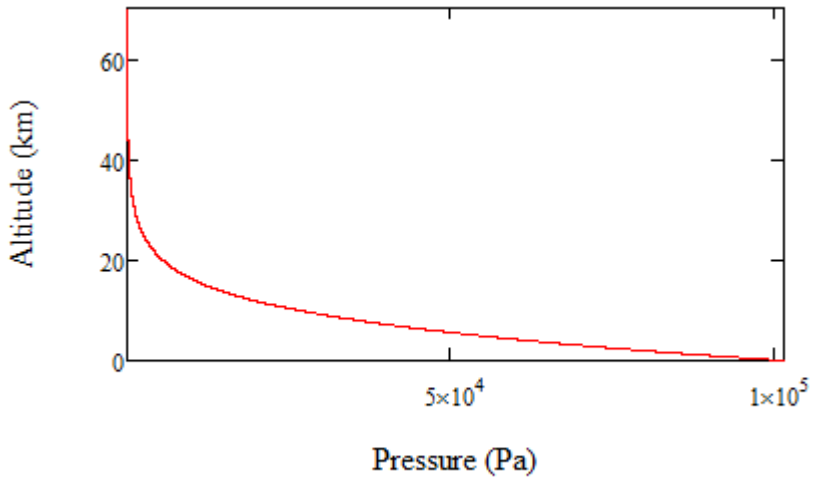

Figure 4. Pressure as a function of Altitude

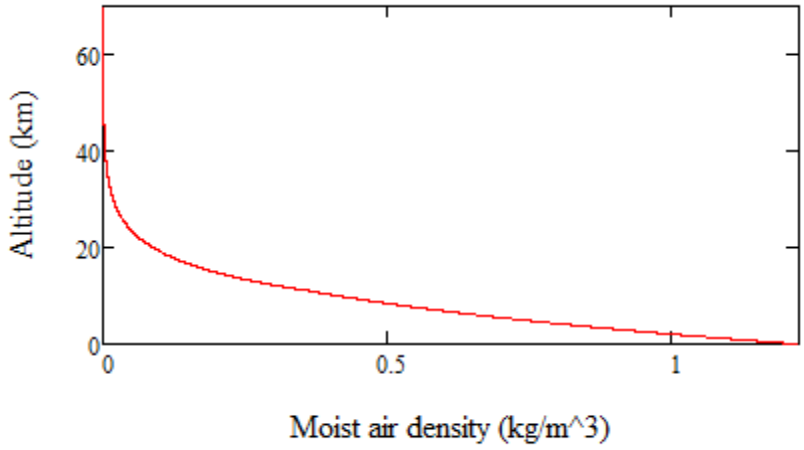

Figure 5. Air Density as a function of altitude.

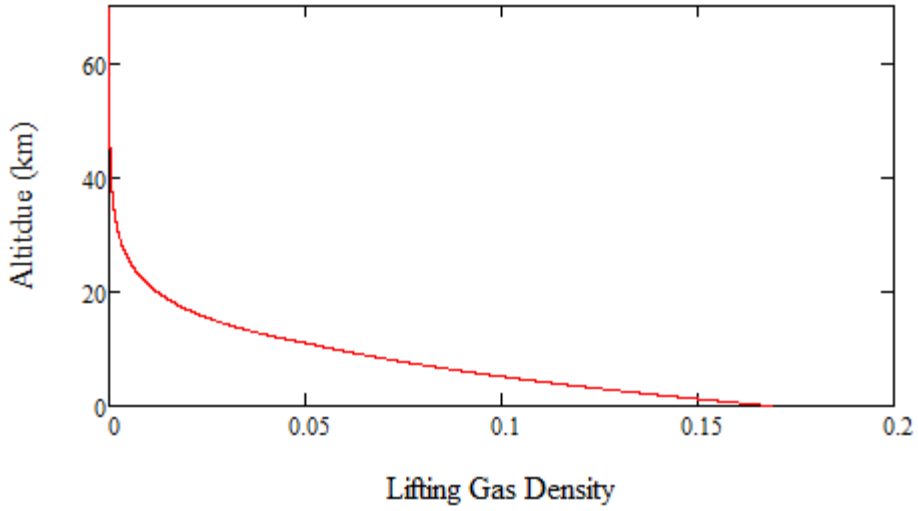

Figure 6. Lifting gas density as a function of altitude

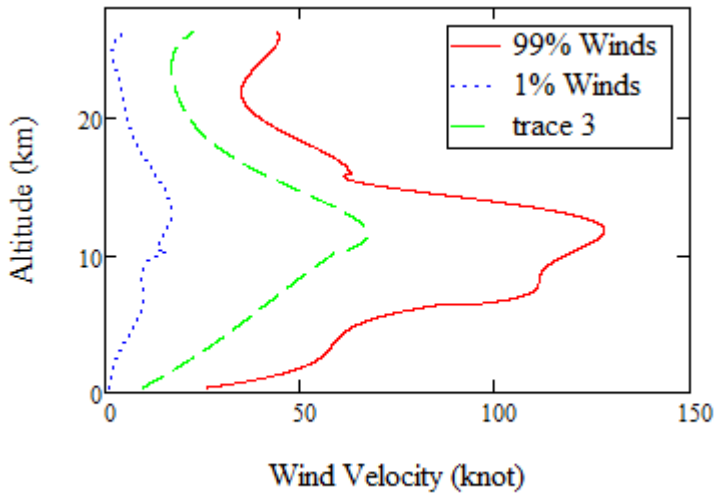

Figure 7. Wind Profile for Akron, OH

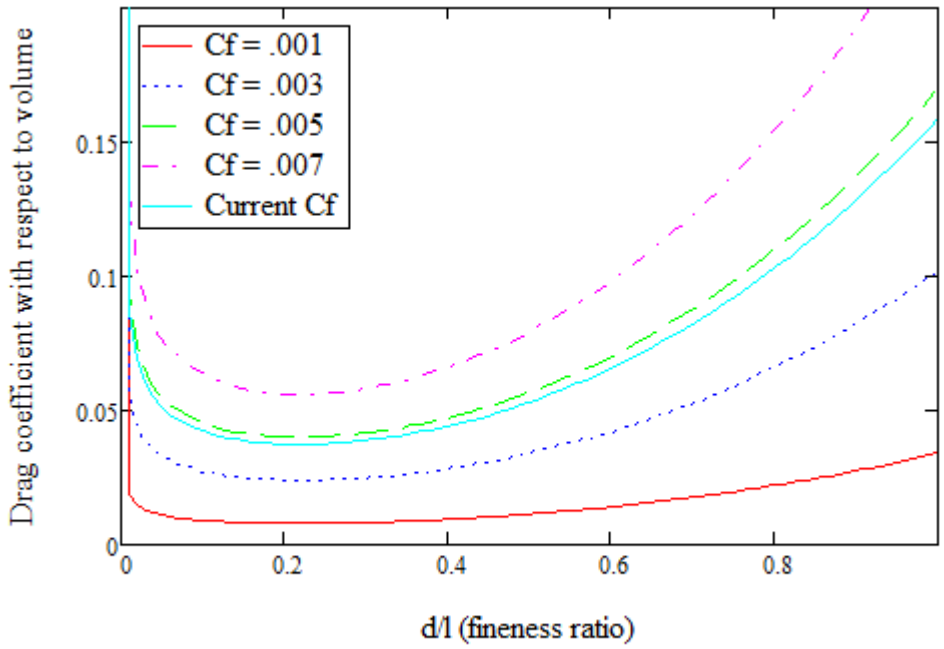

Figure 8. Volumetric drag coefficient vs. fineness ratio

Akron Power

$H := 0, .01 .. 26$

$REHULL_{akron} := Reynolds\left(\rho_{moist.air}(h), U_{99\%.akron}(h), 1, \mu(temperature(h))\right) = 3.24969 \times 10^{5}$

$CFTURB_{akron} := c_{fturb}\left(Reynolds\left(\rho_{moist.air}(h), U_{99\%.akron}(h), 1, \mu(temperature(h))\right)\right) = 5.68806 \times 10^{-3}$

$$C_DV_{akron}(cft, d_l) := cft \cdot \left[4 \cdot \left(\frac{1}{d_l}\right)^{\left(\frac{1}{3}\right)} + 6 \cdot (d_l)^{1.2} + 24 \cdot (d_l)^{2.7}\right]$$

$C_DV_{akron}(CFTURB_{akron}, doverl) = 0.05986$

akronpower(H) :=
- $\mu \leftarrow \mu(temperature(H))$
- $U99\%_{akron} \leftarrow U_{99\%.akron}(H)$
- $\rho \leftarrow \rho_{moist.air}(H)$
- $REHULL_{akron} \leftarrow Reynolds(\rho_{moist.air}(H), U_{99\%.akron}(H), 1, \mu)$
- $CFTURB_{akron} \leftarrow c_{fturb}(REHULL_{akron})$
- $CDV_{akron} \leftarrow C_DV_{akron}(CFTURB_{akron}, doverl)$
- $p_{akron} \leftarrow .5 \cdot \rho \cdot U99\%_{akron}^{3} \cdot CDV_{akron} \cdot \left(volume^{\frac{2}{3}}\right)$

altitude := 0, .1 .. 26

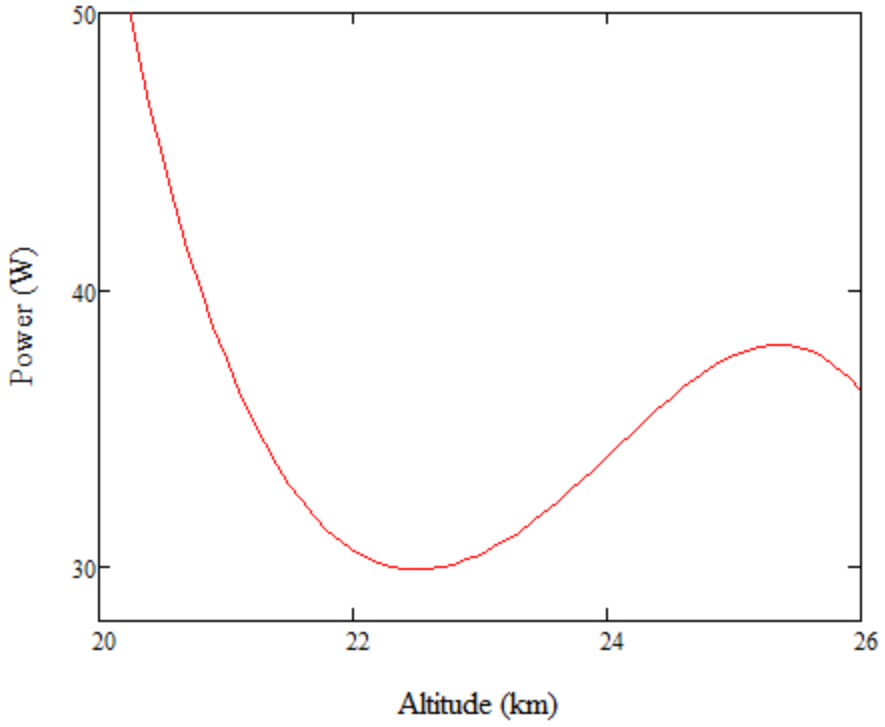

Figure 9. Power Required over Akron, OH

listakron := 20, 20.5 .. 26

listakron =

20
20.5
21
21.5
22
22.5
23
...

akronpower(listakron)

55.9307	W
44.81112	
37.45308	
32.93387	
30.56596	
29.85176	
30.41201	
...	

$U_{99\%.akron}$(listakron)

20.37467	$\frac{m}{s}$
19.26234	
18.4869	
18.06642	
17.9982	
18.25868	
18.80349	
...	

$CDV_{akron}(H) :=$ | $\mu \leftarrow \mu(temperature(H))$

$U99\%_{akron} \leftarrow U_{99\%.akron}(H)$

$\rho \leftarrow \rho_{moist.air}(H)$

$REHULL_{akron} \leftarrow Reynolds(\rho_{moist.air}(H), U_{99\%.akron}(H), 1, \mu)$

$CFTURB_{akron} \leftarrow c_{fturb}(REHULL_{akron})$

$CDVakron \leftarrow C_DV_{akron}(CFTURB_{akron}, doverl)$

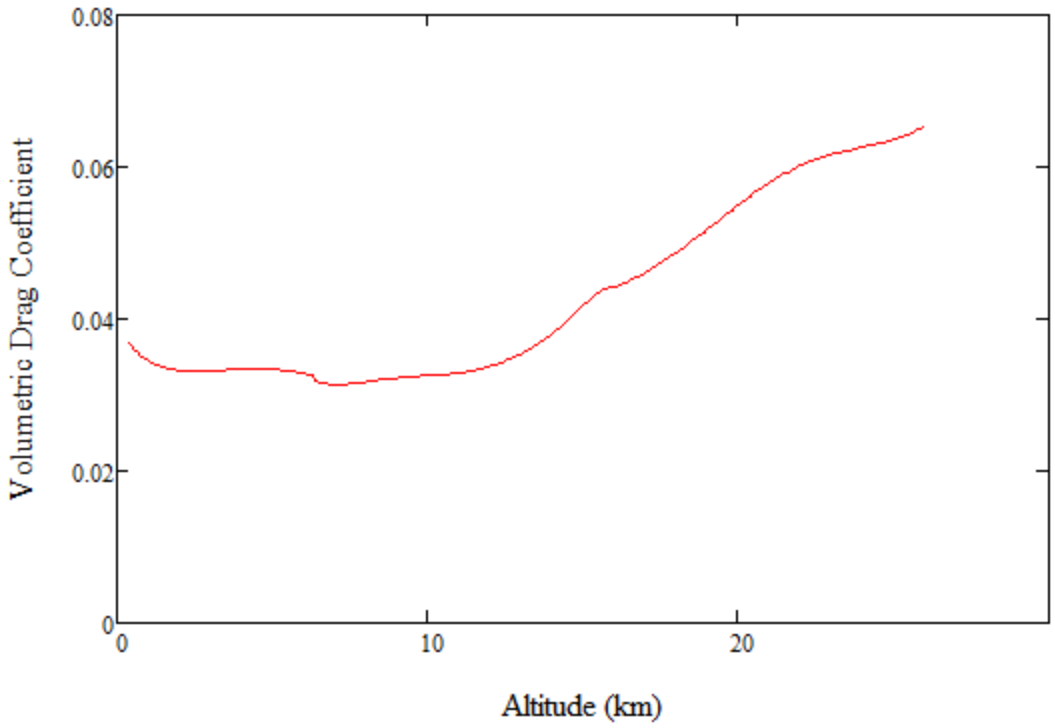

Figure 10. Volumetric drag coefficient as a function of altitude

listcdvakron := .5, 1 .. 26

listcdvakron

0.5
1
1.5
2
2.5
3
...

CDV_{akron}(listcdvakron)

0.03633
0.0345
0.03363
0.03323
0.03311
0.03315
...

White Sands Power

$$REHULL_{WS} := Reynolds\left(\rho_{moist.air}(h), U_{99\%.WS}(h), 1, \mu(temperature(h))\right) = 2.7869 \times 10^{5}$$

$$CFTURB_{WS} := c_{fturb}\left(Reynolds\left(\rho_{moist.air}(h), U_{99\%.WS}(h), 1, \mu(temperature(h))\right)\right) = 5.86554 \times 10^{-3}$$

$$C_DV_{WS}(cft, d_1) := cft \cdot \left[4 \cdot \left(\frac{1}{d_1}\right)^{\left(\frac{1}{3}\right)} + 6 \cdot (d_1)^{1.2} + 24 \cdot (d_1)^{2.7}\right]$$

$$C_DV_{WS}\left(CFTURB_{WS}, doverl\right) = 0.06173$$

$$WSpower(H) := \left| \begin{array}{l} \mu \leftarrow \mu(temperature(H)) \\ U99\%_{WS} \leftarrow U_{99\%.WS}(H) \\ \rho \leftarrow \rho_{moist.air}(H) \\ REHULL_{WS} \leftarrow Reynolds\left(\rho_{moist.air}(H), U_{99\%.WS}(H), 1, \mu\right) \\ CFTURB_{WS} \leftarrow c_{fturb}\left(REHULL_{WS}\right) \\ CDV_{WS} \leftarrow C_DV_{WS}\left(CFTURB_{WS}, doverl\right) \\ \\ P_{WS} \leftarrow .5 \cdot \rho \cdot U99\%_{WS}^{3} \cdot CDV_{WS} \cdot \left(volume^{\frac{2}{3}}\right) \end{array} \right.$$

$$altitude := 0, .1 .. 26$$

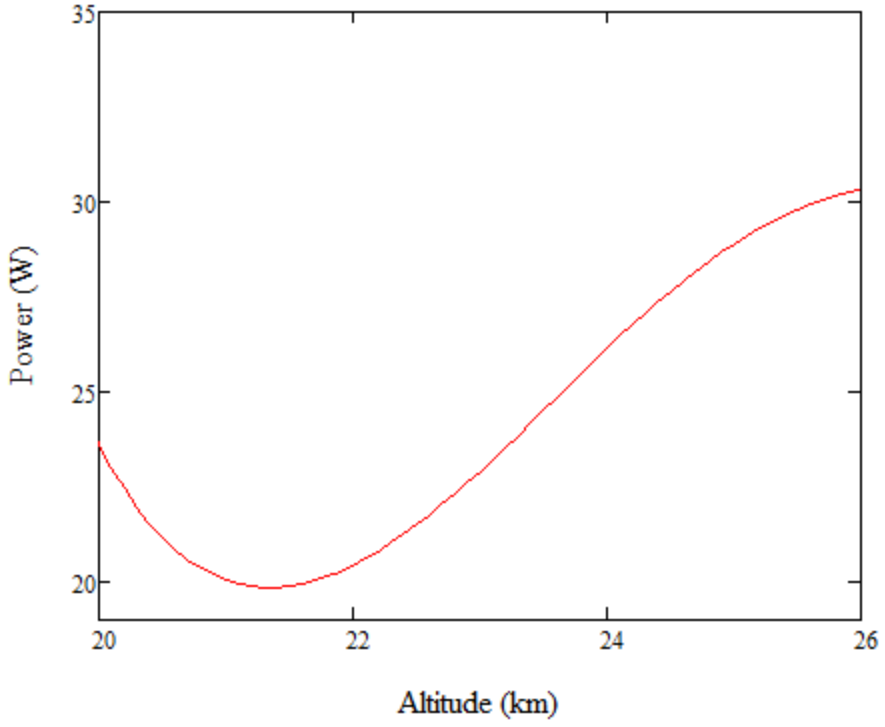

Figure 11. Power required over White Sands, NM

$$listWS := 20, 20.5 .. 26$$

listWS =

20
20.5
21
21.5
22
22.5
23
...

WSpower(listWS)

23.61996	W
21.17867	
20.05978	
19.89739	
20.44204	
21.50305	
22.91338	
...	

$U_{99\%.WS}$(listWS)

14.97569	$\frac{m}{s}$
14.73885	
14.79179	
15.09082	
15.58947	
16.24005	
16.99517	
...	

$$CDV_{WS}(H) := \begin{array}{l} \mu \leftarrow \mu(\text{temperature}(H)) \\ U99\%_{WS} \leftarrow U_{99\%.WS}(H) \\ \rho \leftarrow \rho_{moist.air}(H) \\ REHULL_{WS} \leftarrow \text{Reynolds}\left(\rho_{moist.air}(H), U_{99\%.WS}(H), 1, \mu\right) \\ CFTURB_{WS} \leftarrow c_{fturb}\left(REHULL_{WS}\right) \\ CDV_{WS} \leftarrow C_DV_{WS}\left(CFTURB_{WS}, doverl\right) \end{array}$$

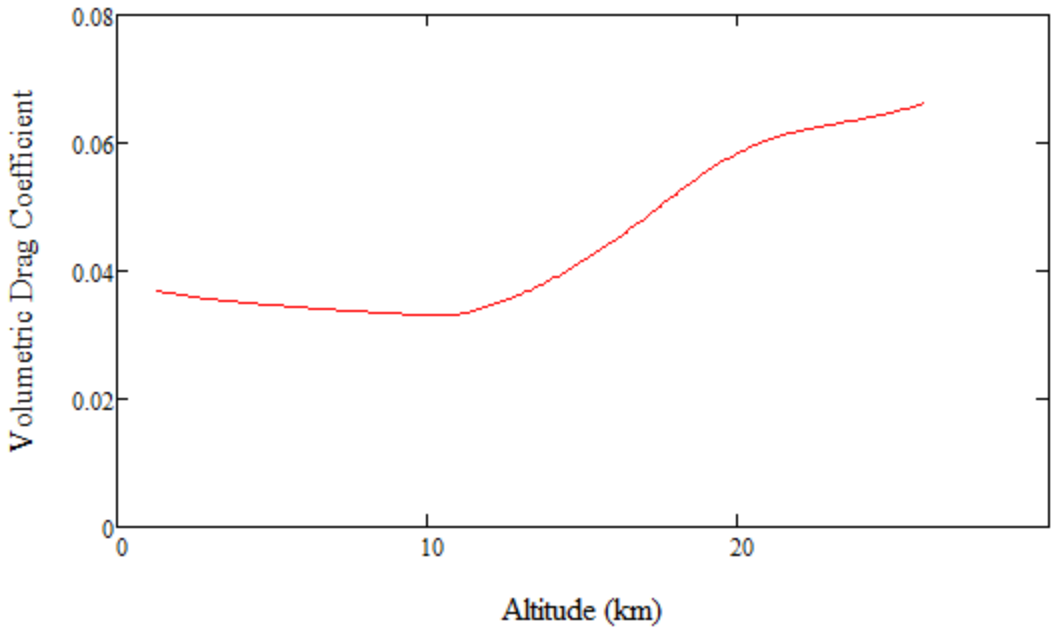

Figure 12. Volumetric drag coefficient as a function of altitude

listcdvws := 1.5, 1.75.. 26

listcdvws =

1.5
1.75
2
2.25
2.5
2.75
...

CDV_{WS}(listcdvws)

0.03669
0.03647
0.03627
0.03608
0.03591
0.03575
...